A Biochemical and Molecular Analysis of Functional Differences between Dystrophin and Utrophin

A DISSERTATION
SUBMITTED TO THE FACULTY OF THE GRADUATE SCHOOL
OF THE UNIVERSITY OF MINNESOTA
BY

Joseph John Belanto

IN PARTIAL FULFILLMENT OF THE REQUIREMENTS
FOR THE DEGREE OF
DOCTOR OF PHILOSOPHY

Advisor, James M. Ervasti Ph.D.

November, 2013

Acknowledgments

I would like to thank my advisor Jim Ervasti for being a wonderful mentor. He has provided an incredible place to work and an excellent environment in which to do research. He is always available to chat about anything work or non-work related. His open door policy has been an invaluable resource in my training.

I would like to thank the members of the Ervasti Lab. Working with such great people every day makes it really easy to come into lab even if the day is not going well. Everyone is willing to help each other, be it with protocols, running experiments, or just discussing ideas. Thank you Ben Perrin, Chris Chamberlain, Dana Strandjord, Jackie McCourt, Alli O'Rourke, JT Olthoff, Xiaobai Patrinostro, Katrina Rhett, Tung Nguyen, Chris Scherber, and Paul Chatterton. I would also like to thank past members of the lab Michele Jaeger and Davin Henderson.

I would like to thank our collaborator Dawn Lowe and her entire lab, especially Michael Eckhoff and Tara Mader. None of the physiology presented here would have been possible without their generous time and technical expertise.

I would like to thank our collaborator Melissa Gardner and her entire lab. None of the TIRF microscopy would have been possible without their instruction, time, and troubleshooting help throughout the microtubule dynamics experiments.

I would like to thank my wonderful committee members, Anja Bielinsky, Harry Orr, Mary Porter, and Alex Sobeck. They have provided great guidance and support during my graduate career for which I am extremely thankful.

I would like to thank Kay Davies and Jeffrey Chamberlain for providing the transgenic mouse models that allowed this work to occur.

I would like to thank my fellow graduate students, especially Dana Strandjord, Keli Holzapfel, Frazer Heinis, Chris Braden, Juan Diaz Quiroz, Michelle Smith, and Jeremy Herrera. My sanity is intact in no small part because of their friendship and our happy hours.

I would like to thank my family, Pete, Loren, Ryan, and Jordyn Belanto for their unending support.

I would like to acknowledge the Mouse Genetics Core at The Scripps Research Institute for generation of transgenic mice.

I would like to acknowledge Dave Thomas and the Minnesota Muscle Training grant (AR007612), 3M and the 3M Science and Technology Fellowship, and the Doctoral Dissertation Fellowship for supporting my graduate career.

Dedication

This dissertation is dedicated to my late grandparents, Joe and Lois Belanto.

Abstract

The *DMD* gene resides on the X chromosome and encodes the protein dystrophin, a 427kD cytoplasmic protein responsible for linking the costameric actin cytoskeleton to the extracellular matrix via the associated dystrophin-glycoprotein complex. Mutations in dystrophin that abolish or reduce its expression lead to Duchenne muscular dystrophy (DMD) or the less severe Becker muscular dystrophy. Patients with DMD become wheelchair bound in their early teens and succumb to fatal cardiac and/or respiratory failure in their mid-twenties to early thirties. There is currently no effective or widely available treatment for DMD beyond ventilatory support and the use of corticosteroids. A long-known but poorly understood phenotype of the dystrophin-deficient *mdx* mouse is that the subsarcolemmal microtubule lattice is disorganized, the consequences of which are mostly unknown.

Many therapies for treating dystrophin deficiency aim at upregulating its autosomal homolog utrophin due to its structural similarity and ability to bind an almost identical repertoire of proteins that dystrophin binds. It was previously shown that utrophin cannot bind neuronal nitric oxide synthase (nNOS) even though dystrophin binds nNOS, establishing for the first time a functional difference between dystrophin and utrophin. Here, we show that transgenic overexpression of utrophin on the *mdx* mouse background (Fiona-*mdx*) is not sufficient to rescue the disorganized microtubule network of the *mdx* mouse. Moreover, transgenic overexpression of dystrophins on the *mdx* mouse background results in rescue of microtubule lattice organization. Thus, we have

elucidated a second functional difference between dystrophin and utrophin. Additionally, Fiona-*mdx* mice lack full recovery of cage activity after a bout of mild exercise. Our results suggest that any deficiency in nNOS binding or microtubule lattice function caused by loss of dystrophin may not be restored by upregulation of utrophin. Therefore, it remains important to determine other specific pathologies to which aberrant nNOS localization or microtubule disorganization associated with loss of dystrophin protein expression contributes.

Previously, our lab reported that dystrophin directly binds to microtubules and organizes them beneath the sarcolemma. Microtubules are composed of α- and β-tubulin monomers arranged in heterodimeric protofilaments which form a hollow, cylindrical tube along which the cell transports intracellular cargo using the motor proteins dyneins and kinesins. Using *in vitro* microtubule cosedimentation assays, we show that dystrophin binds to microtubules with strong affinity (K_D=0.33μM). Through the use of various recombinant constructs tested via *in vitro* microtubule cosedimentation we show that spectrin-like repeats 20-22 of the dystrophin central rod are responsible for microtubule binding activity. However, we show that these repeats require flanking regions of dystrophin for proper binding activity, making microtubule binding a context-dependent function of dystrophin. Additionally, we show that recombinant utrophin does not bind microtubules *in vitro*, corroborating our *in vivo* findings of the disorganized subsarcolemmal microtubule lattice of the Fiona-*mdx* mouse. We also provide evidence showing that dystrophin functions as a molecular guidepost to organize subsarcolemmal microtubules into a rectilinear lattice.

To further elucidate the function of subsarcolemmal microtubule lattice organization and the consequences of its disorganization, we have generated a transgenic mouse expressing a dystrophin incapable of microtubule binding activity while still maintaining all other known functions. Our initial studies show that the microtubule lattice of this mouse when crossed onto the dystrophin-deficient *mdx* mouse background remains disorganized even in the presence of 160% WT levels of dystrophin and the fact that transgenic dystrophin incorporates into the dystrophin-glycoprotein complex. This model will be useful for discerning phenotypes present in the Fiona-*mdx* mouse that are specifically related to microtubule disorganization since nNOS localization is intact in this mouse.

Table of Contents

List of Tables

List of Figures

Chapter One

Introduction

Dystrophin and Duchenne Muscular Dystrophy

Dystrophin is a 427kD cytoplasmic protein predominantly expressed in striated muscle. The *DMD* gene, which encodes dystrophin, resides on the X chromosome in both humans and mice and spans over 2.4 megabases of DNA, making it the largest gene in any known genome (Hoffman et al., 1987). The genomic locus of *DMD* consists of 79 exons within which exist multiple tissue-specific promoters encoding various dystrophin isoforms (Nudel et al., 1989; Bar et al., 1990; Górecki et al., 1992; Byers et al., 1993; Pillers et al., 1993; Roberts et al., 1993; Lidov et al., 1995). These isoforms include three full-length dystrophin isoforms expressed in cardiac muscle (Dp427c), skeletal muscle (Dp427m), and Purkinje cells (Dp427p); a 260kD isoform expressed in the retina (Dp260); a 140kD isoform expressed in the central nervous system (Dp140); a 116kD isoform expressed in Schwann cells (Dp116); and a 71kD isoform expressed highly in the liver and in various other non-muscle tissues (Dp71).

Due to its vast size, the *DMD* gene is statistically more prone to mutation than smaller genes. Mutations in dystrophin which abolish or reduce its function lead to Duchenne muscular dystrophy (DMD) or a milder form of the disease, Becker muscular dystrophy (Worton and Thompson, 1988). Approximately one in every 4000 boys is born with DMD (Mendell et al., 2012), all of whom will inevitably become wheelchair-bound and succumb to fatal cardiac arrest or respiratory failure during their twenties, with a small percentage reaching their early thirties (Rall and Grimm, 2012). Of these mutations, a portion occur *de novo* and therefore maternal screening may not be sufficient to guarantee

genetic fidelity. Current treatment is limited to respiratory therapy, which prolongs life, and corticosteroids, which are minimally effective and can cause serious side effects (Angelini, 2007).

The dystrophin protein consists of an N-terminal tandem calponin-homology domain which interacts with filamentous γ-actin; twenty-four spectrin-like repeats with four flexible hinge regions within which lies a second actin binding domain and the neuronal nitric oxide synthase (nNOS) binding domain; a cysteine-rich domain containing WW, EF-hand, and ZZ domains known to interact with β-dystroglycan at the muscle plasma membrane, or sarcolemma; and a C-terminal domain known to interact with α-dystrobrevin and α-syntrophin (Koenig et al., 1988; Koenig and Kunkel, 1990; Way et al., 1992; Bork and Sudol, 1994; Ponting et al., 1996; Rybakova and Ervasti, 1997). Each spectrin-like repeat is a triple alpha helical bundle, which each helix designated α1-3. In striated muscle, dystrophin localizes to the sarcolemma at a region referred to as the costamere (Porter et al., 1992) and links cytoplasmic γ-actin filaments at its N-terminus with β-dystroglycan at its C-terminus (Figures 1-1 and 1-2). Thus, dystrophin is thought to stabilize the sarcolemma during muscle contraction to decrease damage incurred as a result of normal muscle function. In the absence of dystrophin, costameric proteins mislocalize, leading to membrane instability (Mokri and Engel, 1998) and muscle weakness (Carlson and Makiejus, 1990).

The protein β-dystroglycan spans the sarcolemma and interacts with laminin in the extracellular matrix via the heavily glycosylated α-dystroglycan (Ervasti and Campbell, 1993). These two proteins were initially described as

components of a larger protein complex eventually named the dystrophin-glycoprotein complex (DGC) which was later shown to include the sarcoglycans, sarcospan, dystrobrevin, and syntrophin (Ervasti and Campbell, 1991). The presence of the dystroglycans, sarcoglycans, and other DGC member proteins at the sarcolemma requires dystrophin and patients with DMD show reduced levels of these DGC component proteins in muscle biopsies.

Utrophin and the *mdx* Mouse

Utrophin is the autosomal homolog of dystrophin (Matsumura et al., 1992; Kramarcy et al., 1994; Winder et al., 1995; Blake et al., 2002). In both humans and mice, utrophin is ubiquitously expressed in all tissues throughout development and adulthood. During muscle development, utrophin localizes to the sarcolemma where it serves the same role that dystrophin does later in development. However, as development progresses, utrophin is lost at the sarcolemma as dystrophin expression begins to rise and the former becomes sequestered to the neuromuscular and myotendinous junctions (Matsumura et al., 1992; Kramarcy et al., 1994; Winder et al., 1995; Gramolini et al., 1997; Blake et al., 2002).

The utrophin gene *UTRN* resides on chromosome 6 in humans and chromosome 10 in mice. In both humans and mice, *UTRN* consists of 72 exons and spans approximately 900 kilobases of DNA (Pearce et al., 1993). The utrophin protein consists of an N-terminal tandem calponin-homology domain which interacts with filamentous γ-actin; twenty-two spectrin-like repeats with four flexible hinge regions, of which the first ten repeats participate in actin binding; a cysteine-rich domain which interacts with β-dystroglycan; and a C-terminal domain. The dystrophin and utrophin proteins are 85-87% similar and 74-79% identical in the N-terminal actin binding and cysteine rich domains, whereas the spectrin-like repeats show approximately 50% overall similarity (Figure 1-3). No human diseases have been associated with mutations in utrophin, indicating that it may be embryonic lethal in humans. However, a utrophin deficient mouse

model exists which shows no overt phenotypes aside from reduced acetylcholine receptor clustering at the neuromuscular junction, suggesting that utrophin deficiency may simply not cause disease (Deconinck, 1997).

The mouse model most widely used to study DMD is the *mdx* mouse, which contains a nonsense mutation in exon 23 of the dystrophin transcript, ablating dystrophin protein expression (Bulfield et al., 1984). The relatively mild dystrophic phenotype of the dystrophin-deficient *mdx* mouse is partially credited to the upregulation of utrophin (Tinsley et al., 1998; Blake et al., 2002). Additionally, increased utrophin levels correlate with improved prognosis in DMD patients (Kleopa et al., 2006). Therefore, some potential therapies in development for treating DMD attempt to upregulate utrophin.

While the *mdx* mouse does not fully recapitulate DMD patient phenotypes, there are many phenotypes which it does manifest. The sarcolemma has increased permeability based on increased uptake of Evans blue dye, a membrane impermeable dye, and increased serum creatine kinase levels, a protein normally sequestered in the cytoplasm (Menke and Jockusch, 1991; Clarke et al., 1993; Matsuda et al., 1995). Additionally, the *mdx* mouse displays increased muscle weakness, especially in the diaphragm muscle, accompanied by repetitive rounds of muscle degeneration and regeneration leading to centrally nucleated muscle fibers (Carlson and Makiejus, 1990; Cox et al., 1993; Warner et al., 2002). Lastly, the *mdx* mouse is highly susceptible to eccentric contraction induced injury, losing approximately 85-90% of its force generating capacity after

only five successive eccentric contractions (Moens et al., 1993; Petrof et al., 1993).

In addition to the aforementioned physiological phenotypes of the *mdx* mouse, there are also molecular phenotypes associated with dystrophin deficiency. In the absence of dystrophin, the *mdx* mouse shows substantial reduction in abundance of DGC components (Ervasti et al., 1990; Ohlendieck and Campbell, 1991). The increased levels of utrophin in the *mdx* mouse have been shown to associate with the DGC components to form a so-called utrophin-glycoprotein complex (UGC), but the presence of the UGC is insufficient to rescue the physiological phenotypes described above (Matsumura et al., 1992). However, transgenic overexpression of utrophin in the *mdx* mouse has been shown to increase the amount of UGCs present at the sarcolemma and ameliorate all measured dystrophic parameters of the *mdx* mouse (Tinsley et al., 1998), indicating that utrophin protein levels in the *mdx* mouse may simply be too low to fully compensate for the lack of dystrophin. Like dystrophin, utrophin couples membrane-bound dystrophin-associated proteins with costameric actin filaments (Matsumura et al., 1992; Rybakova et al., 2002). However, utrophin does not localize neuronal nitric oxide synthase to the sarcolemma (Li et al., 2010; Lai et al., 2013) as was previously shown for dystrophin (Lai et al., 2009), indicating that utrophin and dystrophin are not completely interchangeable.

Neuronal Nitric Oxide Synthase

Neuronal nitric oxide synthase (nNOS) belongs to the nitric oxide synthase family of enzymes, which also includes endothelial nitric oxide synthase (eNOS) and inducible nitric oxide synthase (iNOS). Of these three genes, eNOS exists in four splice variants, nNOS exists in three splice variants, whereas iNOS does not have any splice variants (Förstermann and Kleinert, 1995). All NOS enzymes are responsible for catalyzing the formation of nitric oxide, which plays roles in vasodilation and signaling (Förstermann et al., 1994).

nNOS is an approximately 160kD enzyme expressed in various tissues of the body, most notably brain, skeletal muscle, and cardiac muscle (Schmidt et al., 1992; Förstermann et al., 1994; Michel and Feron, 1997). In skeletal muscle, nNOS localizes to myotendinous junctions and to costameres (Chang et al., 1996). These subcellular locations are hotspots for force transduction and signaling, strengthening the hypothesis of the proposed function of nNOS in signaling and vasodilation. nNOS activity is highly calcium dependent (Förstermann et al., 1994). At low calcium concentrations, such as those present in muscle at rest (100nM), nNOS is inactive. When muscle begins to contract, calcium concentrations rise (500nM), and nNOS becomes active. This corresponds well with the increased need for vasodilation of the surrounding vasculature to insure increased oxygen delivery to actively contracting muscle.

In the absence of dystrophin, the costameric localization of nNOS is lost. This initial observation was also accompanied with data from both human and mouse showing that the overall expression of nNOS was reduced in the absence

of dystrophin (Chang et al., 1996). This led researches to begin to hypothesize that nNOS may be a component of the DGC. Initial evidence in support of this hypothesis came when syntrophin was shown to directly interact with nNOS (Brenman et al., 1995; Hillier, 1999). The protein syntrophin is an established component of the DGC that binds to the C-terminus of dystrophin (Ahn and Kunkel, 1995; Suzuki et al., 1995). Based on this work, nNOS was hypothesized to interact with dystrophin and the DGC through its interaction with syntrophin.

Approximately ten years after these initial discoveries, spectrin-like repeats 16 and 17 of the central rod domain of dystrophin were shown to be necessary for sarcolemmal localization of nNOS (Lai et al., 2009). Mice expressing a dystrophin lacking these repeats failed to show sarcolemmal nNOS localization. Through subsequent work, utrophin was shown to lack the nNOS localization activity present in dystrophin, revealing the first molecular difference between these two closely related proteins (Li et al., 2010). The minimal nNOS binding domain was shown to be the α1 helix of dystrophin repeat 17 (Lai et al., 2013). Replacing the homologous helix in utrophin with the α1 helix of dystrophin repeat 17 did not confer nNOS binding activity to utrophin. However, replacing the homologous region of utrophin with dystrophin repeats 16 and 17 conferred nNOS binding activity to utrophin, indicating that nNOS binding in dystrophin is context-dependent, relying on flanking regions in dystrophin for proper activity.

In terms of physiology, sarcolemmal localization of nNOS is required for proper recovery of activity after mild exercise. When mice lacking sarcolemmal localization of nNOS were subjected to mild exercise, they showed greatly

reduced cage activity (Kobayashi et al., 2008). In the presence of sarcolemmal nNOS, WT mice exhibit a nominal decrease in activity after exercise. However, in the absence of sarcolemmal nNOS, this decrease in activity is greatly exacerbated. The *mdx* mouse shows an even greater exacerbation of this loss of activity, presumably due to the combined lack of nNOS and dystrophin. The researchers hypothesized that the lack of vasodilation in the absence of nNOS results in decreased oxygen delivery to muscles and thus weakness and loss of activity. Vasodilators such as phosphodiesterase 5A inhibitors have been shown to be beneficial and alleviate some of the activity loss associated with exercise (Kobayashi et al., 2008), providing evidence for this hypothesis.

Since the Fiona-*mdx* mouse transgenically overexpresses utrophin, but utrophin cannot localize nNOS to the sarcolemma, we initially began our study by rigorously characterizing the physiological differences associated with transgenic overexpression of utrophin. This may be helpful in delineating the benefits and drawbacks associated with utrophin-based therapies for treating DMD.

Microtubules

Microtubule protofilaments are composed of α- and β-tubulin heterodimers arranged head to tail. Eleven to thirteen of these protofilaments self-assemble into a hollow tube known as a microtubule (Wade and Chrétien, 1993) along which the motor proteins dyneins and kinesins travel in order to shuttle cargo throughout the cell. Microtubules are polarized, having a (-) end and (+) end. The (-) end is capped with a ring of γ-tubulin anchored at a structure known as the microtubule organizing center, whereas polymerization and depolymerization occur at the (+) end (Figure 1-4A). Microtubules are essential in all eukaryotic cells for mitosis, cell growth, and cell motility (Figure 1-4B, C, D) (Kirschner and Mitchison, 1986).

Tubulin monomers are approximately 55kD in size. A single α-tubulin will self-assemble with a single β-tubulin monomer to form a heterodimer. Each monomer binds a single GTP molecule with that of β-tubulin being hydrolyzed to GDP over time. Since the β-tubulin monomer is exposed at the (+) end of the microtubule, GTP hydrolysis at the terminal β-tubulin drives the phenomenon known as dynamic instability (Figure 1-5). Dynamic instability refers to the fact that the (+) end of a microtubule will undergo long waves of relatively slow polymerization followed by short bursts of relatively fast depolymerization. This allows for rapid microtubule reorganization within the cell and is the driving force that separates chromosomes during cell division.

To date, seven α-tubulin and eight β-tubulin genes have been discovered. Within a given family, each tubulin shows great similarity to each other except at

its C-terminal tail region. This region is where most tubulin posttranslational modifications occur. Both α- and β-tubulin are subject to posttranslational modifications such as detyrosination, acetylation, polyglycation, and polyglutamylation (Hammond et al., 2008). These posttranslational modifications are thought to regulate microtubule stability, polymerization dynamics, and protein-protein interactions, as well as provide the basis for which motors travel along which microtubules.

Studies of microtubule function in striated muscle are rarer than studies in other tissues, but they do exist. Multiple groups have shown that proper microtubule function is necessary for myotube formation, which occurs when singly nucleated myoblast cells fuse to become multinucleated myotubes (Saitoh et al., 1988; Chang et al., 2002; Perez et al., 2002). Additionally, the microtubule (+) end binding protein EB1 has been shown to be necessary in this process (Zhang et al., 2009). While Golgi-derived vesicles require proper microtubule organization for transport throughout the cell, the Golgi itself requires proper microtubule organization for accurate localization and function within the cell (Ralston et al., 1999, 2001). Apart from these phenotypes, little is known about the molecular pathology of microtubule perturbations in striated muscle.

In WT skeletal muscle, microtubules are organized into a rectilinear lattice beneath the sarcolemma. However, in *mdx* muscle tissue the microtubule lattice becomes disorganized (Percival et al., 2007; Ayalon et al., 2008; Prins et al., 2009), the pathological consequences of which are mostly unknown. Recently, it was shown that the altered microtubule network in *mdx* cardiac tissue contributes

to increased reactive oxygen species and aberrant calcium regulation, suggesting that microtubule lattice derangement in the *mdx* mouse directly contributes to the molecular pathogenesis of DMD (Prosser et al., 2011; Khairallah et al., 2012).

While the *mdx* mouse expresses increased levels of endogenous utrophin (Rybakova et al., 2002) the skeletal muscle microtubule lattice remains disorganized (Percival et al., 2007; Ayalon et al., 2008; Prins et al., 2009) suggesting that the microtubule binding function of dystrophin may not be conserved in utrophin. On the other hand, the increased endogenous utrophin expression in the *mdx* mouse is insufficient to mechanically anchor costameric actin filaments to the sarcolemma while transgenic utrophin overexpression restores coupling (Rybakova et al., 2002), indicating that utrophin protein levels in the *mdx* mouse may simply be too low to properly organize microtubules.

Potential Therapies for Duchenne Muscular Dystrophy

The development of transgenic mice overexpressing utrophin on the *mdx* mouse background has provided proof of principle that utrophin upregulation can functionally compensate for the absence of dystrophin (Tinsley et al., 1998). Subsequent work has shown that the protein levels produced from expression of the endogenous utrophin gene can substitute for transgenic overexpression when upregulated. In one study, transgenic mice were created harboring artificial zinc-finger transcription factors targeted to the utrophin promoter. The muscle tissue of these mice showed a marked increase in utrophin expression and its presence at the sarcolemma comparable to the levels of dystrophin in WT mice (Mattei et al., 2007). However, since transgenic overexpression is not an option for treatment of humans, high throughput small molecule screens have been undertaken to identify drugs that could possibly be used to achieve utrophin overexpression. This would offer systemic delivery of a drug to patients and would require no genetic manipulation to achieve therapeutic benefit.

Nonsense mutations account for 35-40% of mutations in the dystrophin gene (Roberts et al., 1994). Dystrophin mRNA harboring these nonsense mutations can cause nonsense mediated decay of the mRNA or, if translated, produces a truncated protein that at minimum lacks the C-terminal β-dystroglycan binding domain, rendering it incapable of coupling muscle contraction with force transmission. Earlier studies on the antibiotic gentamicin showed that it could cause the ribosome to skip over nonsense mutations and allow for full translation of the otherwise intact mRNA (Barton-Davis et al., 1999).

These findings opened the door for high throughput screens aimed at finding nonsense mutation read-through drugs that could be used not only to treat DMD patients with nonsense mutations but other diseases caused by these mutations. Drawbacks to this type of therapy are that drugs would have to be administered for the life of the patient, which can be rather costly. In addition, 60-65% of DMD patients would not benefit from this therapy since their mutations are not nonsense mutations.

As an alternative to drugs that allow read-through of nonsense mutations, exon skipping provides a means to bypass the exon harboring the nonsense mutation altogether. This therapeutic strategy can be employed not only for nonsense mutations, but also missense mutations that may affect protein folding or stability as well as insertions or deletions that may affect the reading frame of the mRNA. It is important to note that in order to remain in frame it may be necessary to bypass multiple exons. Blocking splice site recognition can be achieved by using antisense oligonucleotides or oligonucleotide mimics such as morpholino oligomers, which have a modified backbone in place of the normal phosphate backbone (van Deutekom et al., 2001). These modified oligomers have a longer half-life since their composition is not one the cell normally encounters, which reduces the likelihood they will be degraded. In one study, exon 23 of the *mdx* mouse was targeted for skipping using morpholinos (Yin et al., 2009). The *mdx* mice treated with these morpholinos expressed sarcolemma-associated dystrophin in multiple muscle tissues and this increased expression correlated with increased grip strength, reduced serum creatine kinase levels,

and fewer centrally nucleated fibers, all of which point to phenotypic restoration toward that of WT mice.

Restoration of dystrophin expression can also be achieved by cellular introduction of full-length or truncated dystrophin constructs. Since a new, normal dystrophin gene is introduced to the cell, gene delivery bypasses the need for personalized therapy based on individual patient mutations, which is an advantage over exon skipping therapies. Viral-mediated transduction is the most prominent method of gene delivery. Earlier methods, such as direct intramuscular injection of plasmid DNA coding for dystrophin, showed very poor efficacy and is not very amenable to humans as injection of every muscle cell is not feasible (Acsadi et al., 1991). However, these initial experiments provided proof of principle. Recombinant adeno-associated virus (rAAV) has become the main viral vehicle used for delivering dystrophin DNA in a systemic manner. However, the limited carrying capacity of rAAV prevents the full-length dystrophin construct from being transduced. Therefore, truncated versions of dystrophin harboring deletions in the internal rod domain and/or the C-terminus were used.

Finally, systemic delivery of dystrophin or utrophin protein can potentially treat DMD patients. Since it is not plausible to inject every muscle cell with protein directly, some method of allowing the protein to enter the cell must be devised. One potential solution to this issue comes from the lysine-rich domain of the HIV-1 transactivator of transcription (TAT) protein. When fused to a protein of interest, this sequence allows for cellular entry of the entire protein via macropinocytosis (Schwarze et al., 2000). Fusing TAT to dystrophin or utrophin

and injecting it intraperitoneally or intravenously allows for systemic delivery of recombinant protein that will be able to traverse cell membranes. Functional recovery of the dystrophic phenotype in *mdx* mice treated with a fusion protein of TAT and a truncated version of utrophin (TAT-microutrophin) has proven effective (Sonnemann et al., 2009). Intraperitoneal injection of TAT-microutrophin showed that it entered all organs, including skeletal and cardiac tissue, and was found to localize to the sarcolemma. This sarcolemmal localization coincided with restoration of the normal glycoprotein complex along with increased grip strength and decreased susceptibility to contraction-induced injury.

Figures

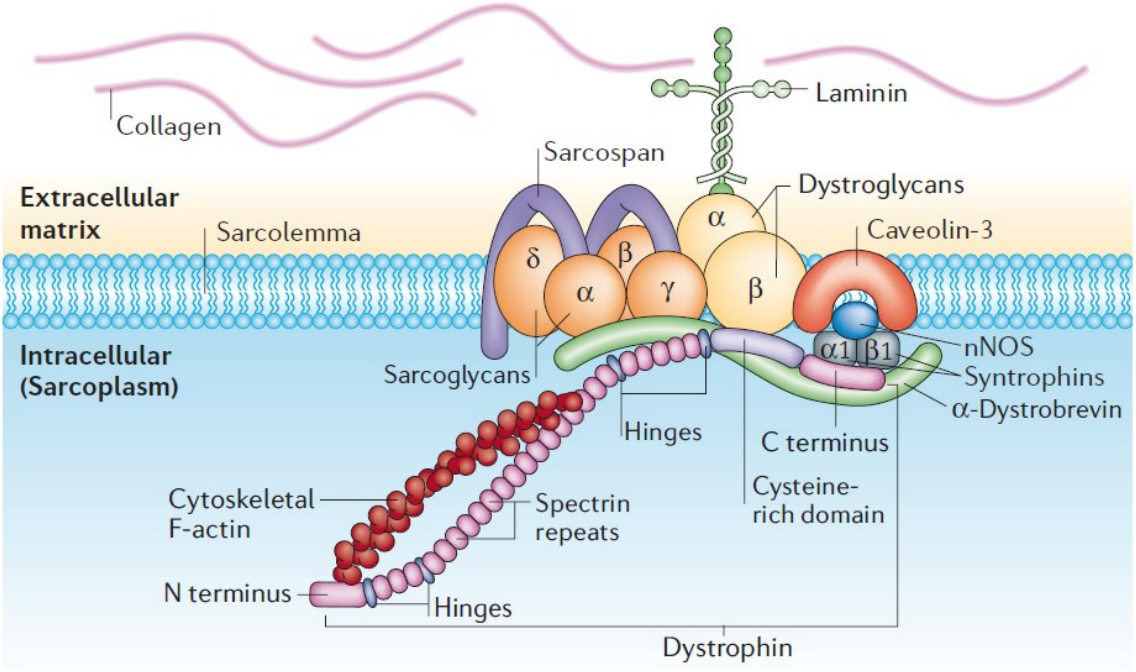

Figure 1-1: The dystrophin-glycoprotein complex. Schematic representation of the dystrophin-glycoprotein complex. From Davies and Nowak, 2006.

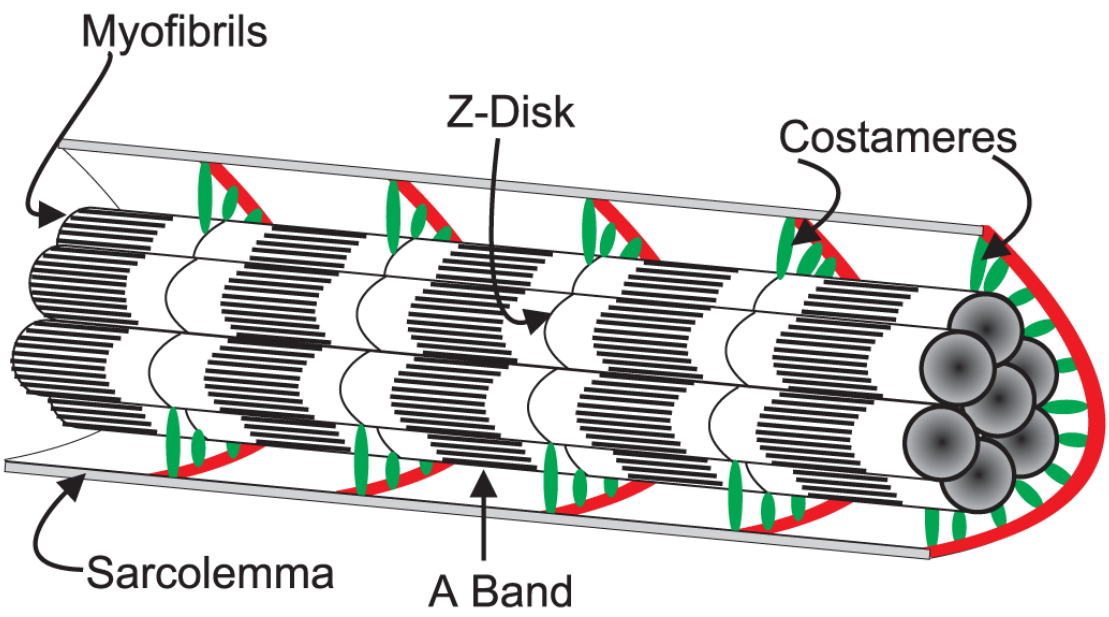

Figure 1-2: Schematic representation of a muscle fiber. Representative structure of a single muscle fiber. Dystrophin is highly enriched at costameres where it links cytoplasmic γ-actin with transmembrane β-dystroglycan. This linkage is thought to stabilize the sarcolemma during muscle contraction to prevent damage. From Ervasti, 2003.

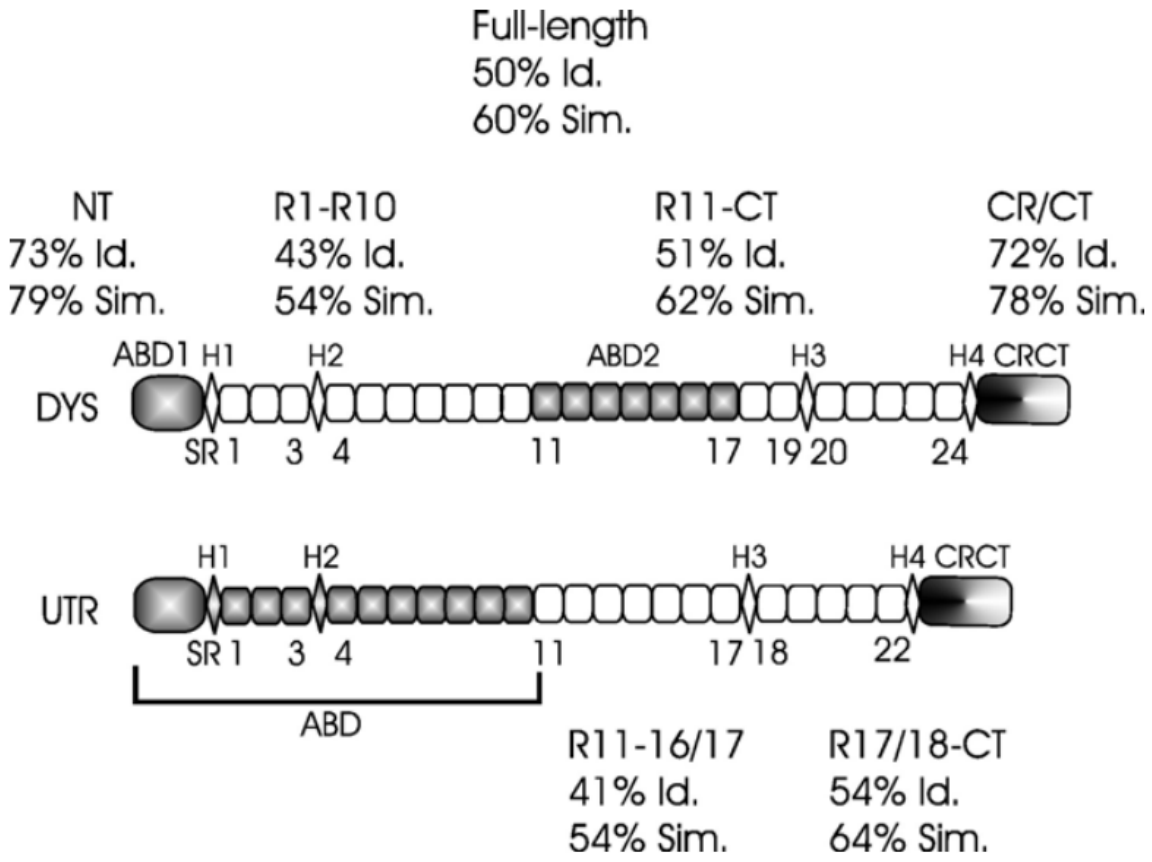

Figure 1-3: Homology between dystrophin and utrophin. Schematic representation showing percentage similarity and identity of homologous regions of dystrophin and utrophin. From Ervasti, 2007.

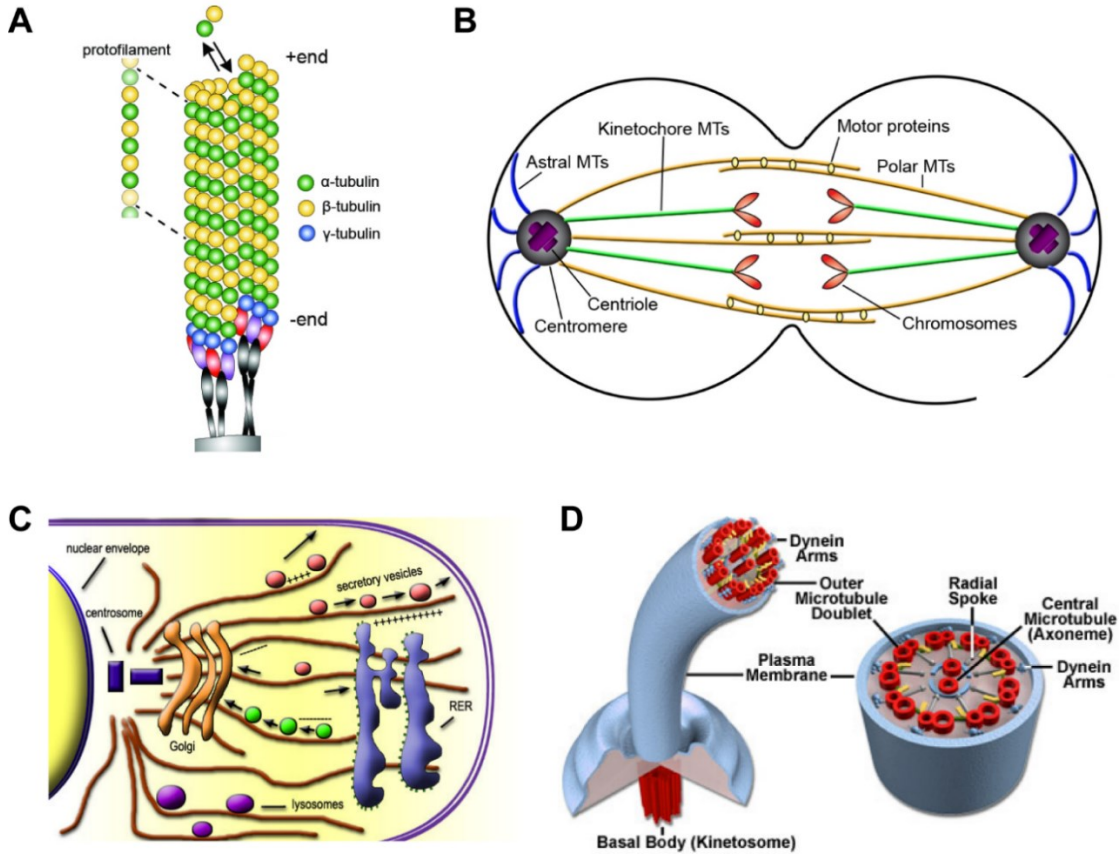

Figure 1-4: Structure and cellular functions of microtubules. (A) Schematic representation of the structure of a microtubule. α- and β-tubulin heterodimers self-assemble into protofilments which then self-assemble into hollow microtubules. IN cells, microtubules are capped at their (-) end by a ring of γ-tubulin, which is then anchored to the microtubule organizing center (pink, purple, and black). (B) During cytokinesis, microtubules are responsible for separating sister chromatids at the cleavage furrow. (C) Intracellular vesicle transport between the nucleus, Golgi complex, endoplasmic reticulum, and plasma membrane requires motor movement along microtubules. (D) Movement in many microorganisms relies on the movement of dynein motors along microtubule doublets in specialized structures known as flagella or cilia.

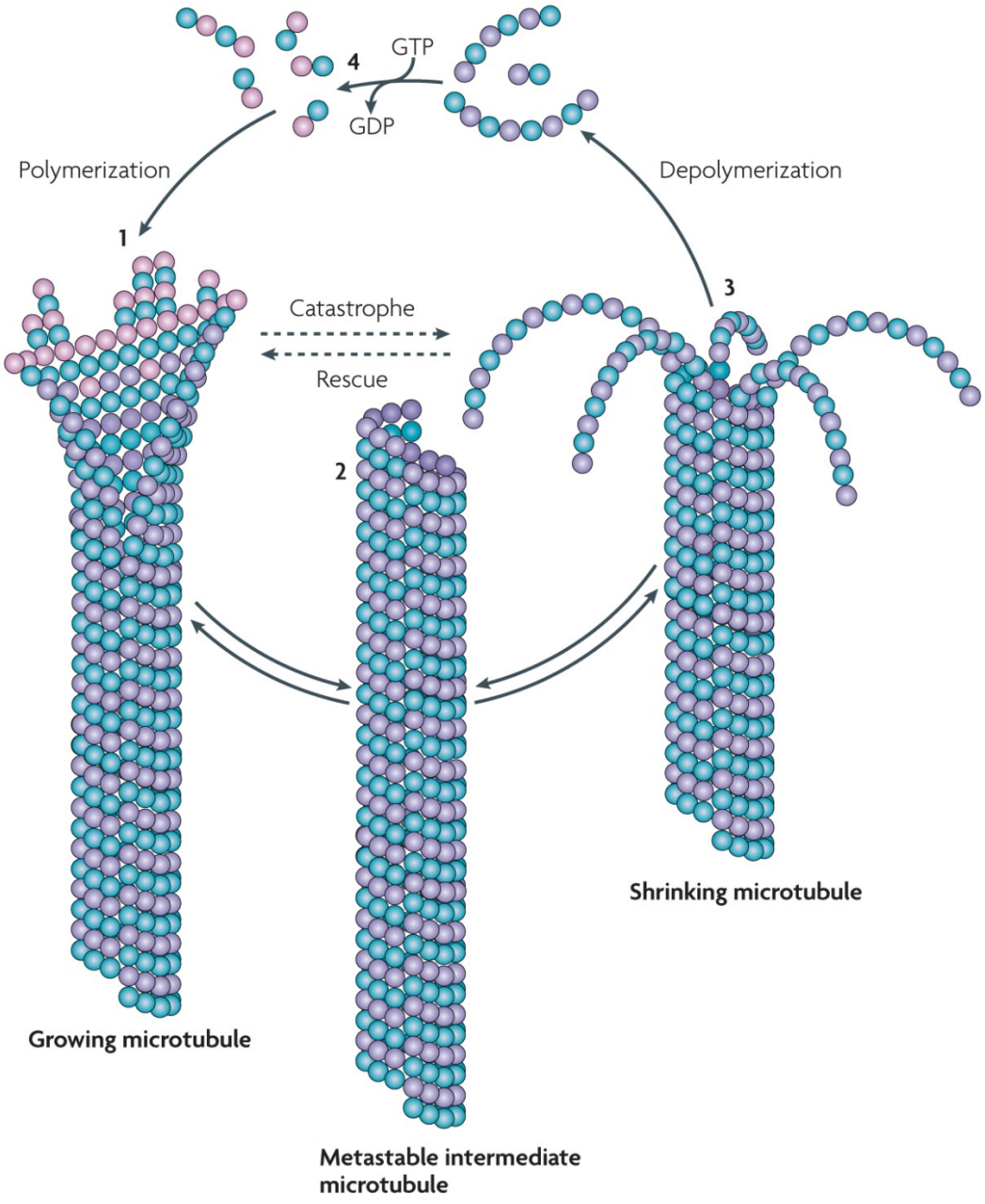

Figure 1-5: Model of microtubule dynamic instability. Microtubule (+) end dynamics are regulated by the presence of either GTP or GDP at the terminal β-tubulin subunit. When in the GTP-bound state, the microtubule continues to polymerize steadily. When in the GDP-bound state, the microtubule undergoes rapid depolymerization. The switch from polymerization to depolymerization is

known as catastrophe whereas the reverse is known as rescue. Rescue occurs via the addition of a GTP-bound heterodimer to the depolymerizing (+) end, which can be accomplished by microtubule interacting proteins. Adapted from Akhmanova and Steinmetz, 2008.

Chapter Two

Analysis of Differences between Dystrophin and Utrophin

Joseph Belanto performed all experiments except for the following: The data presented in Figures 2-5 and 2-6 were generated by Michael Eckhoff, Tara Mader, and Dr. Dawn Lowe. Dr. Kay E. Davies provided Fiona mice and Dr. Jeffrey S. Chamberlain provided Dys-TG-*mdx* and mini-Dys-TG-*mdx* mice.

Summary

Dystrophin and utrophin are highly homologous proteins capable of linking subsarcolemmal γ-actin filaments in the cytoplasm with laminin in the extracellular matrix via the heavily glycosylated transmembrane β-dystroglycan. Despite exhibiting several overlapping functions, endogenous dystrophin and utrophin occupy different subcellular locations within muscle cells: dystrophin resides primarily at costameres whereas utrophin localizes to the neuromuscular and myotendinous junctions. In DMD patients who lack dystrophin, utrophin protein is upregulated and can be found in place of dystrophin at costameres. Unfortunately, this utrophin upregulation is insufficient to fully compensate for the absence of dystrophin. However, transgenic overexpression of utrophin has proven effective in ameliorating dystrophin-deficiency in mice and is therefore being pursued as a potential therapy to treat DMD. Here, we rigorously analyzed different mouse models to determine which, if any, phenotypes of the dystrophin-deficient *mdx* mouse remain in the presence of transgenically overexpressed utrophin. We find that utrophin cannot compensate for dystrophin in regards to subsarcolemmal microtubule lattice organization, recovery of activity after mild exercise, or loss of torque production after eccentric contraction. Therefore, we conclude that while utrophin-based therapies for DMD will provide great benefit, they will not ameliorate all DMD patient phenotypes.

Introduction

Duchenne muscular dystrophy (DMD) is a lethal X-linked disease found in approximately one of every 5000 live male births (Mendell et al., 2012). DMD is caused by loss of function mutations in the *DMD* gene which encodes the protein dystrophin (Hoffman et al., 1987). Dystrophin binds cytoplasmic γ-actin filaments at its N-terminus and second third of the central rod domain to link them to β-dystroglycan at its C-terminus. Through this interaction dystrophin is hypothesized to reduce normally incurred muscle damage via stabilization of the sarcolemma during muscle contraction. Full-body muscle weakness (Carlson and Makiejus, 1990) is a hallmark of dystrophin deficiency and usually manifests in the first decade of life as the initial missed developmental milestone.

The *mdx* mouse faithfully models some of the phenotypes associated with DMD and is the most widely used mouse model to study DMD (Bulfield et al., 1984). Similar to DMD patients, the *mdx* mouse displays widespread muscle weakness, undergoes repetitive rounds of muscle degeneration and regeneration (Carlson and Makiejus, 1990; Cox et al., 1993; Warner et al., 2002), and is highly susceptible to eccentric contraction induced injury, losing almost all force generating capacity after multiple contractions (Moens et al., 1993; Petrof et al., 1993). However, the *mdx* mouse has a normal lifespan and has an overall milder phenotype than DMD patients, indicating that the mouse may have better compensatory mechanisms than humans for dealing with dystrophin deficiency.

We and others (Ralston et al., 1999; Percival et al., 2007; Ayalon et al., 2008; Prins et al., 2009) have shown that skeletal muscle microtubules are

organized into a rectilinear lattice beneath the sarcolemma and that loss of dystrophin in the *mdx* mouse results in a loss of this microtubule organization. While the *mdx* mouse expresses increased levels of endogenous utrophin (Rybakova et al., 2002) the skeletal muscle microtubule lattice remains disorganized (Percival et al., 2007; Ayalon et al., 2008; Prins et al., 2009) suggesting that the microtubule binding function of dystrophin may not be conserved in utrophin. On the other hand, the increased endogenous utrophin expression in the *mdx* mouse is insufficient to mechanically anchor costameric actin filaments to the sarcolemma while transgenic utrophin overexpression restores coupling (Rybakova et al., 2002), indicating that utrophin protein levels in *mdx* mice may simply be too low to properly organize microtubules. This raises the question as to whether dystrophin and utrophin are completely interchangeable in regards to this and other molecular and physiological functions.

One established phenotype of the Fiona-*mdx* mouse, a mouse model which transgenically overexpresses full-length utrophin on the dystrophin-deficient *mdx* mouse background, is that neuronal nitric oxide synthase (nNOS) does not localize to the sarcolemma whereas localization occurs in the presence of dystrophin (Lai et al., 2009; Li et al., 2010), indicating that utrophin cannot fully compensate for the lack of dystrophin. While the Fiona-*mdx* mouse has been analyzed for various dystrophic phenotypes, a rigorous evaluation of other possible phenotypes is lacking. Here, we have performed experiments to further elucidate phenotypes of the *mdx* mouse that specifically associated with the loss

of nNOS localization and/or microtubule disorganization. To do this, we have utilized the Dys-TG-*mdx* mouse (nNOS localization, microtubule organization), the mini-Dys-TG-*mdx* mouse (no nNOS localization, microtubule organization), and the Fiona-*mdx* mouse (no nNOS localization, no microtubule organization). We find that loss of nNOS localization regardless of microtubule organization contributes to loss of activity after mild exercise whereas loss of microtubule organization regardless of nNOS localization contributes to torque loss following eccentric contraction in anterior muscles.

Results

In this study, we utilized three previously developed transgenic mouse models crossed onto the dystrophin-deficient *mdx* mouse background. The first transgenically overexpresses full-length utrophin (Fiona-*mdx*), the second transgenically overexpresses nearly full-length dystrophin (Dys-TG-*mdx*), and the last transgenically overexpresses a miniaturized dystrophin (mini-Dys-TG-*mdx*) lacking spectrin-like repeats 4 to 19 (Tinsley et al., 1998; Crawford et al., 2000; Li et al., 2006). Western blotting of quadriceps tissue lysates verified that the transgenic proteins were being overexpressed above WT levels in all transgenic lines (Figure 2-1). To begin to address which molecular and physiological phenotypes of the *mdx* mouse are not rescued be transgenic overexpression of utrophin or dystrophin, we first analyzed microtubule lattice organization in different mouse models (Figure 2-2). Unlike WT mice, which show subsarcolemmal microtubule lattice organization (Figure 2-2A), we find that the microtubule lattice in the Fiona-*mdx* mouse remained disorganized with morphology similar to that seen in the *mdx* mouse (Figure 2-2B, C). The Dys-TG-*mdx* and mini-Dys-TG-mdx mice showed rescued microtubule lattice organization qualitatively comparable to that of WT mice (Figure 2-2D, E). These data indicate that transgenic utrophin overexpression in skeletal muscle is insufficient to organize the microtubule cytoskeleton in the *mdx* mouse. Interestingly, microtubules remained organized in both WT and *mdx* mice in the interior of muscle fibers (Figure 2-3), a cellular location in which dystrophin is absent,

indicating that interior organization may be mediated by a different protein or set of proteins present in both WT and *mdx* mice.

To elucidate other phenotypes of the Fiona-*mdx* mouse potentially related to the loss of nNOS localization or microtubule lattice organization, we first evaluated physical activity after mild exercise to assess activity-induced inactivity. The Campbell group has established that the *mdx* mouse shows greatly reduced physical activity after mild exercise (Kobayashi et al., 2008), but the effect of transgenic overexpression of utrophin or dystrophin had yet to be evaluated. Similar to previously reported data (Kobayashi et al., 2008), we find that WT mice were approximately 50% less active following mild treadmill exercise whereas *mdx* mice were 95% less active (Figure 2-4). The Dys-TG-*mdx* mouse showed activity comparable to that of WT mice after mild exercise (not statistically different from each other). However, the Fiona-*mdx* and mini-Dys-TG-*mdx* mice both showed intermediate loss of activity, each having approximately 25% of initial activity (not statistically different from each other). WT mice and Dys-TG-*mdx* mice were both statistically different from Fiona-*mdx* and mini-Dys-TG-*mdx* mice and all four lines were statistically different from *mdx* mice. These data indicated that while transgenic overexpression of utrophin in *mdx* mice significantly improves activity after mild exercise, it does not restore activity to levels measured after transgenic dystrophin overexpression. Interestingly, the mini-Dys-TG-*mdx* mouse, which shows rescued microtubule morphology (Figure 2-2E), but lacks the nNOS binding domain (Li et al., 2010) mirrors the phenotype of the Fiona-*mdx* mouse, suggesting that loss of nNOS localization contributes to

mild exercise-induced inactivity whereas microtubule lattice organization does not.

Next, we narrowed our focus down from the phenotypic characteristics of the entire animal to examining specific muscle groups. We began by measuring the force production in isolated extensor digitorum longus muscles after repeated eccentric contractions. Eccentric contractions occur when a muscle is being forcibly lengthened while it is contracting. In this assay, *mdx* mice begin to show statistically significant loss of force production after a single eccentric contraction (Figure 2-5), which plateaus to 15% of WT force production after five eccentric contractions. Comparison of Fiona-*mdx* and Dys-TG-*mdx* mice revealed no statistically significant force loss, even after ten consecutive eccentric contractions. These data indicate that transgenic overexpression of utrophin can compensate for the loss of dystrophin in regards to force production in isolated extensor digitorum longus muscles after repeated eccentric contractions.

Subsequently, we measured torque production *in vivo* in the anterior (extensor digitorum longus and tibialis anterior) and the posterior (soleus and gastrocnemius) muscle groups of live mice after subjecting muscles to repeated rounds of eccentric contraction. In these assays, *mdx* mice showed drastic loss of torque production as compared to WT mice (Figure 2-6) in both the anterior and posterior muscle groups. The Dys-TG-*mdx* mice showed no loss of torque production as compared to WT mice in either muscle group. Conversely, the Fiona-*mdx* mice showed intermediate loss of torque production in the anterior muscle group (Figure 2-6A) but normal torque production in the posterior muscle

group (Figure 2-6B). This intermediate loss of torque production mirrors the intermediate loss of activity we observed after mild exercise in the Fiona-*mdx* mice (Figure 2-4). However, mini-Dys-TG-*mdx* mice do not show this intermediate loss of torque production in the anterior muscle group, which is in contrast to the loss of exercise-induced inactivity seen for these mice (Figure 2-4). For the anterior muscle group, WT mice, Dys-TG-*mdx* mice, and mini-Dys-TG-*mdx* mice are statistically different from Fiona-*mdx* mice and all mice are statistically different from *mdx* mice. Interestingly, the mini-Dys-TG-*mdx* mouse, which shows rescued microtubule morphology (Figure 2-2E), but lacks the nNOS binding domain (Li et al., 2010) does not mirror the phenotype of the Fiona-*mdx* mouse, suggesting that microtubule disorganization rather than loss of nNOS localization contributes to loss of torque production in the anterior muscles.

One final phenotype of the *mdx* mouse that we thought was possibly linked to either the loss of nNOS localization or loss of microtubule organization is patterning of the neuromuscular junction (Lyons and Slater, 1991). A neuromuscular junction occurs at the location where a motor neuron innervates a muscle fiber. At this synapse, the sarcolemma is extensively folded, acetylcholine receptors are highly concentrated, and myonuclei tend to cluster. These myonuclei are specialized and upregulate the transcription of certain genes not highly expressed in other myonuclei, such as utrophin (Gramolini et al., 1997). In WT mice, the neuromuscular junction patterning appears much like a pretzel, folding in upon itself (Figure 2-7A). In contrast, the neuromuscular junction of the *mdx* mouse loses this patterning and instead appears like a cluster of grapes

(Figure 2-7B). The neuromuscular junction of the Fiona-*mdx* mouse was qualitatively similar to that of WT mice, as was the neuromuscular junction of the Dys-TG-*mdx* mouse (Figure 2-7C, D), indicating that transgenic overexpression of utrophin ameliorates the aberrant neuromuscular junction patterning seen in *mdx* mice.

Discussion

Many DMD therapies in development aim to upregulate endogenous utrophin as a surrogate for dystrophin. This approach has the theoretical advantage of bypassing any immune response that may develop against dystrophin, since a DMD patient's immune system may identify dystrophin as foreign (Wang et al., 2007; Mendell et al., 2010; Flanigan et al., 2013). Additionally, DMD patients already harbor an intact, functional utrophin gene, so there is no need for genetic manipulation, only transcriptional or translational upregulation. However, utrophin cannot bind nNOS (Li et al., 2010) or microtubules (Figure 2-2C) and thus may lack other previously overlooked functions of dystrophin. Therefore, we sought to identify previously unknown pathologies of DMD that cannot be compensated for by transgenic overexpression of utrophin.

The proper sarcolemmal localization of nNOS to the sarcolemma has been implicated in vasodilation to increase oxygen delivery to muscle during exercise. The lack of nNOS localization leads to decreased blood flow to the muscles and subsequently exercised-induced fatigue. Mice specifically lacking nNOS exhibit reduced cage activity after mild exercise, which is exacerbated in *mdx* mice (Kobayashi et al., 2008), presumably due to the additional lack of dystrophin. Here we show for the first time that transgenic overexpression of utrophin partially rescues this phenotype of the *mdx* mouse, but does restore activity to WT levels. Our data suggests that utrophin cannot fully substitute for dystrophin in maintaining activity after exercise most probably due to a lack of

nNOS localization at the sarcolemma. In support of this hypothesis, transgenic overexpression of mini dystrophin shows the same intermediate recovery of activity after mild exercise. This mouse also lacks sarcolemmal nNOS localization, but unlike the Fiona-*mdx* mouse, mini-Dys-TG-*mdx* mice show recovery in microtubule lattice organization (Figure 2-2). We conclude that exercise-induced inactivity is principally caused by loss of nNOS localization rather than by microtubule lattice disorganization.

Increased reactive oxygen species and aberrant calcium regulation have been proposed to stem from microtubule lattice derangement in the *mdx* mouse, providing the first evidence for a pathological microtubule-associated phenotype in DMD (Prosser et al., 2011; Khairallah et al., 2012). Here, we show that lack of microtubule organization also contributes to loss of torque production in anterior crural muscles. The Fiona-*mdx* mouse loses torque production after eccentric contractions *in vivo* whereas the mini-Dys-TG-*mdx* mouse retains WT levels of torque production. We conclude that contraction-induced torque loss of anterior crural muscles is associated with microtubule disorganization rather than nNOS mislocalization.

Since transgenic overexpression of utrophin fails to rescue nNOS localization and microtubule disorganization, and the mini-Dys-TG-*mdx* mouse restores microtubule lattice organization (Figure 2-2E) but does not restore nNOS localization to the sarcolemma (Li et al., 2010), we utilized these mouse lines to begin to distinguish between nNOS-associated and microtubule-associated phenotypes. We show, for the first time, that exercise-induced

inactivity following mild exercise is an nNOS-associated phenotype whereas loss of torque production in anterior crural muscles is a microtubule-associated phenotype. However, a caveat to these findings is that the field lacks a mouse model which restores nNOS localization but fails to rescue microtubule lattice disorganization. The appendix outlines the generation of a mouse model to address this issue.

Figures

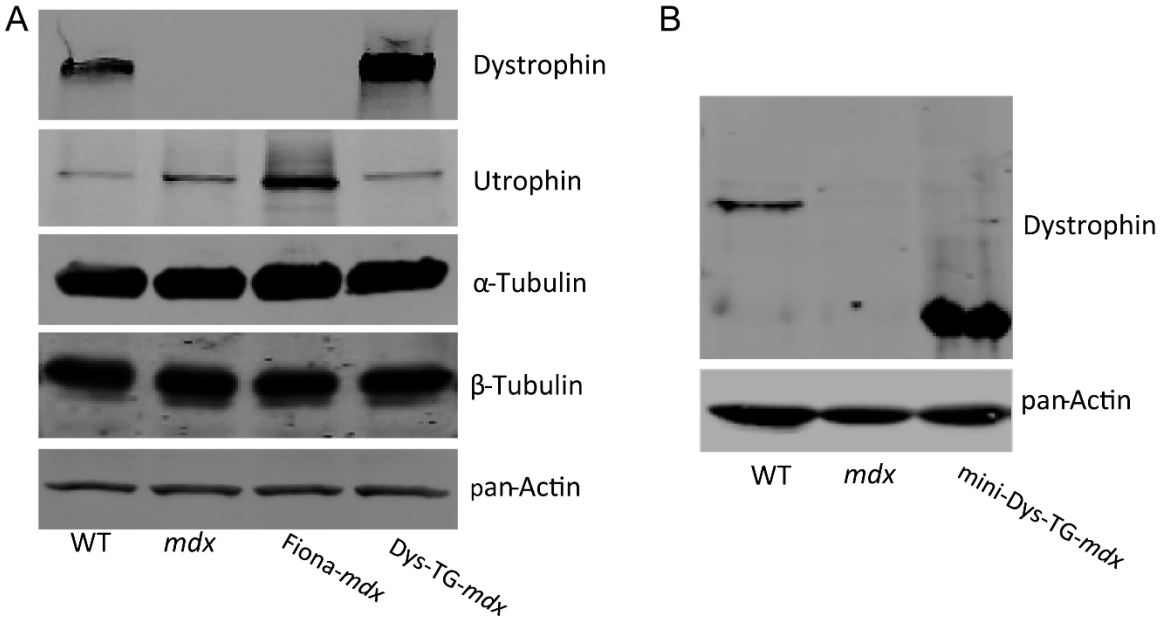

Figure 2-1: Western blotting for dystrophin and utrophin in transgenic mouse lines. (A) The *mdx* mouse expresses approximately 250% of WT levels of utrophin in the absence of dystrophin expression. The Fiona-*mdx* mouse expresses approximately 1000% of WT levels of utrophin and 400% of *mdx* levels of utrophin. The Dys-TG-*mdx* mouse express approximately 300% of WT levels of dystrophin. Tubulin and actin shown as loading controls. (B) The mini-Dys-TG-*mdx* mouse expresses approximately 600% of WT levels of dystrophin. Full-length dystrophin is 427kD whereas mini dystrophin is approximately 220kD. Actin shown as a loading control. All lanes are 60µg of total quadriceps lysate.

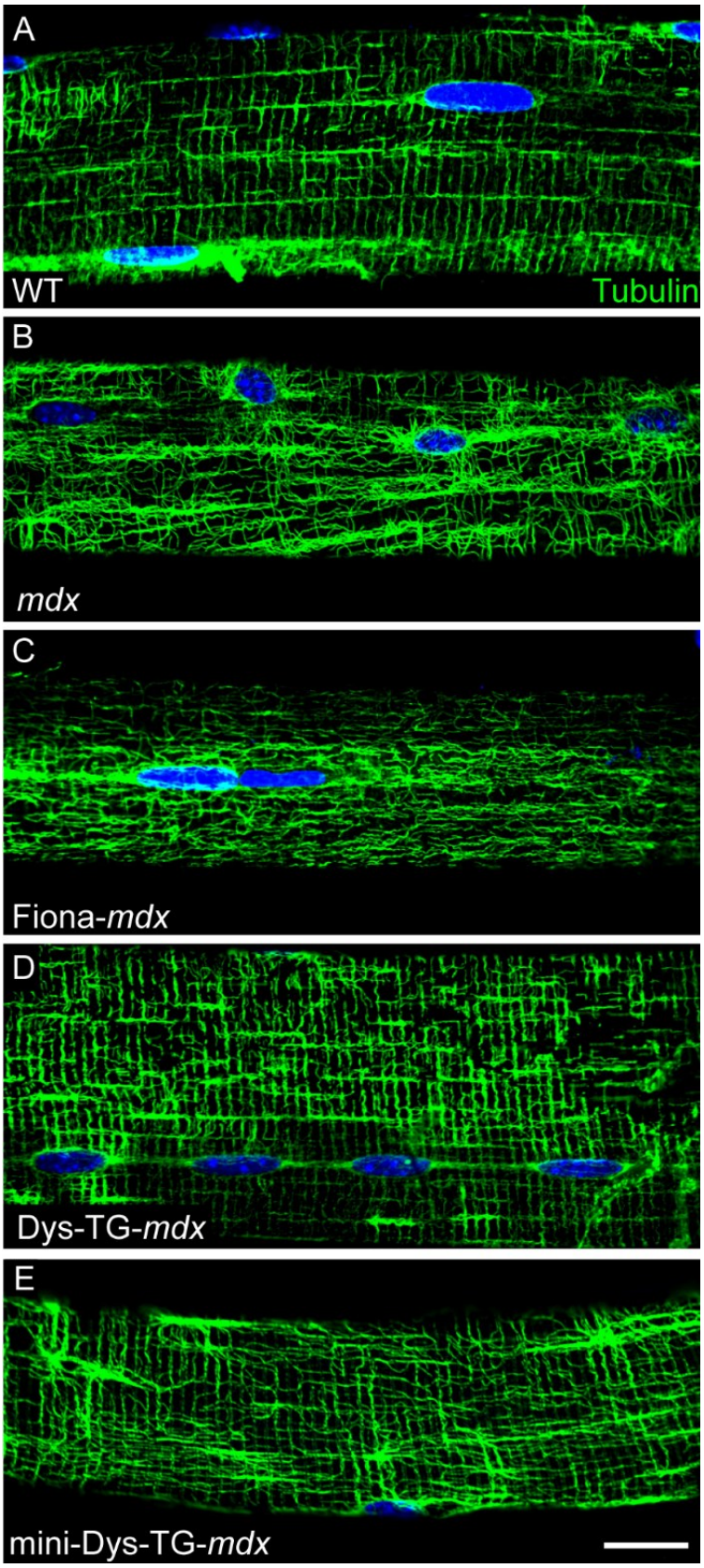
A
WT
Tubulin
B
mdx
C
Fiona-mdx
D
Dys-TG-mdx
E
mini-Dys-TG-mdx

Figure 2-2: Mouse extensor digitorum longus muscle sarcolemmal microtubule imaging. (A) When dystrophin is present (WT), microtubules are organized into a rectilinear lattice beneath the sarcolemma. (B) In the absence of dystrophin (*mdx*), the microtubule lattice becomes disordered. (C) Transgenic overexpression of utrophin in the absence of dystrophin (Fiona-*mdx*) does not rescue the disorganized microtubule lattice. (D) Transgenic expression of nearly full-length dystrophin in the absence of endogenous dystrophin (Dys-TG-*mdx*) results in an organized microtubule lattice. (E) Transgenic expression of mini dystrophin (mini-Dys-TG-*mdx*) also rescues the microtubule lattice. Single extensor digitorum longus muscle fibers were mechanically teased from profusion fixed mice and immunostained for tubulin and counterstained with DAPI to visualize nuclei. Bar, 20μm.

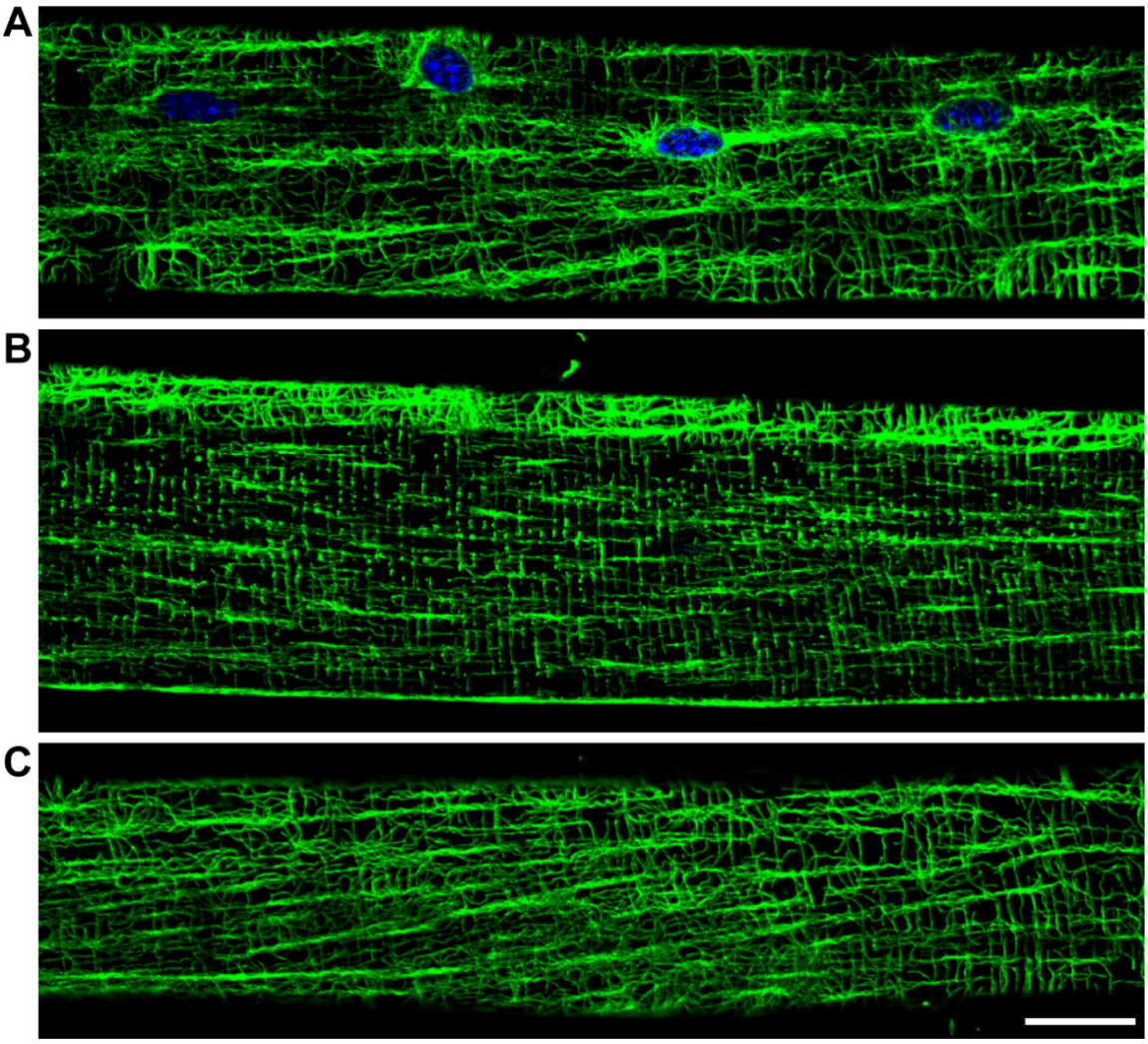

Figure 2-3: Mouse extensor digitorum longus muscle internal microtubule imaging. All images are of the same fiber. A and C are from opposite faces of the same fiber whereas B images the same fiber internally. (A) and (C) Subsarcolemmal microtubule lattice is disorganized in the *mdx* mouse. (B) Interior microtubule lattice is normal. A is the same image as from Figure 2-2B. Bar, 20μm.

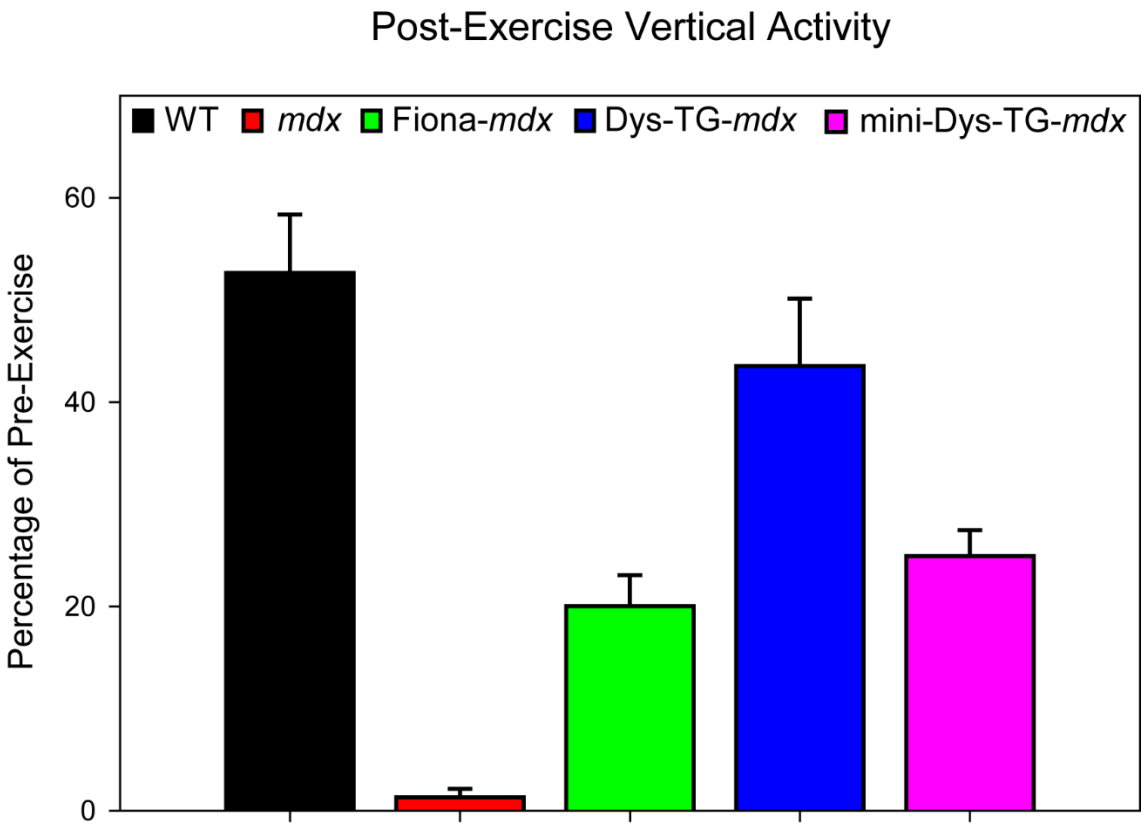

Figure 2-4: Activity following mild treadmill exercise. WT mice exhibited approximately 50% of initial activity after mild exercise whereas post-exercise activity in *mdx* mice dropped greater than 95% of their initial activity. Transgenic overexpression of dystrophin in mdx mice (Dys-TG-*mdx*) restored post-exercise activity levels similar to WT whereas transgenic overexpression of utrophin (Fiona-*mdx*) or mini dystrophin (mini-Dys-TG-*mdx*) yielded intermediate (~25%) restoration of activity. Post exercise activity levels in WT mice and Dys-TG-*mdx* mice were not statistically different from each other, but were statistically different from Fiona-*mdx* and mini-Dys-TG-*mdx* mice, which were not statistically different from each other, and all 4 lines were statistically different from *mdx* mice ($p<0.05$).

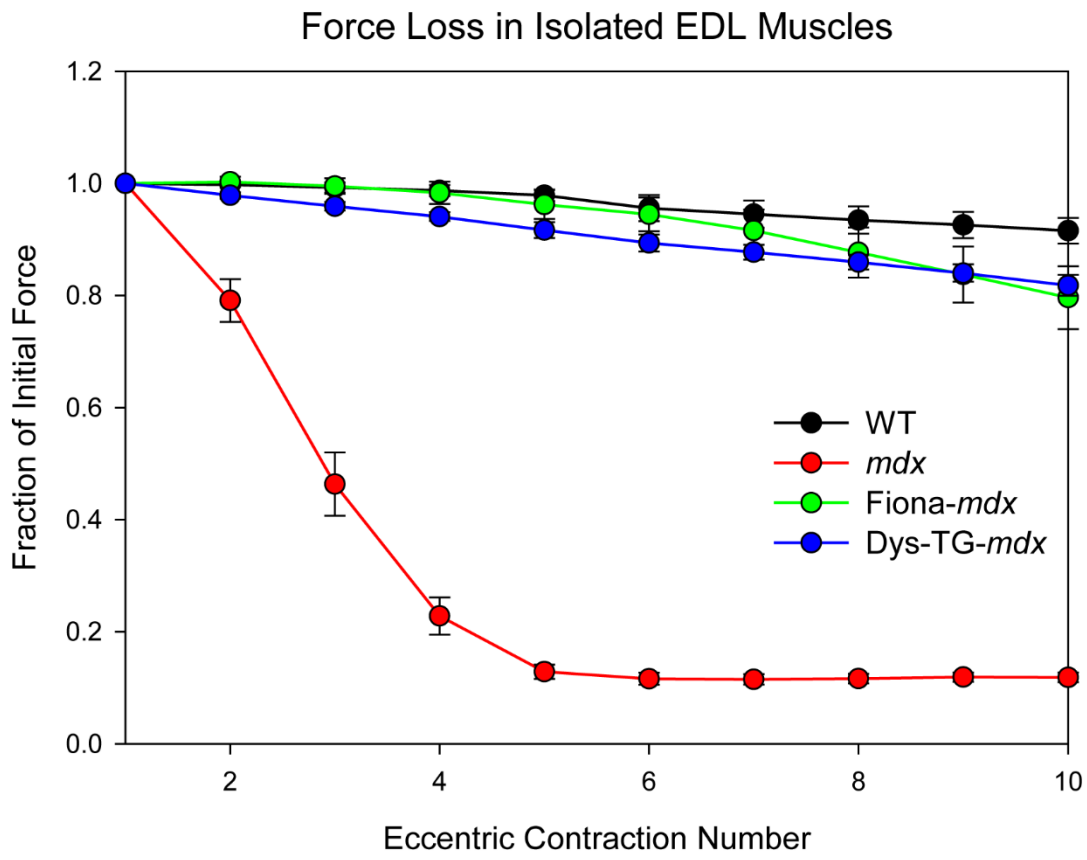

Figure 2-5: *Ex vivo* force loss in isolated EDL muscles. Statistically significant loss of force production ($p<0.05$) in *mdx* mice as compared to WT mice occurs after a single eccentric contraction. Examining Fiona-*mdx* and Dys-TG-*mdx* mice revealed no statistically significant force loss, even after ten consecutive eccentric contractions.

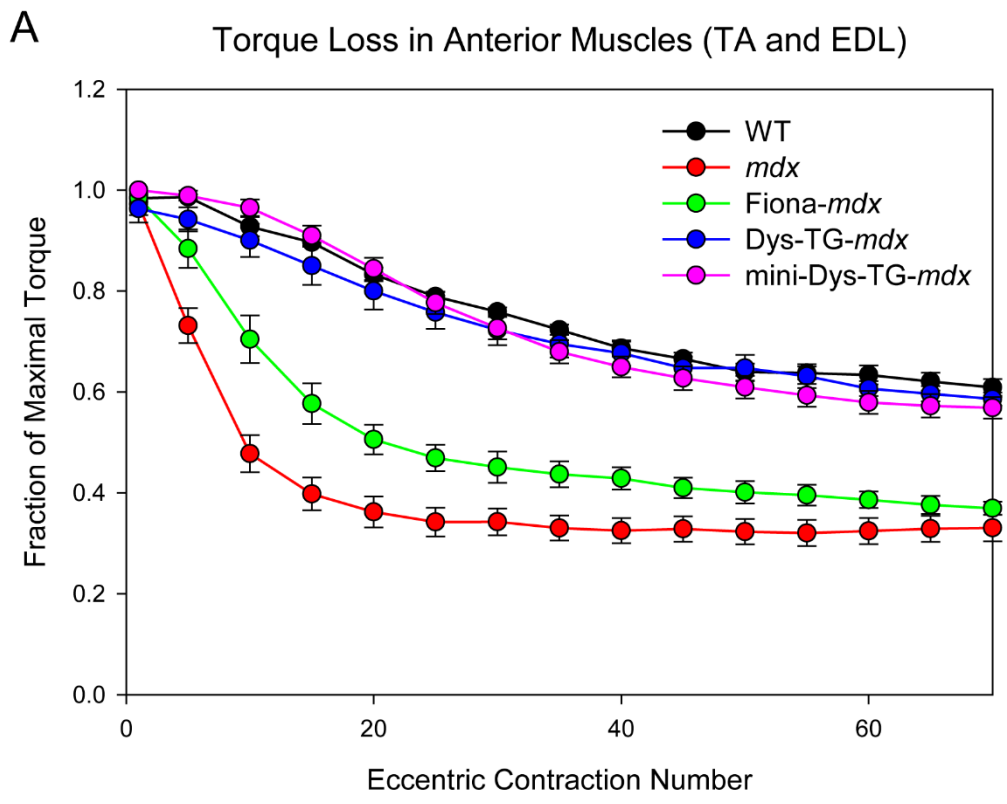
A
Torque Loss in Anterior Muscles (TA and EDL)
Fraction of Maximal Torque
Eccentric Contraction Number
WT
mdx
Fiona-mdx
Dys-TG-mdx
mini-Dys-TG-mdx
0.0
0.2
0.4
0.6
0.8
1.0
1.2
0
20
40
60

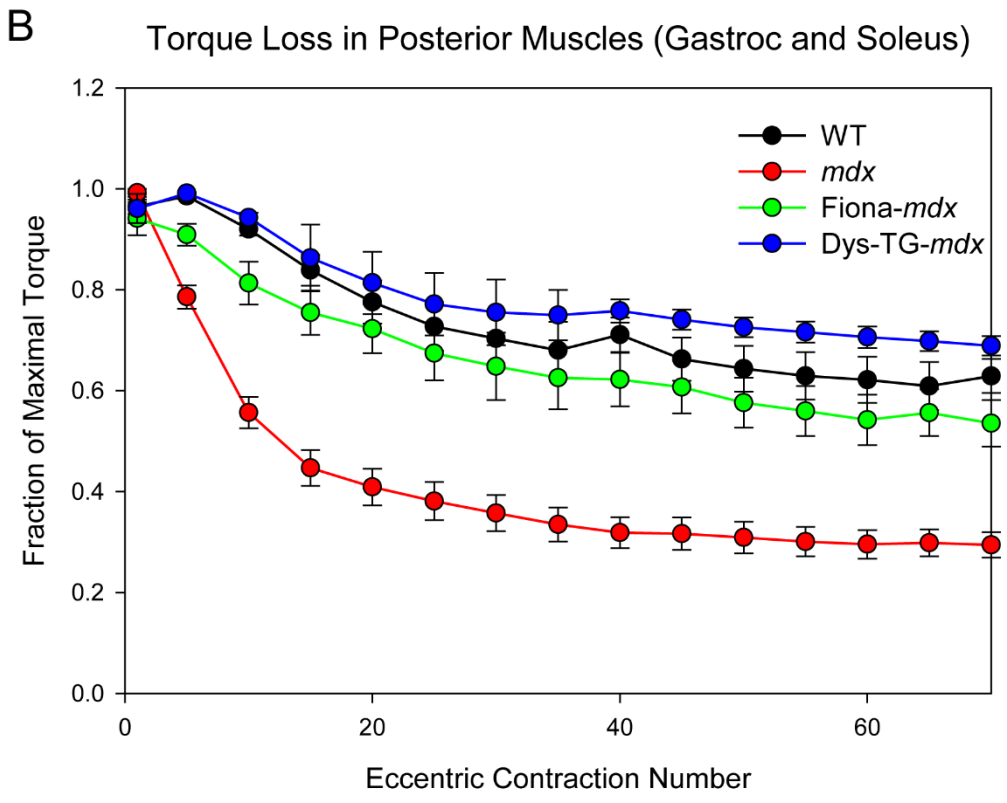
B
Torque Loss in Posterior Muscles (Gastroc and Soleus)
Fraction of Maximal Torque
Eccentric Contraction Number
WT
mdx
Fiona-mdx
Dys-TG-mdx
0.0
0.2
0.4
0.6
0.8
1.0
1.2
0
20
40
60

Figure 2-6: *In vivo* torque loss in anterior and posterior muscle groups. (A) As compared to WT mice, *mdx* mice showed drastic loss of torque production in the anterior muscle group. Additionally, Dys-TG-*mdx* and mini-Dys-TG-*mdx* mice showed no loss of torque production as compared to WT mice. Conversely, the Fiona-*mdx* mice showed intermediate loss of torque production in the anterior muscle group, comparable to intermediate loss of activity seen in Figure 2-4. WT, Dys-TG-*mdx* and Fiona-*mdx* mice (not statistically different from each other) are statistically different from *mdx* mice. $p<0.05$ for all statistically significant differences. (B) As compared to WT mice, *mdx* mice showed drastic loss of torque production in the posterior muscle group. Additionally, Fiona-*mdx* mice and Dys-TG-*mdx* mice showed no loss of torque production as compared to WT mice. WT, Dys-TG-*mdx* and mini-Dys-TG-*mdx* mice (not statistically different from each other) are statistically different from Fiona-*mdx* mice and all mice are statistically different from *mdx* mice. $p<0.05$ for all statistically significant differences.

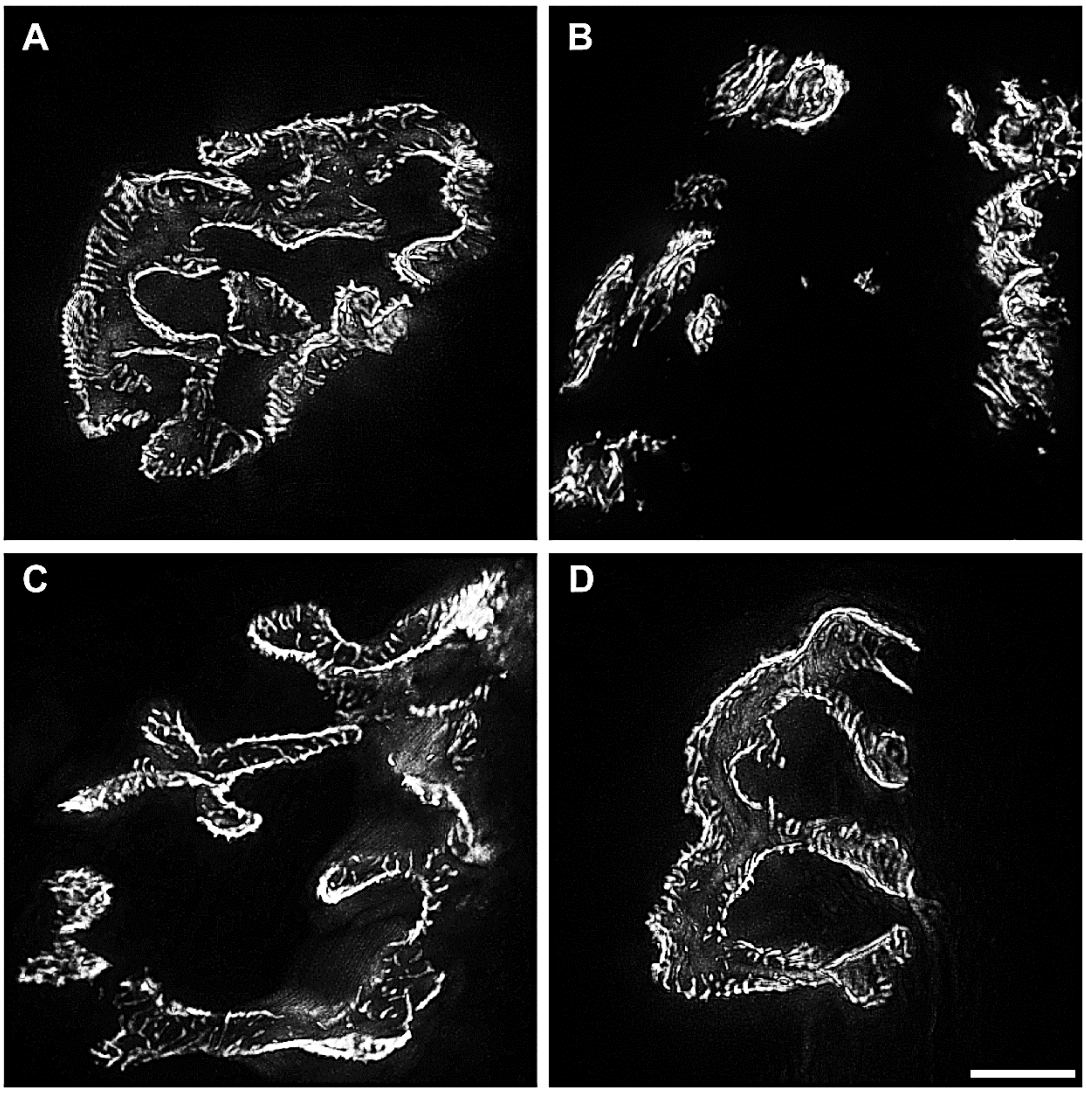

Figure 2-7: Mouse neuromuscular junction imaging. (A) Neuromuscular junction morphology in a WT mouse resembles a pretzel. (B) This morphology is lost in the *mdx* mouse and instead appear as a cluster of grapes. (C) The Fiona-*mdx* mouse shows rescued neuromuscular junction morphology. (D) The Dys-TG-*mdx* mouse shows rescued neuromuscular junction morphology. Bar, 5μm.

Chapter Three

Dystrophin Repeats 20-22 Act as a Context-Dependent Molecular Guidepost to Organize Microtubules

Joseph Belanto purified all proteins and performed all experiments except for the following: Katrina Rhett performed all differential scanning fluorimetry experiments.

Summary

Dystrophin links the cortical actin cytoskeleton of striated muscle to the extracellular matrix via the dystrophin-glycoprotein complex. Mutations in dystrophin that abolish or reduce its function/expression lead to Duchenne or Becker muscular dystrophy. Dystrophin also directly binds to microtubules, and its absence results in microtubule disorganization, which contributes to disease pathology. Here we show that the dystrophin homolog utrophin lacks microtubule binding activity *in vitro*. By analyzing a series of deletion and chimeric dystrophin constructs, we have mapped the microtubule binding domain to spectrin-like repeats 20-22, but find that binding activity is context-dependent. *In vitro* analysis revealed that dystrophin stalled microtubule polymerization, but had no effect on microtubule dynamics when measured in bulk solution. We conclude that dystrophin functions as a context-dependent molecular guidepost to organize the subsarcolemmal microtubule lattice in skeletal muscle.

Introduction

Dystrophin is a 427kD cytoplasmic protein predominantly expressed in striated muscle (Hoffman et al., 1987). Loss of function mutations in dystrophin lead to the disease Duchenne muscular dystrophy (DMD), an X-linked lethal disease with no cure (Worton and Thompson, 1988). The dystrophin protein interacts with cytosplasmic and membrane-spanning proteins such as filamentous γ-actin, intermediate filament proteins, neuronal nitric oxide synthase (nNOS), β-dystroglycan, α-dystrobrevin and α-syntrophin (Koenig et al., 1988; Koenig and Kunkel, 1990; Way et al., 1992; Bork and Sudol, 1994; Ponting et al., 1996; Rybakova and Ervasti, 1997). Our lab previously showed that in addition to the aforementioned molecular interactions, dystrophin directly interacts with microtubules (Prins et al., 2009), suggesting classification of dystrophin as a cytolinker.

Microtubules have not been as intensely studied in striated muscle as in other tissues. However, the available studies reveal that microtubules are essential in muscle for myotube formation, the process by which single muscle cells fuse to form elongated, multinucleated muscle fibers (Saitoh et al., 1988; Chang et al., 2002; Perez et al., 2002). Additionally, proper microtubule function is required for correct Golgi localization and function within muscle cells (Ralston et al., 1999, 2001). In WT skeletal muscle, microtubules are organized into a rectilinear lattice beneath the sarcolemma. However, in *mdx* muscle tissue the microtubule lattice becomes disorganized, the pathological consequences of which are mostly unknown. Recently, it was shown that the altered microtubule

network in *mdx* cardiac tissue contributes to increased reactive oxygen species and aberrant calcium regulation, suggesting that microtubule lattice derangement in the *mdx* mouse directly contributes to the molecular pathogenesis of DMD (Prosser et al., 2011; Khairallah et al., 2012).

The protein ankyrin-B simultaneously interacts with dystrophin, β2-spectrin, and dynactin-4, and is thought to deliver dystrophin to the sarcolemma via the microtubule cytoskeleton. Once at the sarcolemma, proper localization of dystrophin to the costamere requires ankyrin-G (Ayalon et al., 2008, 2011). Most recently, it was shown that proper localization of ankyrin-B to the sarcolemma relies on the scaffolding protein obscurin, underscoring the large interplay of proteins required for proper localization of dystrophin to costameres (Randazzo et al., 2013). Knockdown or knockout studies of ankyrin-B, ankyrin-G, β2-spectrin, dynactin-4, and obscurin have shown that each is required for proper costameric localization of dystrophin, and that lack of this localization leads to phenotypes similar to those seen in the dystrophin-deficient *mdx* mouse (Ayalon et al., 2008, 2011; Randazzo et al., 2013).

The minimal microtubule binding domain of dystrophin has not been biochemically established. Initial studies from our lab indicated that dystrophin repeat 24 and hinge 4 were necessary for microtubule binding; however, these assays were performed using whole muscle microtubule cosedimentation assays in which other proteins may facilitate indirect protein-protein interactions (Prins et al., 2009). Therefore, we set out to express and purify various dystrophin isoforms and deletion constructs to biochemically determine the minimal

domain(s) within dystrophin necessary for microtubule binding activity. We find dystrophin repeat 24 and hinge 4 do not directly participate in microtubule binding activity. Instead, repeats 20-22 of dystrophin are the minimal microtubule binding domain. Additionally, we show that this microtubule binding is context-specific insofar as it is dependent on flanking regions of dystrophin for proper function.

In addition to delineating the minimal microtubule binding domain in dystrophin, we show that in accordance with our previous mouse studies, recombinant utrophin cannot bind microtubules *in vitro*. Our results also demonstrate that dystrophin functions as a context-dependent molecular guidepost for microtubule lattice organization through a direct interaction of spectrin-like repeats 20-22 and microtubules, providing a molecular mechanism for subsarcolemmal microtubule lattice organization.

Results

To begin to elucidate the microtubule binding properties of dystrophin, we expressed and purified full-length recombinant mouse dystrophin and utrophin (Rybakova et al., 2002, 2006) for comparison of microtubule binding activity *in vitro* using a microtubule cosedimentation assay (Figure 3-1A). Dystrophin displayed specific, high affinity binding to microtubules (K_D=0.33μM) similar to previously published data for Dp260 (Prins et al., 2009) while utrophin showed no concentration-dependent, saturable binding (Figure 3-1B). Additionally, we analyzed both constructs via differential scanning fluorimetry (DSF) to determine whether they had similar thermal stabilities (Niesen et al., 2007). Both dystrophin and utrophin displayed a single, cooperative DSF transition, indicating well-folded proteins with similar melting temperatures (Figure 3-1C and Table 3-1). These data indicate that dystrophin binds microtubules with high affinity in a concentration-dependent, saturable manner and that utrophin does not exhibit any microtubule binding activity *in vitro*.

To identify the regions of dystrophin necessary for interaction with microtubules, we measured microtubule binding activity in an array of naturally occurring dystrophin isoforms, truncation, and internal deletion constructs (Figure 3-2). Only full-length dystrophin (K_D=0.33μM), Dp260 (K_D=0.26μM), and mini Dys (K_D=0.38μM) showed specific microtubule binding (Figure 3-3). While the three microtubule binding constructs share a large region of dystrophin spanning from hinge 3 to the C-terminus, other constructs containing this same region, such as Dys 18-CT, failed to bind microtubules. Therefore, we used DSF to analyze all

constructs to determine if they had similar melting temperatures. Most constructs gave similar results as full-length dystrophin (Figure 3-4 and Table 3-1). However, Dp140, Dp116, Dys 15-24, and Dys 18-CT displayed DSF denaturation curves with two distinct melting temperatures (Figure 3-4 and Table 3-1). We hypothesized that Dp140, Dp116, Dys 15-24, and Dys 18-CT adopted conformations that prevent their binding to microtubules and eliminated them from our delineation of the microtubule binding domain. Based on data for the remaining constructs, we hypothesize that the microtubule binding domain of dystrophin resides within repeats 20-24.

To test the roles of dystrophin repeats 20-24 in microtubule binding activity and to determine their sufficiency in conferring microtubule binding activity, we substituted dystrophin repeats 20-24 for the homologous repeats of utrophin, repeats 18-22 (Figure 3-5). Using the *in vitro* microtubule cosedimentation assay, Dys R20-24$_{Utr}$ displayed no specific microtubule binding activity, indicating that a region present within repeats 20-24 was necessary for microtubule binding activity. However, Utr R18-22$_{Dys}$, in which utrophin repeats 18-22 were exchanged for dystrophin repeats 20-24, displayed no specific microtubule binding activity, indicating that dystrophin repeats 20-24 were not sufficient for microtubule binding activity. Together these data indicated that a region within dystrophin repeats 20-24 was necessary but not sufficient for microtubule binding activity.

To define the minimal microtubule binding domain within dystrophin repeats 20-24, we constructed multiple Dp260 deletion constructs in which single

dystrophin repeats were deleted (Figure 3-6A) and hybrid constructs in which varying numbers of homologous utrophin repeats were substituted into Dp260 (Figure 3-7A). Dp260 was chosen as a template rather than full-length dystrophin due to its smaller size, ease of cloning, higher protein expression, and similar microtubule binding characteristics to those of full-length dystrophin. All constructs tested were analyzed by DSF and shown to have melting temperatures similar to those of Dp260 (Figures 3-6B and 3-7B and Table 3-1). Individual deletion of each repeat within dystrophin repeats 20-24 did not appreciably affect the microtubule binding activity of Dp260 (Figure 3-6A and Table 3-1), indicating that no single repeat acts as the microtubule binding domain. Additionally, the exchange of dystrophin repeats 23 or 24 (Dp260 R24$_{Utr}$ and Dp260 R23-24$_{Utr}$) did not affect microtubule binding activity. The substitution of dystrophin repeat 20 (Dp260 R20$_{Utr}$) resulted in a modest decrease in microtubule binding affinity, similar to that of the substitution of repeat 22 (Dp260 R22-24$_{Utr}$). However, the substitution of two or all repeats within the region of dystrophin repeats 20-22 (Dp260 R20-21$_{Utr}$, Dp260 R20-22$_{Utr}$, Dp260 R20-23$_{Utr}$, Dp260 R21-24$_{Utr}$, and Dp260 R20-24$_{Utr}$) resulted in complete loss of specific microtubule binding activity (Figure 3-7A and Table 3-1). These data indicate that dystrophin repeats 20-22 are the most important for microtubule binding activity.

Finally, constructs encoding only dystrophin repeats 20-22 or 20-24 failed to show any microtubule binding activity (Figure 3-8A and Figure 3-9). Interestingly, although both constructs displayed a single thermal transition when analyzed by DSF, we noticed a marked shift to higher denaturation temperatures

for both constructs (Figure 3-8B and Table 3-1). To more clearly illustrate differences in thermal stabilities, the data shown in Figure 3-10 are derivative plots of the data collected during a DSF experiment. When viewed in this manner, each peak of the curve more clearly defines the melting temperature(s) for the protein. Dys 20-22 and Dys 20-24 displayed a single melting temperature higher than any of the constructs shown in Figure 3-4 (Table 3-1), suggesting that the isolated repeats adopted a more thermally stable but microtubule non-binding conformation. Interestingly, Utr R18-22$_{Dys}$, which failed to bind microtubules even though it contains the microtubule binding domain of dystrophin, also exhibited a similar second DSF peak at the higher temperature suggesting that dystrophin repeats 20-24 adopt the same microtubule non-binding conformation as they do in isolation when in the context of utrophin (Figure 3-10B and Table 3-1). This provides evidence as to why Utr R18-22$_{Dys}$ does not bind microtubules. By comparison, dystrophin lacked this second DSF peak and exhibited a single, broad melting temperature indicative of proper microtubule binding domain conformation. In summary, our data suggest that dystrophin repeats 20-22 are necessary but not sufficient for microtubule binding activity due to context-dependent folding of this region that is influenced by more distal sequences in dystrophin.

Known microtubule binding proteins display a wide range of functions, including affecting tubulin polymerization dynamics, affecting microtubule depolymerization dynamics, bundling microtubules, and localizing microtubules to a specific location within the cell. To better understand the cellular role of

dystrophin binding to microtubules, we performed experiments to address the possibility that dystrophin plays a part in one or more of these functions.

To determine if dystrophin affected tubulin polymerization, we performed tubulin polymerization assays in the presence or absence of dystrophin, utrophin, tau, and excess calcium (Figure 3-11A). Tau is a known enhancer of tubulin polymerization (Cleveland et al., 1977) whereas high calcium concentrations are known to decrease the rate of tubulin polymerization (Weisenberg, 1972; O'Brien et al., 1997). As expected, an increase in tubulin polymerization rate was seen in the presence of tau (5.64mOD/min) whereas excess calcium inhibited polymerization (0.03mOD/min). Whether or not dystrophin was present, tubulin showed no measurable difference in its polymerization rate (2.42mOD/min and 2.46mOD/min for tubulin and tubulin plus dystrophin, respectively). The same held true when utrophin was present (2.38mOD/min). These data suggested that dystrophin had no effect on tubulin polymerization dynamics.

To test whether dystrophin affected microtubule depolymerization, tubulin was first polymerized into microtubules prior to switching the temperature to 4°C, which induces microtubule depolymerization. Over the course of 30 minutes, the rate of tubulin depolymerization (-8.75%/min) was no different than when dystrophin or utrophin was present (-8.01%/min and -6.92%/min, respectively) (Figure 3-11B). Tau partially reduced the rate of microtubule depolymerization (-2.62%/min) whereas excess calcium neither decreased nor increased the rate of microtubule depolymerization (-8.75%/min). These data suggested that dystrophin had no effect on microtubule depolymerization dynamics.

To test whether or not dystrophin bundled microtubules, we incubated both red and green fluorescently labeled microtubules alone, with dystrophin, with utrophin, or with tau, a known microtubule bundling protein (Lewis et al., 1989). A positive bundling event was detected as yellow fluorescence, indicating the close apposition of red and green microtubules. While tau induced microtubule bundling (Figure 3-11C), neither dystrophin nor utrophin showed any induction of microtubule bundling. In addition to events in which tau bundled two individual microtubules (upper panel, arrows), there were also many instances in which large numbers of microtubules were bundled into large clusters (lower panel), which was not seen under any other conditions assayed. Together these data suggested that dystrophin had no microtubule bundling activity.

We and others have shown that subsarcolemmal microtubules are organized into a rectilinear lattice in the presence of dystrophin (Figure 2-2A, D, E), indicating that dystrophin plays a role in microtubule localization/organization. To determine how this localization occurred at the single microtubule level, we coupled either dystrophin or utrophin to fluorescent microparticles and imaged the dystrophin/microtubule or utrophin/microtubule interaction as free fluorescent tubulin was allowed to polymerize off immobile seeds (Hendricks et al., 2012). Kymographs of the data indicated that as a microtubule interacted with a dystrophin-coated microparticle, the microtubule paused as it interacted with dystrophin before depolymerizing (Figure 3-12A, C, E, G). In contrast, when a microtubule encountered a utrophin-coated microparticle, the microtubule immediately depolymerized (Figure 3-12B, D, F, G). We hypothesize that

dystrophin localized microtubules by acting as a guidepost to anchor microtubules to a specific location when directly encountering them, but not affecting their overall dynamics when in close proximity. In a muscle cell, this tethering would occur at the costamere where dystrophin localizes.

Discussion

Microtubules are essential in all eukaryotic cells for mitosis, cell growth, and cell motility (Kirschner and Mitchison, 1986). In this study, we sought to further understand the properties of the dystrophin/microtubule interaction. We show for the first time that the dystrophin homolog utrophin exhibits no microtubule binding activity *in vitro* and that transgenic overexpression of utrophin on the *mdx* background fails to rescue microtubule lattice disorganization *in vivo*. It has already been shown that transgenic utrophin overexpression fails to localize nNOS to the sarcolemma (Li et al., 2010), providing the first evidence of a major functional difference between dystrophin and utrophin. Here, we have elucidated a second functional difference in regards to microtubule interaction, reinforcing the idea that while dystrophin and utrophin share many functions, they are not completely functionally interchangeable. Understanding the differences between these two proteins can better inform future therapeutic avenues of research, such as the use of miniaturized dystrophin constructs, by elucidating the domains within dystrophin necessary for full functionality.

Our finding that dystrophin repeats 20-22 confer microtubule binding to full-length dystrophin, Dp260, and mini Dys but not to other dystrophin proteins containing these repeats, such as Dp140, Dys 15-24, and Dys 18-CT, or to utrophin when substituted for the homologous repeats, further adds to the evidence that dystrophin's protein/protein interactions can be context-specific. We conclude that the presence of repeats 20-22 on their own or within the

context of full-length utrophin is not enough to recapitulate the microtubule binding of full-length dystrophin.

Dystrophin repeats 20-22 have been previously reported to form a thermally stable, cooperative interaction (Mirza et al., 2010), supporting our finding that these repeats have a higher thermal denaturation temperature in isolation than the other portions of dystrophin or than that of full-length dystrophin. This work also cited repeats 16 and 17, the dystrophin repeats initially shown to localize nNOS, as another highly stable, cooperative interaction. The documented thermal cooperation of dystrophin repeats 20-22 also supports the idea that they work in concert to interact with microtubules, much as the thermally stable repeats 16 and 17 function together to localize nNOS to the sarcolemma. Additionally, our lab has provided evidence that while portions of dystrophin may display different thermodynamic characteristics when in isolation, full-length dystrophin displays its own thermodynamic characteristic instead of displaying those of each portion (Henderson et al., 2011). This indicates that the rod domain repeats impact one another and that when in isolation behave in a manner that may differ from their behavior when in the context of full-length protein. Due to size limitations, miniaturized gene therapy constructs are being researched for treating DMD. Our data suggest that deletion of one dystrophin domain may have consequences for the proper function of more distal domains.

We also studied the effect of dystrophin on microtubule dynamics for the first time. We observed that dystrophin does not affect tubulin polymerization, microtubule depolymerization, or bundle microtubules. However, we did observe

a tethering effect when a single dynamic microtubule interacted with a stationary dystrophin molecule, providing a basis for the role of dystrophin in microtubule localization. To the best of our ability, we attempted to model the *in vivo* interaction of microtubules with dystrophin in an *in vitro* system in an attempt to understand how dystrophin localizes microtubules within striated muscle. To this end, coupling dystrophin to an immobile fluorescent microparticle was our way of recreating the normally stationary location of dystrophin at the costamere. Then, permitting tubulin to polymerize and analyzing the dystrophin/microtubule interaction when they came into proximity allowed us to visualize what we believe occurs *in vivo*. Based on the data presented, we hypothesize that dystrophin acts a molecular guidepost, localizing microtubules to the costamere where dystrophin resides.

In summary, we have shown that repeats 20-22 of dystrophin directly interact with microtubules in a context-dependent manner resulting in microtubule lattice organization beneath the sarcolemma. Due to dystrophin acting as a molecular guidepost, microtubules become anchored to the costamere in muscle cells with microtubule lattice organization being the direct result of this. We have also shown that utrophin cannot interact with microtubules, illustrating a second functional difference between dystrophin and utrophin.

Figures

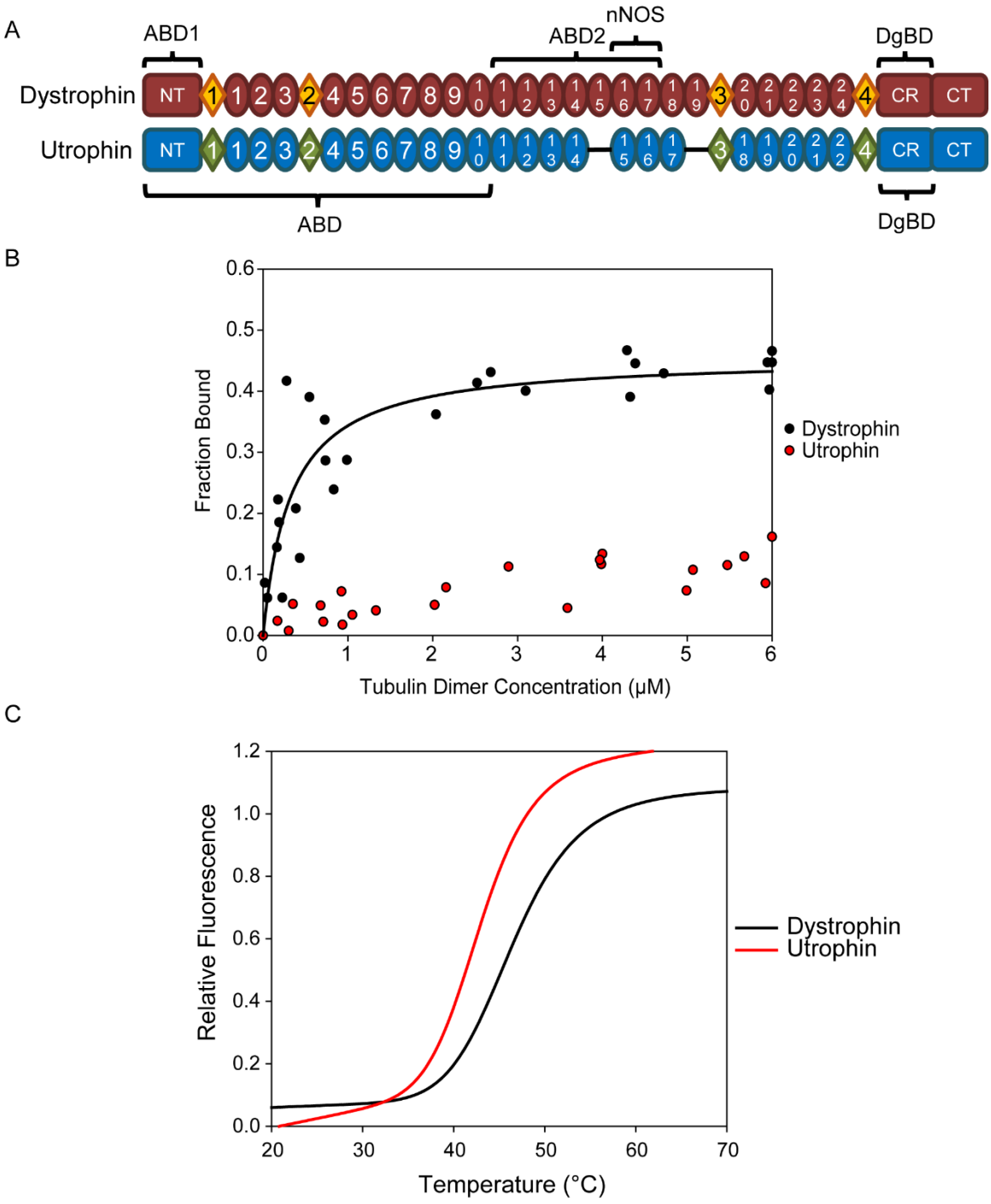

Figure 3-1: Domain structure, microtubule binding properties, and differential scanning fluorimetry of dystrophin and utrophin. (A) Schematic

representation of dystrophin and utrophin proteins. Ovals represent spectrin-like repeats, diamonds represent hinge regions. Homologous repeats are aligned. Dystrophin repeats 15 and 19 do not have homologous repeats in utrophin. ABD, actin binding domain; nNOS, nNOS binding domain; DgBD, β-dystroglycan binding domain; NT, N-terminus; CT, C-terminus; CR, cysteine rich domain (B) Microtubule binding curve of dystrophin and utrophin. Dystrophin binds microtubules with high affinity (K_D=0.33μM) whereas utrophin displays no specific microtubule binding. (C) DSF analyses of dystrophin and utrophin show that both unfold in a single transition at similar temperatures.

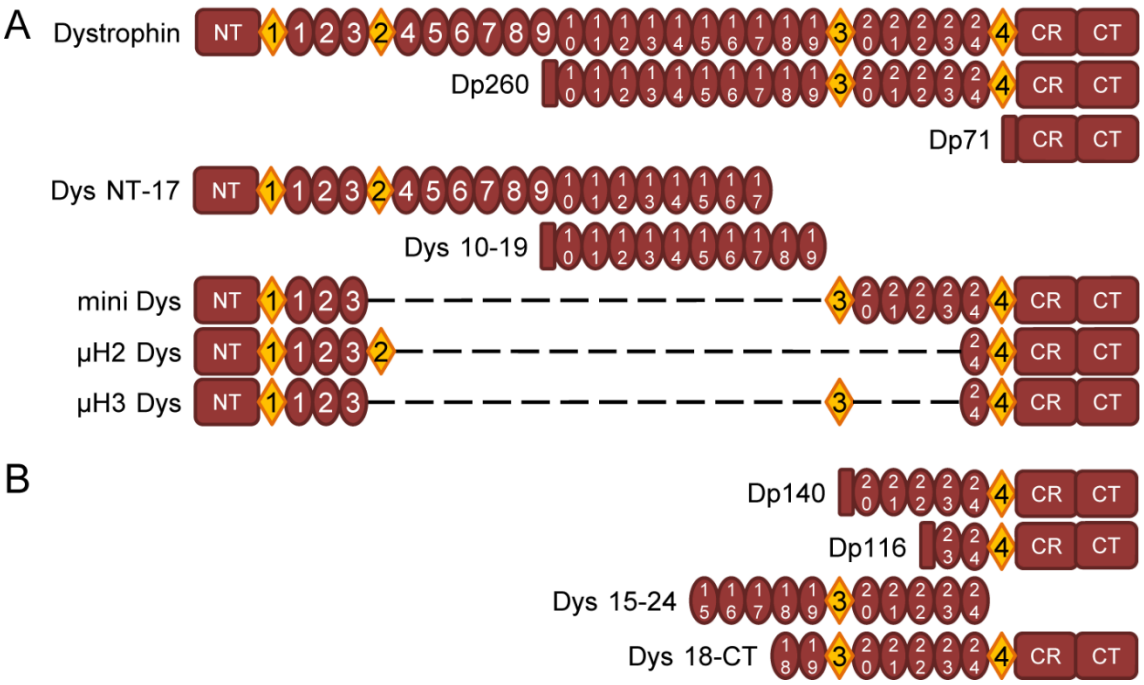

Figure 3-2: Domain structure of proteins analyzed. (A-B) Schematic representations of different dystrophin constructs tested in *in vitro* microtubule cosedimentation assays. Ovals and diamonds are as in Figure 3-1. Based on the unique domains present in the constructs that bind microtubules (shown in A), the microtubule binding domain lies within repeats 20-24.

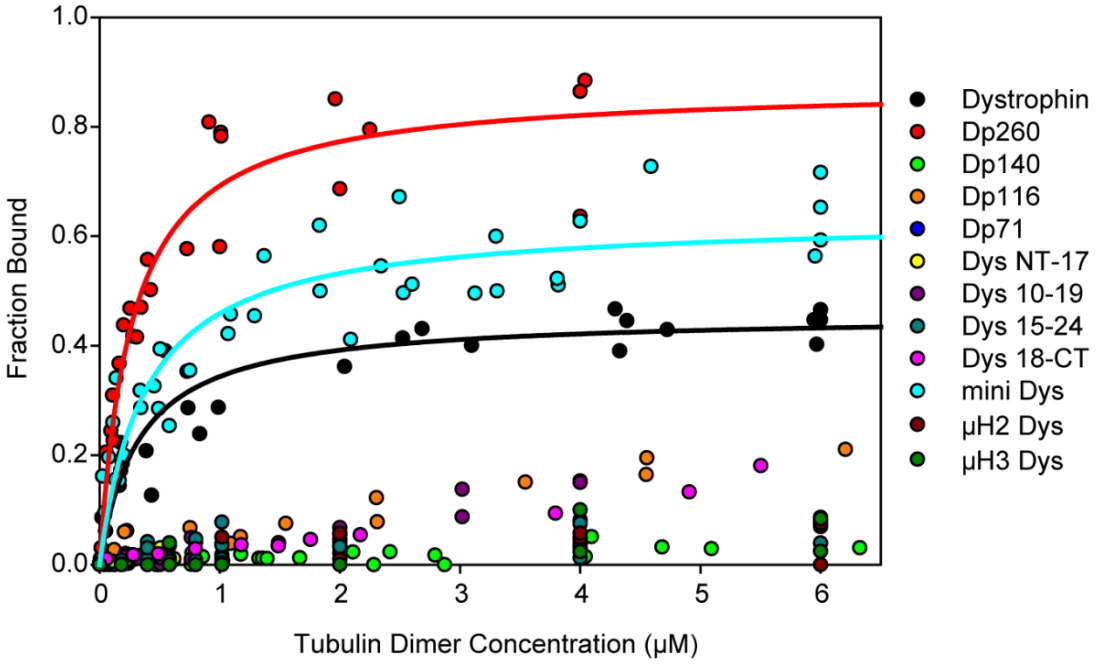

Figure 3-3: Microtubule binding properties of constructs analyzed. Microtubule binding curves of all constructs shown in Figure 3-2. Only dystrophin, Dp260, and mini Dys show specific microtubule binding (K_D=0.33μM, 0.26μM, and 0.38μM, respectively). No other construct shows specific microtubule interaction.

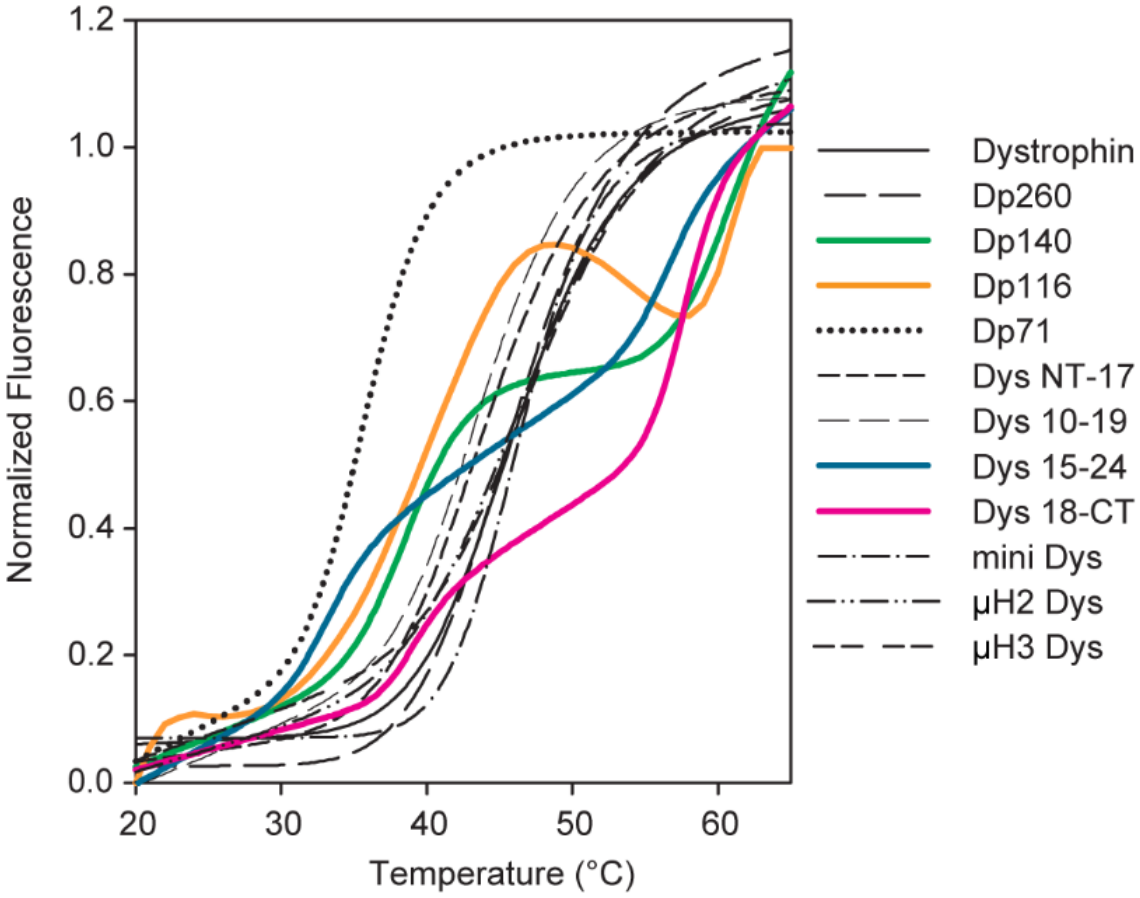

Figure 3-4: Differential scanning fluorimetry of constructs analyzed. DSF analysis of all constructs shown in A and B. Dp140, Dp116, Dys 15-24, and Dys 18-CT display thermal denaturation curves different from that of full-length dystrophin, indicating that they are folded in a different manner.

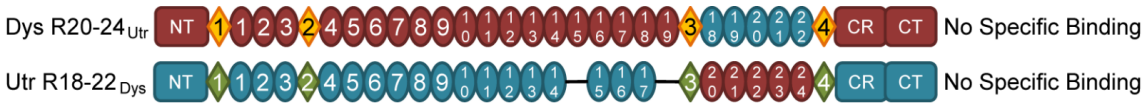

Figure 3-5: Domain structure and microtubule binding properties of full-length dystrophin and utrophin swap constructs. Substituting dystrophin repeats 20-24 for utrophin repeats 18-22 ablates specific microtubule binding. However, substituting utrophin repeats 18-22 for dystrophin repeats 20-24 does not confer microtubule binding to utrophin. Ovals and diamonds are as in Figure 3-1.

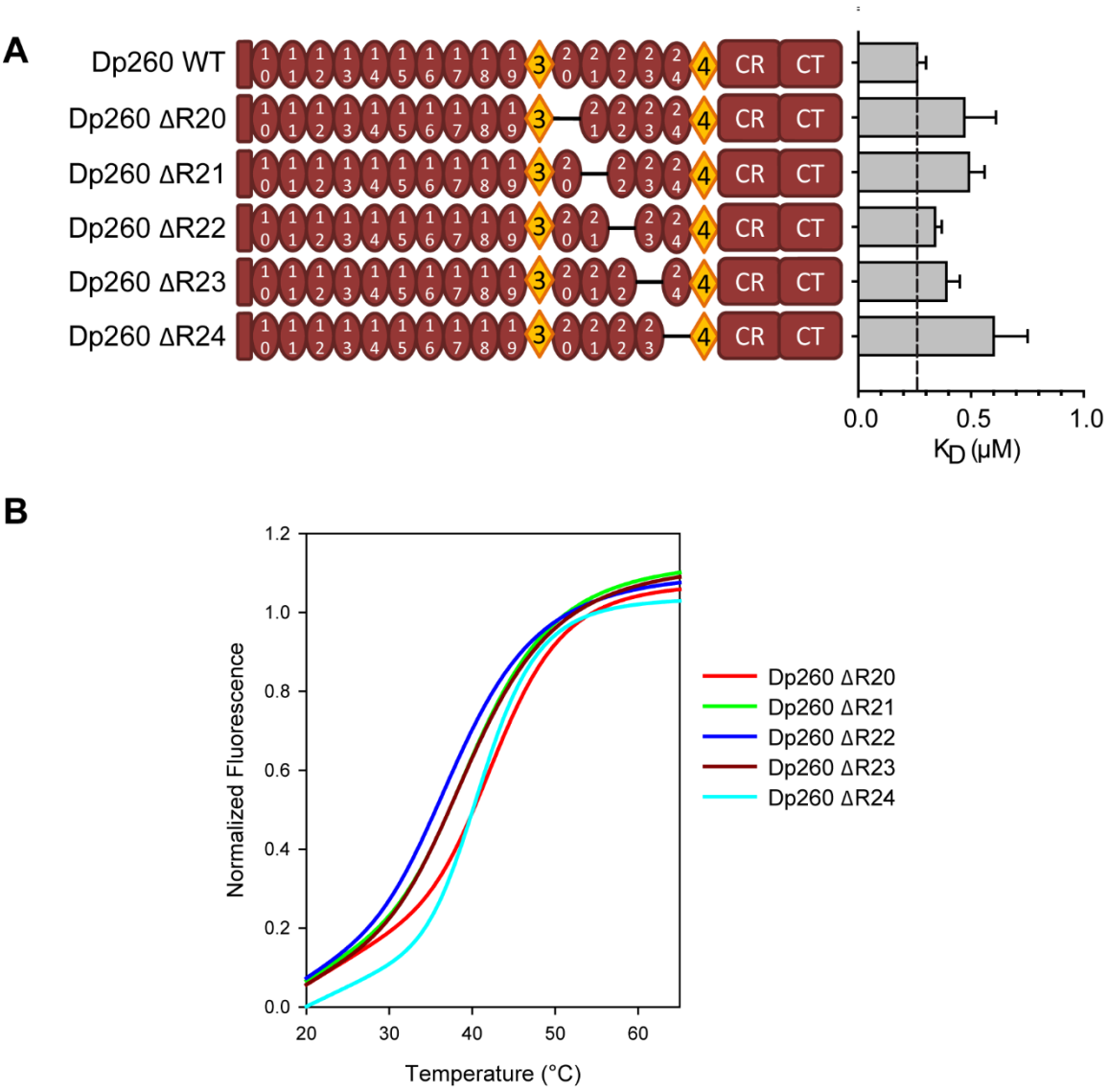

Figure 3-6: Domain structure, microtubule binding properties, and differential scanning fluorimetry of Dp260 deletion constructs. (A) Dp260 single repeat deletion constructs show no significant loss of microtubule binding activity, indicating that no single repeat functions as the microtubule binding domain of dystrophin. (B) DSF analysis shows that all constructs unfold in a single transition at similar temperatures to Dp260.

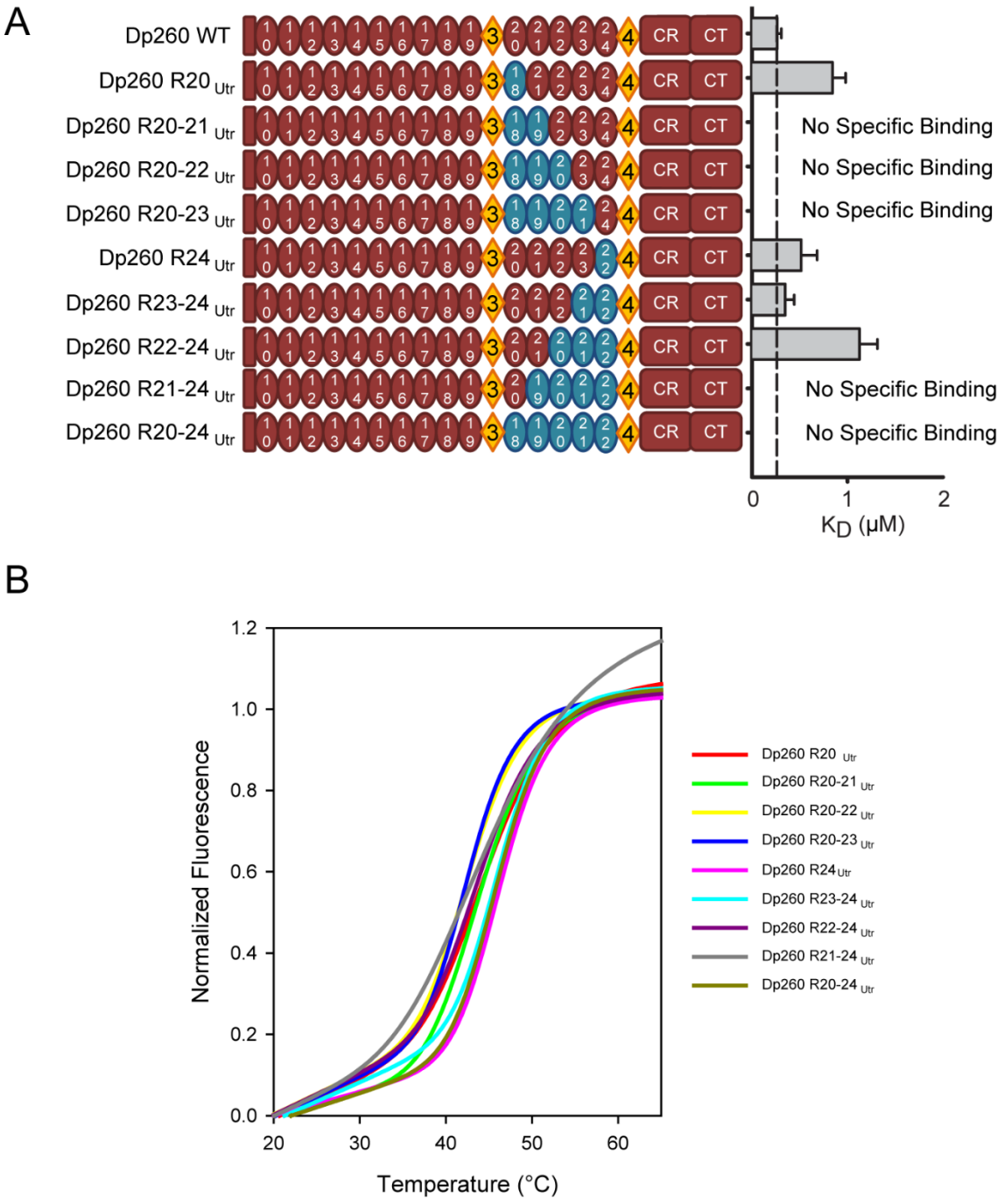

Figure 3-7: Domain structure, microtubule binding properties, and differential scanning fluorimetry of Dp260/utrophin swap constructs. (A) Dp260/Utrophin hybrid constructs with varying numbers of utrophin repeats

substituted into dystrophin repeats 20-24 reveals that repeats 20-22 are the most important for microtubule binding. Loss of dystrophin repeats 23 or 24 does not affect microtubule binding. Loss of repeat 20 or 22 results in a slight decrease in microtubule binding whereas losing two or all repeats within 20-22 ablates microtubule binding. Ovals and diamonds are as in Figure 3-1. (B) DSF analysis shows that all constructs unfold in a single transition at similar temperatures to Dp260.

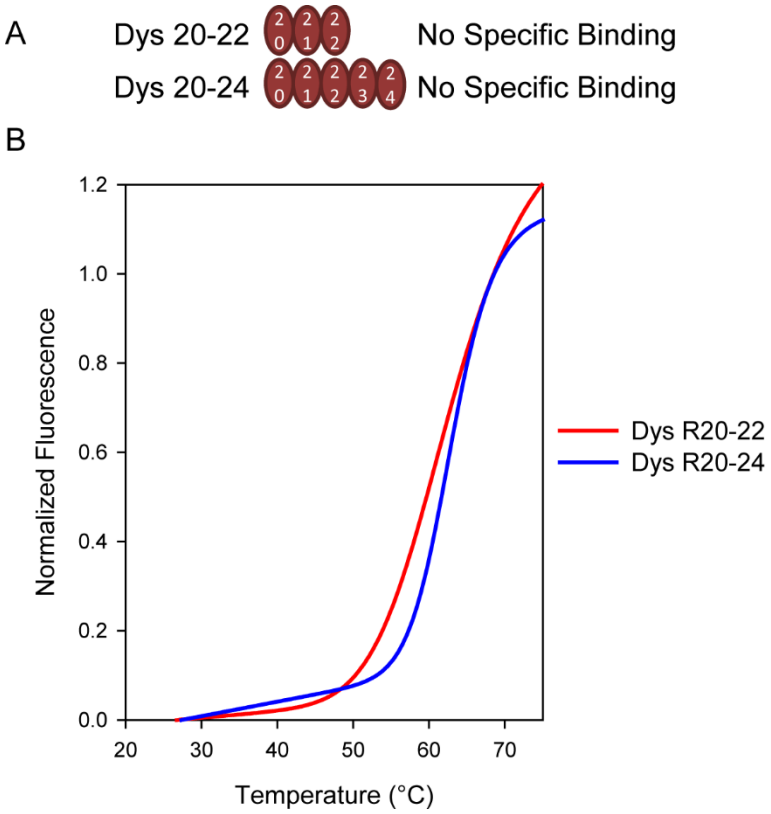

Figure 3-8: Domain structure, microtubule binding properties, and differential scanning fluorimetry of isolated dystrophin repeats 20-22 and repeats 20-24. (A) Schematic representation of constructs assayed. Ovals are as in Figure 3-1. (B) DSF analysis shows that both constructs unfold in a single transition at higher temperatures than dystrophin.

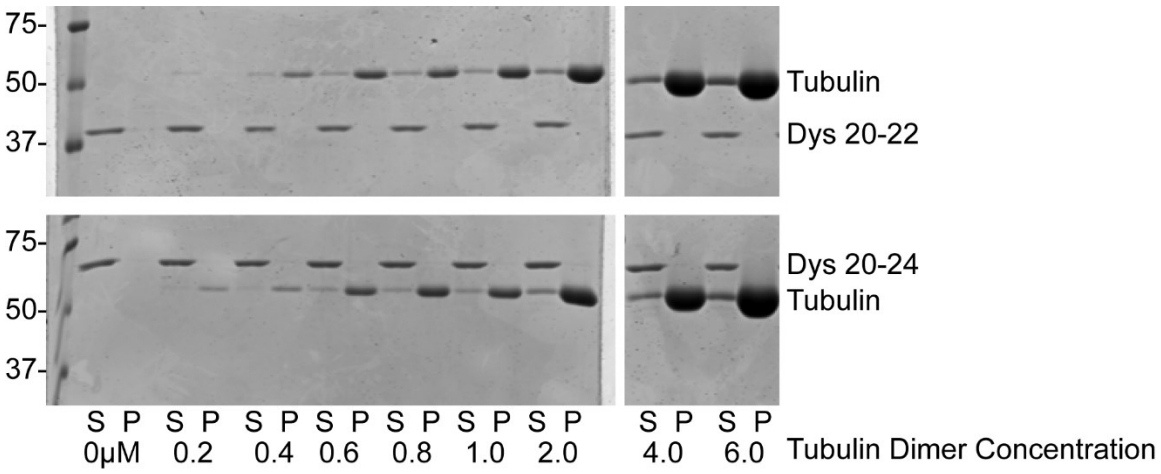

Figure 3-9: Raw data for Figure 3-8. Coomassie stained SDS-PAGE gels of microtubule cosedimentation assays performed in the presence of Dys 20-22 (upper) and Dys 20-24 (lower). Both constructs fail to cosediment with microtubules as tubulin dimer concentration is increased from 0 μM or 6 μM, indicating that no microtubule binding is occurring. S, supernatant (fraction not bound to microtubules); P, pellet (fraction bound to microtubules).

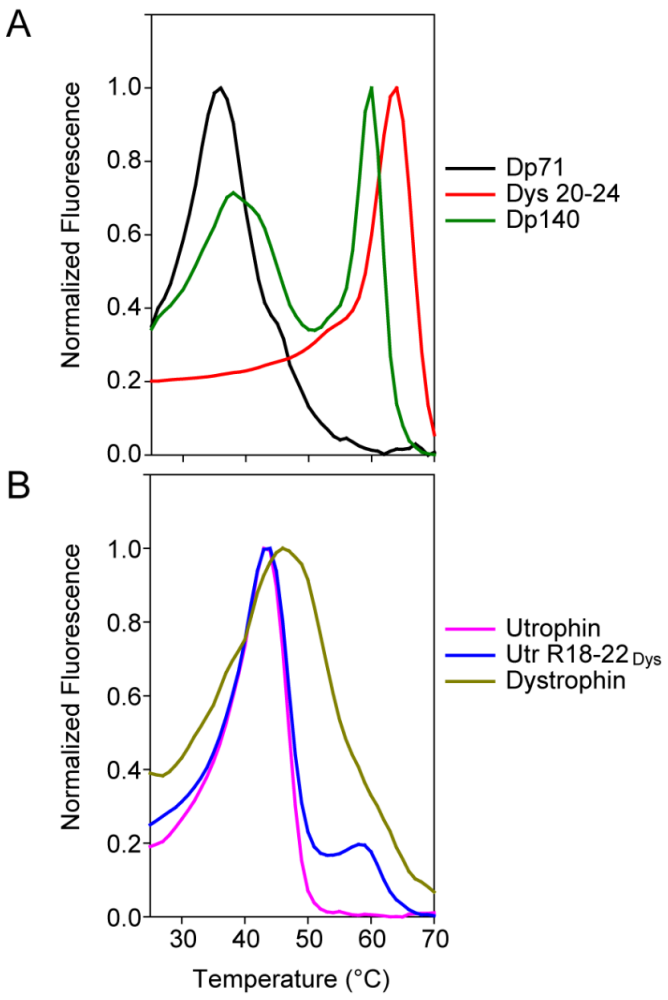

Figure 3-10: Differential scanning fluorimetry derivate curves. Derivative plots of DSF data for Dp140, Dp71, and Dys 20-24. Dp140 exhibits thermal characteristics of Dp71 and Dys 20-24. The higher thermal denaturation temperature of Dys 20-24 is indicative of the microtubule non-binding conformation. (B) Dystrophin does not exhibit a high thermal denaturation peak, indicating that repeats 20-22 are in a microtubule binding conformation. Dystrophin repeats 20-24 exhibit the high thermal denaturation temperature when placed within utrophin, indicating that utrophin does not provide the proper context for the microtubule binding domain of dystrophin to bind microtubules.

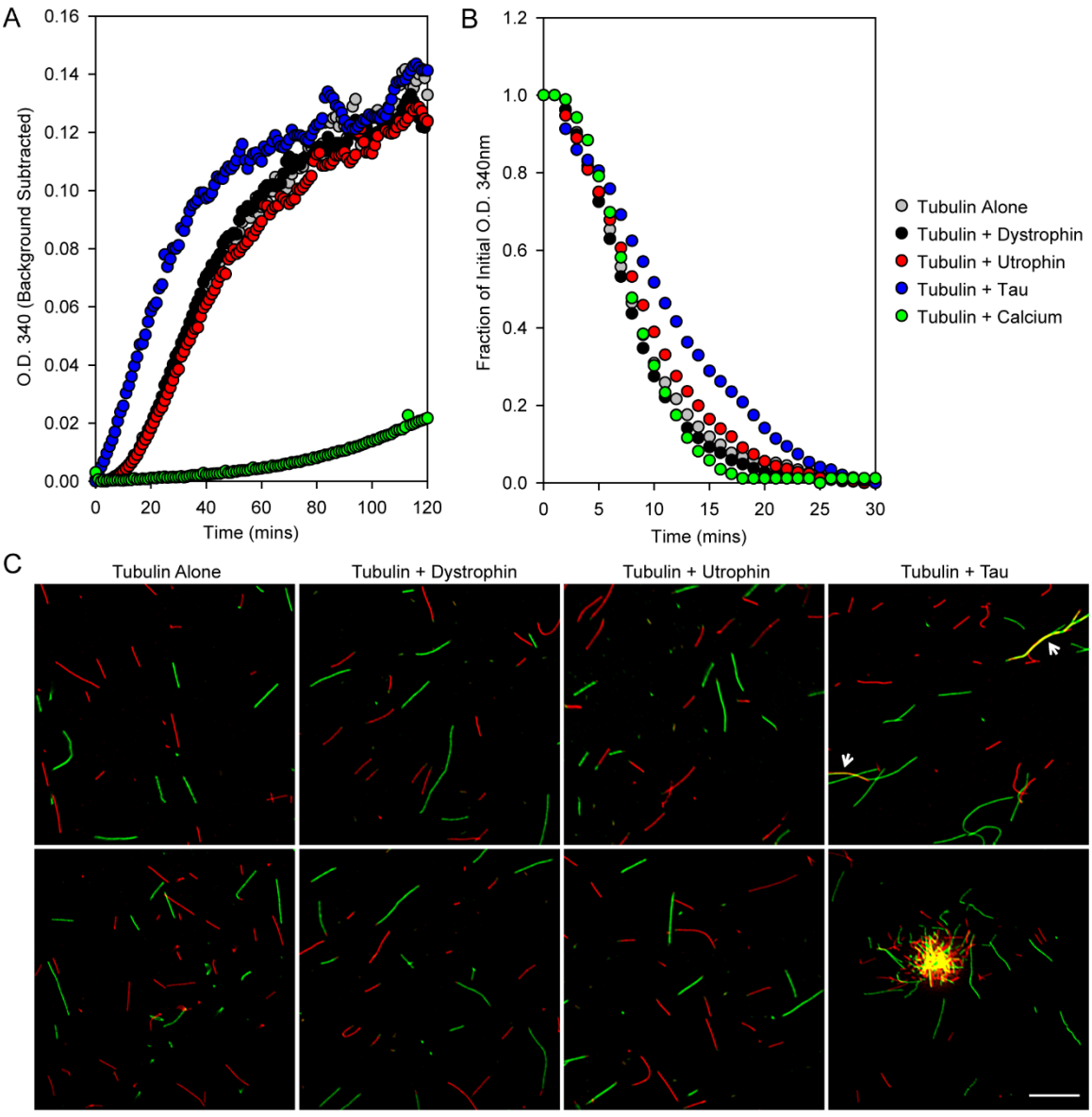

Figure 3-11: Effect of dystrophin and utrophin on tubulin polymerization, microtubule depolymerization, and microtubule bundling. (A) Tubulin polymerization assay. Tubulin polymerized at the same rate when alone, with dystrophin, or with utrophin (2.42 mOD/min, 2.46 mOD/min, and 2.38 mOD/min, respectively), indicating that dystrophin does not affect tubulin polymerization. Tau increased the rate of tubulin polymerization (5.64 mOD/min) and shortened

the microtubule nucleation phase whereas calcium drastically decreased the rate of polymerization (0.03 mOD/min). (B) Microtubule depolymerization assay. The rate of microtubule depolymerization was approximately the same when microtubules were incubated alone, with dystrophin, with utrophin, or with calcium (-8.75%/min, -8.01%/min, -6.92%/min, and -8.75%/min, respectively), indicating that dystrophin has no effect on microtubule depolymerization. Tau partially reduced the rate of microtubule depolymerization (-2.62%/min). (C) Microtubule bundling assay. Microtubules alone, with dystrophin, or with utrophin display no evidence of microtubule bundling as evidenced by the lack of yellow fluorescence. Tau exhibits microtubule bundling activity of individual microtubules as evidenced by yellow fluorescence (arrows, upper panel). Additionally, large tau/microtubule bundles were frequently observed (lower panel). Bar, 10 μm.

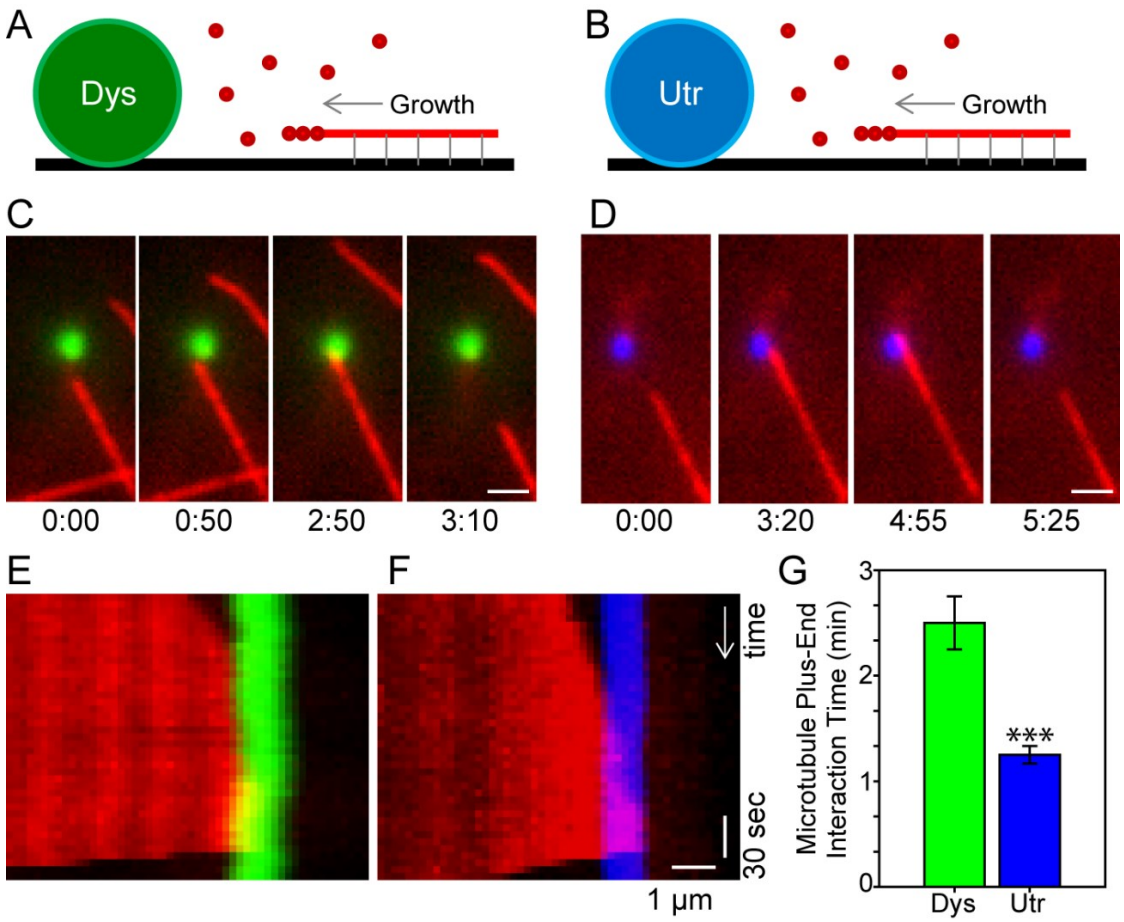

Figure 3-12: Effect of dystrophin and utrophin on microtubule localization. (A-B) Schematic representation of assay performed. Dystrophin (Dys, green) or utrophin (Utr, blue) coated YG microparticles and red fluorescent microtubule seeds were immobilized via anti-biotin to TIRF imaging chambers. Free red fluorescent tubulin was flowed into the chamber and the polymerization and depolymerization of microtubules as they interacted with the microparticles imaged over time. (C) Time lapse images of a direct dystrophin/microtubule interaction. As the microtubule interacts with dystrophin, its polymerization rate decreases as the microtubule becomes anchored to dystrophin. This interaction increases the time until catastrophe. Bar, 2 µm. (D) Time lapse images of a direct

utrophin/microtubule interaction. A microtubule that encounters a utrophin-coated microparticle does not become anchored and immediately undergoes catastrophe. Bar, 2 μm. (E) Kymograph of the data presented in C. (F) Kymograph of the data presented in D. (G) The dystrophin/microtubule (n=6) interaction time is significantly greater than the utrophin/microtubule (n=8) interaction time. Values shown are means with standard errors. ***, $P < 0.001$.

Tables

Construct	T_M1 (°C)	T_M2 (°C)	K_D (μM)
Dystrophin	46.6 ± 0.9		0.33 ± 0.08
Dp260	46.4 ± 1.6		0.26 ± 0.04
Dp140	39.3 ± 0.6	60.7 ± 3.1	No Specific Binding
Dp116	40.6 ± 1.2	61.2 ± 0.6	No Specific Binding
Dp71	36.3 ± 0.3		No Specific Binding
Dys NT-17	44.8 ± 1.1		No Specific Binding
Dys 10-19	44.7 ± 1.3		No Specific Binding
Dys 15-24	33.2 ± 0.3	56.7 ± 0.6	No Specific Binding
Dys 18-CT	38.9 ± 0.5	57.7 ± 0.5	No Specific Binding
mini Dys	46.5 ± 0.6		0.38 ± 0.07
μH2 Dys	48.0 ± 1.5		No Specific Binding
μH3 Dys	48.3 ± 1.5		No Specific Binding
Utrophin	43.1 ± 1.6		No Specific Binding
Dp260 ΔR20	44.6 ± 2.0		0.47 ± 0.14
Dp260 ΔR21	42.3 ± 3.9		0.49 ± 0.07
Dp260 ΔR22	40.6 ± 3.2		0.34 ± 0.03
Dp260 ΔR23	42.2 ± 2.7		0.39 ± 0.06
Dp260 ΔR24	42.1 ± 0.6		0.60 ± 0.15
Dp260 $R20_{Utr}$	45.8 ± 1.0		0.84 ± 0.15
Dp260 $R20\text{-}21_{Utr}$	44.6 ± 0.2		No Specific Binding
Dp260 $R20\text{-}22_{Utr}$	43.4 ± 0.4		No Specific Binding
Dp260 $R20\text{-}23_{Utr}$	43.1 ± 0.3		No Specific Binding
Dp260 $R24_{Utr}$	46.7 ± 0.3		0.52 ± 0.17
Dp260 $R23\text{-}24_{Utr}$	46.7 ± 0.5		0.35 ± 0.09
Dp260 $R22\text{-}24_{Utr}$	44.9 ± 0.5		1.13 ± 0.19
Dp260 $R21\text{-}24_{Utr}$	46.3 ± 6.0		No Specific Binding
Dp260 $R20\text{-}24_{Utr}$	46.5 ± 0.4		No Specific Binding
Dys 20-22		62.7 ± 4.2	No Specific Binding
Dys 20-24		63.0 ± 1.8	No Specific Binding
Dys $R20\text{-}24_{Utr}$	46.7 ± 1.2		No Specific Binding
Utr $R18\text{-}22_{Dys}$	43.0 ± 0.6	58.0 ± 1.1	No Specific Binding

Table 3-1: Differential scanning fluorimetry melting temperatures and microtubule dissociation constants for all constructs.

Chapter Four

Conclusions and Discussion

Dystrophin is thought to stabilize the sarcolemma against contraction-induced injuries that occur as a result of normal muscle contraction. The exact mechanism through which dystrophin performs this role was initially thought to be by linking the actin cytoskeleton to the extracellular matrix allowing for radial force transduction and reduced membrane damage. However, studies have shown that dystrophin directly interacts with intermediate filament proteins (Bhosle et al., 2006) and microtubules (Prins et al., 2009), indicating that dystrophin may protect against contraction-induced injury via multiple cytoskeletal interactions. Since dystrophin interacts with microtubules whereas its homolog utrophin does not, we sought to determine the physiological relevance of the dystrophin-microtubule interaction and whether any pathologies can be directly attributed to the lack of this interaction as seen in DMD patients and the *mdx* mouse.

Sarcolemmal nNOS has been implicated in effecting vasodilation to increase oxygen delivery to muscle during contraction. Mice lacking nNOS exhibit reduced cage activity after mild exercise (Kobayashi et al., 2008), which is exacerbated in *mdx* mice presumably due to the additional lack of dystrophin. We have shown here that the Fiona-*mdx* mouse, which transgenically overexpresses utrophin, fails to fully rescue this loss of activity. We conclude that utrophin cannot fully compensate for dystrophin in regards to exercise-induced inactivity and that this may partially be explained through a lack of nNOS localization to the sarcolemma. However, since activity is partially recovered from the *mdx* mouse in the Fiona-*mdx* mouse, another aspect of the *mdx* mouse beyond the lack of

nNOS localization to the sarcolemma must contribute to its lack of activity after mild exercise. Since the recovery seen in the mini-Dys-TG-*mdx* mouse is comparable to the Fiona-*mdx* mouse, we believe that the level of recovery seen in the Fiona-*mdx* mouse is not a utrophin-specific phenomenon, but rather that the loss of full-length utrophin or full-length dystrophin below endogenous dystrophin protein levels is the main cause of activity loss.

The exact physiological consequences of microtubule derangement are yet to be fully elucidated, but recent work has shown that the perturbed microtubule lattice in the dystrophin-deficient *mdx* mouse appears to exacerbate the dystrophic phenotype (Khairallah et al., 2012). In this study, the authors show that the loss of force generation seen in the *mdx* mouse upon repeated eccentric contractions can be greatly ameliorated when microtubules are depolymerized using colchicine. They postulate that perturbation of the microtubule lattice may contribute to the loss of force generation and that simply reducing overall microtubule abundance can improve performance. Therefore, therapies attempting to ameliorate DMD and BMD patients' symptoms may need to account for the role that microtubule lattice disorganization plays in muscle weakness. We show for the first time that transgenic utrophin overexpression is incapable of preventing loss of torque production specifically in anterior muscles and that this is a microtubule-related phenotype (Chapter 2). We intend to use our newly generated dystrophin transgenic mouse lines in which the microtubule binding domain has been ablated (Appendix) to further evaluate direct physiological consequence of microtubule lattice disorganization.

Additionally, microtubules have been shown to be integral in the formation of myotubes from myoblasts during muscle development and differentiation (Saitoh et al., 1988; Chang et al., 2002; Perez et al., 2002). The Golgi apparatus requires proper microtubule organization in muscle for both proper localization and proper vesicular trafficking (Ralston et al., 1999, 2001). That *mdx* and Fiona-*mdx* mice survive to adulthood would seem to argue that microtubule organization is not required for myotube formation whereas the Golgi is intimately dependent on microtubule organization, underscoring the different roles that microtubules have within muscle cells and highlighting how much research is still necessary to fully understand the interplay of these processes.

We have mapped the microtubule binding domain of dystrophin to spectrin-like repeats 20-22 of the central rod domain (Chapter 3). These repeats have been previously reported to adopt a thermally stable, highly cooperative conformation when expressed in isolation (Mirza et al., 2010), corroborating our findings. When spectrin-like repeats 20-22 are swapped for the homologous repeats from utrophin, microtubule binding is ablated. However, swapping these repeats into utrophin does not confer microtubule binding activity, indicating that these repeats are not sufficient for microtubule binding. This context-specific interaction of dystrophin and microtubule also holds true for dystrophin and nNOS, indicating that flanking regions of the dystrophin protein are required for the proper function of the protein as a whole.

Context-specific interactions between dystrophin and other binding partners have been previously reported. We recently demonstrated that the

dystrophin/actin interaction is enhanced by the carboxy-terminal third of dystrophin even though no direct dystrophin/actin interaction can be measured for this region (Henderson et al., 2012). Additionally, the second and third alpha helices of dystrophin repeat 16 are necessary but not sufficient for nNOS localization to the sarcolemma (Lai et al., 2013); when these helices were swapped into the homologous region of utrophin, no nNOS localization was observed. Many therapies in development tend to focus on miniaturized dystrophin constructs in which large regions of the rod domain deemed less important are removed. Our results argue that these approaches may be less effective due to the cooperative influences between multiple domains present in dystrophin. In support of this, we have shown that full-length dystrophin displays thermodynamic characteristics unique from those reported by individual domains (Henderson et al., 2011).

In addition to delineating the minimal microtubule binding domain, we have shown for the first time how dystrophin organizes the subsarcolemmal microtubule lattice. While dystrophin does not affect tubulin polymerization, microtubule depolymerization, or bundle microtubules it appears to localize microtubules to the sarcolemma by acting as a molecular guidepost (Chapter 3). When actively polymerizing microtubules encounter a dystrophin molecule, they become anchored and pause before continuing to polymerize. This anchorage helps explain how the presence of dystrophin results in subsarcolemmal microtubule organization. Lack of dystrophin, as in the *mdx* mouse, or the overexpression of utrophin at the sarcolemma, as in the Fiona-*mdx* mouse, does

not allow for proper microtubule guidance and thus results in lattice disorganization.

In conclusion, we have shown: (1) that spectrin-like repeats 20-22 in dystrophin are necessary but not sufficient to organize the subsarcolemmal microtubule lattice, (2) that microtubule organization is achieved through dystrophin acting as a molecular guidepost to orient microtubules, (3) that the microtubule binding activity of dystrophin is not conserved in utrophin, (4) that reduced cage activity after mild exercise in the Fiona-*mdx* and mini-Dys-TG-*mdx* mice is an nNOS-associated phenotype, and (5) that reduced torque production in anterior crural muscles of the Fiona-*mdx* mouse is a microtubule-associated phenotype. Additionally, we have generated a transgenic mouse model expressing a dystrophin lacking microtubule binding activity (Appendix) to further investigate the specific contributions of microtubule disorganization on DMD.

Chapter Five

Materials and Methods

Mice

All animals were housed and treated in accordance with the standards set by the University of Minnesota Institutional Animal Care and Use Committee. Fiona-*mdx* mice were kind gifts from Dr. Kay E. Davies (University of Oxford). Dys-TG-*mdx* and mini-Dys-TG-*mdx* mice were kind gifts from Dr. Jeffrey S. Chamberlain (University of Washington).

Establishment of Transgenic Mice

The human skeletal α-actin (HSA) promoter was cloned in place of the cytomegalovirus promoter in the Gateway version of the mammalian expression vector pcDNA, pDEST40. This new plasmid (pDEST-HSA) was used to create a transgene with the Dys R20-24$_{Utr}$ construct, which was already built in the pENTR/D-TOPO vector using the methods described below. pDEST-HSA-Dys R20-24$_{Utr}$ DNA was restriction digested to linearize the transgene (KasI and NaeI), gel extracted, and sent for pronuclear injection at the Mouse Genetics Core at The Scripps Research Institute. Transgenic founder mice were identified by PCR using HSA-specific primers (Forward: 5'-GTC AGG AGG GGC AAA CCC GC-3', Reverse: 5'-GTC GCT GCC CTT CTC GAG CC-3', Product Size: 187bp). Transgenic founder mice were crossed with C57Bl/10 mice to check for transgene transmission. Dystrophin protein expression was assessed in several different muscles from each transgene transmitting line once crossed onto the *mdx* background using quantitative Western blotting. Three lines transmitted the transgene and had detectable protein expression as detailed in Table A-1.

Reagents

Anti-α-tubulin (DM1A, 1:200), anti-α-tubulin (B512, 1:1000), anti-β-tubulin (D66, 1:1000), anti-pan-actin (C4, 1:1000), anti-laminin (L9393, 1:1000), anti-FLAG (M2, 1:2000), and anti-biotin (BN-34, 1:10) antibodies were purchased from Sigma Aldrich. Anti-dystrophin (Dys1, 1:50), anti-β-dystroglycan (NCL-b-DG, 1:100), anti-α-sarcoglycan (NCL-a-SG, 1:100), and anti-γ-sarcoglycan (NCL-g-SG, 1:100) antibodies were purchased from Leica. Anti-utrophin (8A4, 1:50) antibody was purchased from Santa Cruz Biotechnology. Anti-α-dystroglycan (IIH6C4, WB: 1:500, IF: 1:100) and anti-syntrophin (1351, 1:100) antibodies were purchased from Millipore. Anti-dystrobrevin (23, 1:100) antibody was purchased from BD Biosciences. Anti-nNOS (Z-RNN3, 1:150) antibody, Alexa Fluor secondary antibodies (1:250), Alexa Fluor α-bungarotoxin (1:500), and SYPRO Orange (1:1000) were purchased from Invitrogen. Wheat germ agglutinin agarose beads were purchased from Vector Laboratories. Pre-formed microtubules, tubulin, red fluorescent tubulin, green fluorescent tubulin, biotinylated tubulin, tau, and paclitaxel were purchased from Cytoskeleton. Fluoresbrite fluorescent YG COOH microparticles (polystyrene, 1μm diameter) and PolyLink protein coupling kit were purchased from Polysciences. Primers were purchased from Integrated DNA Technologies.

Muscle Fiber Imaging

Extensor digitorum longus muscles were harvested from profusion-fixed mice and immunostained for α-tubulin (DM1A). Profusion media (50mM PIPES,

5mM EGTA, 2mM $MgSO_4$, 10% DMSO, 0.1% Triton X-100, pH 6.8) containing 4% paraformaldehyde was previously described (Hardham, 1987). Muscles were further post-fixed in 4% paraformaldehyde in phosphate buffered saline (PBS: 8mM NaH_2PO_4, 42mM Na_2HPO_4, 150mM NaCl, pH 7.5) for 48 hours while rotating. Single muscle fibers or bundles of two or three muscle fibers were mechanically teased apart and incubated with anti-α-tubulin overnight with rotation. Goat anti-mouse secondary antibody coupled to Alexa Fluor 488 or 568 was used for visualization. Fibers were mounted on slides using *SlowFade* Gold antifade reagent with DAPI (Invitrogen) to visualize nuclei. Fibers were imaged on the Olympus FluoView FV1000 with the 60X oil immersion objective using the accompanying software. Z-stacks of two to three sarcolemmal images were maximally projected using ImageJ. Brightness and contrast were adjusted using Adobe Photoshop.

Mouse Activity Cage Measurements

Exercise-induced inactivity was assessed as previously described (Kobayashi et al., 2008) with the following modifications. Mice were acclimated to the treadmill for three consecutive days prior to activity cage assessments. Acclimation consisted of 5 minutes at 0 m/min followed by 5 minutes at 9 m/min at 0° incline. On the fourth day, baseline voluntary activity was assessed for 30 minutes prior to exercise using activity cages (AccuScan Instruments Inc.). Mice were then placed on the treadmill set at 15° decline. Mice were acclimated to the treadmill for 5 minutes at 0 m/min. Without the use of electrical shock, mice were

encouraged to walk for 5 minutes at 5 m/min followed by 10 minutes at 15 m/min. After exercise, mice were placed back in the same activity cages and activity monitored for 30 minutes after exercise.

Ex Vivo EDL Force Measurements

The contraction-induced injury protocol consisted of ten eccentric contractions performed on isolated extensor digitorum longus (EDL) muscles harvested from mice anesthetized with sodium pentobarbital (100 mg/kg). EDL muscles were secured to a force transducer with 5-0 suture in a 1.5 mL bath assembly and incubated at 25°C in an oxygenated (95% O_2) Krebs-Ringer bicarbonate buffer solution. Eccentric contractions were performed as follows. EDL muscles were passively shortened to 95% resting length and then stimulated for 200ms while the muscle was simultaneously lengthened to 105% resting length at 0.5 lengths/s. Each eccentric contraction was separated by three minutes of rest before performing the next eccentric contraction. Force production was plotted as a percentage of initial force.

In Vivo Muscle Torque Measurements

Mice were anesthetized with 0.2 mg/kg fentanyl citrate, 10 mg/kg droperidol, and 5mg/kg diazepam. Electrodes were placed on either side of the peroneal nerve of the left hind limb and the left paw placed into a mechanical foot lever. Torque was measured over frequencies ranging from 20 to 400Hz to determine optimal frequency of excitation. Initial torque production was measured

by stimulating muscles for 150ms at 250Hz. The voltage was adjusted between 3-5V to achieve maximal isometric torque. The muscles were injured by 70 electrically-induced eccentric contractions of 150ms each. Each eccentric contraction took place such that the foot was passively moved from 0° to 19° of dorsiflexion relative to the tibialis anterior muscle for 100ms followed by an additional movement from 19° of dorsiflexion to 19° of plantarflexion at an angular velocity of 2°/ms for 50ms. Torque about the ankle joint was measured for each eccentric contraction and plotted as a percentage of initial torque production.

Neuromuscular Junction Imaging

Gastrocnemius muscles from each mouse line were cryopreserved in OCT and 20μm longitudinal sections cut. Sections were fixed in 4% paraformaldehyde in PBS for ten minutes and subsequently washed three times in PBS for five minutes each. Alexa Fluor 488 α-bungarotoxin was incubated on the sections for 30 minutes at 37°C. Sections were washed three times in PBS for five minutes each and slides sealed using *SlowFade* Gold antifade reagent with DAPI to visualize nuclei. Images were acquired on a Deltavision PersonalDV deconvolution microscope equipped with a 100X 1.40 NA oil objective.

Immunofluorescence

Quadriceps muscles from each mouse line were cryopreserved in OCT and 10μm transverse sections cut. Sections were fixed in 4% paraformaldehyde

in PBS for ten minutes and subsequently washed three times in PBS with 0.1% Triton for five minutes each. Primary antibodies were incubated overnight at 4°C in a humidified chamber. The next day, slides were washed three times in PBS with 0.1% Triton for five minutes each and goat anti-mouse or anti-rabbit secondary antibody coupled to Alexa Fluor 488 or 568 was incubated on the sections for 30 minutes at 37°C. Sections were washed three times in PBS with 0.1% Triton for five minutes each and slides sealed using *SlowFade* Gold antifade reagent with DAPI to visualize nuclei. Images were acquired on a Deltavision PersonalDV deconvolution microscope equipped with a 40X 1.35 NA oil objective.

Cloning

All dystrophin and utrophin plasmid constructs were initially inserted and sequence verified in the Gateway entry vector pENTR/D-TOPO (Invitrogen) after PCR amplifying them from existing N-terminally FLAG-tagged pFastBac1 constructs from previous studies (Rybakova et al., 2002, 2006; Prins et al., 2009; Henderson et al., 2010, 2011). All PCRs were performed using PfuII Ultra HS polymerase (Stratagene). Once verified, entry vectors were recombined into the Gateway insect cell destination vector, pDEST8, using LR Clonase II (Invitrogen) and subsequently expressed in Sf9 insect cells using the Bac-to-Bac system (Invitrogen).

Deletion constructs were built as previously described (Imai et al., 1991). Briefly, PCR primers were designed such that they amplified the entire plasmid

except the region being deleted. These linear PCR products were then circularized via the addition of T4 polynucleotide kinase and T4 DNA ligase (New England Biolabs) and sequence verified. Multiple rounds of deletion were performed if necessary to create the desired construct.

Dystrophin/utrophin hybrid constructs were built as follows. Briefly, PCR primers were designed to amplify the entire dystrophin plasmid except the repeats being exchanged with primers containing 15 nucleotide overhangs homologous to the ends of the utrophin repeats being substituted in. Additionally, the homologous utrophin repeats being substituted in were PCR amplified with primers containing 15 nucleotide overhangs homologous to the dystrophin repeats flanking the hybrid region. These two PCR products were mixed in equimolar ratios and assembled into a single vector using the Gibson Assembly Master Mix (New England Biolabs). These vectors were sequence verified, recombined into pDEST8, and expressed as described above.

Protein Expression and Purification

FLAG-tagged dystrophin and utrophin proteins were expressed and purified in Sf9 insect cells using the Bac-to-Bac protocol (Invitrogen). Briefly, recombinant baculoviral DNA was transfected into a small culture of Sf9 insect cells using CellFectin II (Invitrogen). Four days later, the media containing the recombinant baculovirus was harvested and the transfected cells were analyzed for protein expression by anti-FLAG Western blot. Once expression was verified,

large cultures were incubated for three days with amplified baculovirus before being harvested for protein purification.

For purification, cells were lysed using 1% Triton X-100 in phosphate buffered saline containing protease inhibitors (100nM aprotinin, 1mM benzamidine, 10μM E-64, 10μM leupeptin, 1mM pepstatin A, and 1mM phenylmethanesulfonylfluoride) and protein purified using M2 FLAG affinity agarose (Sigma) as previously described (Prins et al., 2009; Henderson et al., 2010, 2011). Proteins were dialyzed into microtubule buffer (50mM HEPES, 50mM KCl, 1mM $MgCl_2$, 1mM EGTA, pH 7.5) overnight at 4°C before being concentrated and used in *in vitro* microtubule cosedimentation assays, DSF analyses, and tubulin dynamics assays.

In vitro Microtubule Cosedimentation Assay

For *in vitro* microtubule cosedimentation assays, 0.75μM dystrophin or utrophin proteins were incubated with pre-formed microtubules ranging from 0μM to 6μM tubulin dimer for 30 minutes at room temperature. Reactions were then centrifuged at 100,000 × g for 30 minutes at room temperature. The supernatant was collected and an equal volume of buffer used to resuspend the pelleted microtubules and interacting protein. Equivalent volumes of supernatant and pellet were run side-by-side using SDS-PAGE, stained using Coomassie blue, and imaged and analyzed via densitometry using the Odyssey infrared scanner (Li-cor). Fraction of protein in the pellet was plotted against the concentration of

tubulin dimer for each sample and the data fit to a one site saturation binding curve using SigmaPlot (Systat Software).

Differential Scanning Fluorimetry

For DSF, the dye SYPRO Orange was incubated with each protein while fluorescence emission was collected in a real time PCR instrument (iCycler, Bio-Rad) as the temperature of the solution was raised from 20°C to 90°C. Data were normalized from 0 to 1 fraction protein unfolded. A curve was fit to the exponential portion of the data using a two-state transition algorithm (Henderson et al., 2011), the inflection point of which was calculated as the melting temperature of that protein. Dp140, Dys 15-24, and Dys 18-CT were fit to a three-state transition algorithm to account for the two inflection points present. Dp116 could not be fit to either transition algorithm and thus the two melting temperatures were determined by fitting each portion of the data to separate two-state transition algorithms. Derivative plot data values were extracted directly from the iCycler, and scaled such that they ranged from 0 to 1.

Tubulin Dynamics Assays

Tubulin polymerization was carried out in a microplate reader (SpectraMax Plus384, Molecular Devices) at 37°C for two hours in the presence or absence of each protein assayed according to the manufacturer's protocol (Cytoskeleton). Proteins of interest were used at 0.65μM while tubulin was used at 3mg/mL (~27μM tubulin dimer). For excess calcium, 2mM $CaCl_2$ was included in the

reaction to compensate for the presence of EGTA (Schoenmakers et al., 1992). The increase in optical density at 340nm was recorded as a measure of increased presence of polymerized microtubules. The logarithmic growth portion of each reaction was used to calculate the rate of polymerization via linear regression using SigmaPlot (Systat Software).

Microtubule depolymerization was carried out by first polymerizing tubulin as above. Buffer or the protein being assayed was then added to the reaction and the temperature switched to 4°C. Loss of the presence of microtubules was measured in the same manner as above over 30 minutes, with a decrease in optical density at 340nm indicating depolymerization of microtubules. The logarithmic portion of each reaction was used to calculate the rate of depolymerization via linear regression.

To assay for microtubule bundling, equivalent amounts of red and green fluorescent tubulin were individually induced to polymerize into microtubules and then combined in equivalent amounts in the presence or absence of the protein being assayed prior to incubation at room temperature for 30 minutes. Final tubulin dimer concentration was 6μM and proteins of interest were at 0.75μM. Reactions were diluted 1:200 in imaging buffer (80mM PIPES, 2mM $MgCl_2$, 0.5mM EGTA, 30% glycerol, 0.5% glutaraldehyde, pH 6.9) before images were acquired on a Deltavision PersonalDV deconvolution microscope equipped with a 60X 1.42 NA oil objective with yellow fluorescence indicative of a positive bundling event.

Protein/microtubule direct interaction studies were performed as previously described (Hendricks et al., 2012). Briefly, COOH YG microparticles were conjugated to biotinylated-BSA and either dystrophin or utrophin using the PolyLink protein coupling kit according to the manufacturer's protocol. Protein-coupled YG microparticles and red fluorescent biotinylated-tubulin containing microtubule seeds were hybridized to a total internal reflection fluorescence (TIRF) imaging chamber using anti-biotin. After hybridization, the chamber was rinsed with BRB80 (80mM PIPES, 1mM $MgCl_2$, 1mM EGTA, pH 6.9). Tubulin polymerization was initialized by adding 10μM tubulin (9:1 unlabeled:red fluorescent tubulin) in imaging buffer (50mM KCl, 20mM glucose, 0.15% methyl cellulose, 10 μg/mL casein, 2 μg/mL glucose oxidase, 1 μg/mL catalase, 10mM DTT, 3mM GTP, 1% Tween). TIRF microscopy was performed using a Nikon Eclipse Ti microscope with Nikon CFI Apochromat 100X 1.49 NA oil objective. An Andor iXon3 EM-CCD camera fitted with a 2.5X projection lens was used for image acquisition. Images were collected every 5 seconds and analyzed using ImageJ. COOH YG microparticles bound to utrophin were pseudo-colored blue using ImageJ.

Wheat Germ Agglutinin Dystrophin-Glycoprotein Complex Enrichment

Muscle tissue was harvested from each mouse line, snap frozen in liquid nitrogen, ground with a mortar and pestle, and lysed for thirty minutes in 1% Triton X-100 in phosphate buffered saline containing protease inhibitors (100nM aprotinin, 1mM benzamidine, 10μM E-64, 10μM leupeptin, 1mM pepstatin A, and

1mM phenylmethanesulfonylfluoride). Lysates were clarified by centrifugation, an aliquot collected as a starting lysate sample, and the remaining lysate incubated with wheat germ agglutinin conjugated agarose beads overnight at 4°C while rotating. The next day, the lysate was removed from the beads and kept as the void fraction. The beads were washed three times with 1% Triton X-100 in phosphate buffered saline. After washing, the beads were boiled in 2X Laemmli sample buffer (5% sodium dodecyl sulfate, 192mM sucrose, 108mM Tris, 710mM β-mercaptoethanol, 0.0007% bromophenol blue) for five minutes. This fraction was taken as the elution.

References

Acsadi, G., G. Dickson, D.R. Love, A. Jani, F.S. Walsh, A. Gurusinghe, J.A. Wolff, and K.E. Davies. 1991. Human dystrophin expression in mdx mice after intramuscular injection of DNA constructs. *Nature*. 352:815–8.

Ahn, A.H., and L.M. Kunkel. 1995. Syntrophin binds to an alternatively spliced exon of dystrophin. *The Journal of cell biology*. 128:363–71.

Akhmanova, A., and M.O. Steinmetz. 2008. Tracking the ends: a dynamic protein network controls the fate of microtubule tips. *Nature reviews. Molecular cell biology*. 9:309–22.

Angelini, C. 2007. The role of corticosteroids in muscular dystrophy: a critical appraisal. *Muscle & Nerve*. 36:424–35.

Ayalon, G., J.Q. Davis, P.B. Scotland, and V. Bennett. 2008. An ankyrin-based mechanism for functional organization of dystrophin and dystroglycan. *Cell*. 135:1189–1200.

Ayalon, G., J.D. Hostettler, J. Hoffman, K. Kizhatil, J.Q. Davis, and V. Bennett. 2011. Ankyrin-B interactions with spectrin and dynactin-4 are required for dystrophin-based protection of skeletal muscle from exercise injury. *The Journal of Biological Chemistry*. 286:7370–8.

Bar, S., E. Barnea, Z. Levy, S. Neuman, D. Yaffe, and U. Nudel. 1990. A novel product of the Duchenne muscular dystrophy gene which greatly differs from the known isoforms in its structure and tissue distribution. *The Biochemical journal*. 272:557–60.

Barton-Davis, E.R., L. Cordier, D.I. Shoturma, S.E. Leland, and H.L. Sweeney. 1999. Aminoglycoside antibiotics restore dystrophin function to skeletal muscles of mdx mice. *The Journal of clinical investigation*. 104:375–81.

Bhosle, R.C., D.E. Michele, K.P. Campbell, Z. Li, and R.M. Robson. 2006. Interactions of intermediate filament protein synemin with dystrophin and utrophin. *Biochemical and Biophysical Research Communications*. 346:768–77.

Blake, D.J., A. Weir, S.E. Newey, and K.E. Davies. 2002. Function and genetics of dystrophin and dystrophin-related proteins in muscle. *Physiological Reviews*. 82:291–329.

Bork, P., and M. Sudol. 1994. The WW domain: a signalling site in dystrophin? *Trends in Biochemical Sciences*. 531–533.

Brenman, J.E., D.S. Chao, H. Xia, K. Aldape, and D.S. Bredt. 1995. Nitric oxide synthase complexed with dystrophin and absent from skeletal muscle sarcolemma in Duchenne muscular dystrophy. *Cell*. 82:743–752.

Bulfield, G., W. Siller, P. Wight, and M. KJ. 1984. X chromosome-linked muscular dystrophy (mdx) in the mouse. *Proceedings of the National Academy of Sciences*. 81:1189–1192.

Byers, T.J., H.G. Lidov, and L.M. Kunkel. 1993. An alternative dystrophin transcript specific to peripheral nerve. *Nature genetics*. 4:77–81.

Carlson, C.G., and R. V Makiejus. 1990. A noninvasive procedure to detect muscle weakness in the mdx mouse. *Muscle & Nerve*. 13:480–4.

Chang, W., D.R. Webster, A.A. Salam, D. Gruber, A. Prasad, J.P. Eiserich, and J.C. Bulinski. 2002. Alteration of the C-terminal amino acid of tubulin specifically inhibits myogenic differentiation. *The Journal of biological chemistry*. 277:30690–8.

Chang, W.J., S.T. Iannaccone, K.S. Lau, B.S. Masters, T.J. McCabe, K. McMillan, R.C. Padre, M.J. Spencer, J.G. Tidball, and J.T. Stull. 1996. Neuronal nitric oxide synthase and dystrophin-deficient muscular dystrophy. *Proceedings of the National Academy of Sciences*. 93:9142–9147.

Clarke, M.S., R. Khakee, and P.L. McNeil. 1993. Loss of cytoplasmic basic fibroblast growth factor from physiologically wounded myofibers of normal and dystrophic muscle. *Journal of cell science*. 106 (Pt 1:121–33.

Cleveland, D., S. Hwo, and M. Kirschner. 1977. Purification of tau, a microtubule-associated protein that induces assembly of microtubules from purified tubulin. *Journal of Molecular Biology*. 116:207–25.

Cox, G.A., N.M. Cole, K. Matsumura, S.F. Phelps, S.D. Hauschka, K.P. Campbell, J.A. Faulkner, and J.S. Chamberlain. 1993. Overexpression of dystrophin in transgenic mdx mice eliminates dystrophic symptoms without toxicity. *Nature*. 364:725–9.

Crawford, G.E., J.A. Faulkner, R.H. Crosbie, K.P. Campbell, S.C. Froehner, and J.S. Chamberlain. 2000. Assembly of the dystrophin-associated protein complex does not require the dystrophin COOH-terminal domain. *The Journal of Cell Biology*. 150:1399–410.

Davies, K.E., and K.J. Nowak. 2006. Molecular mechanisms of muscular dystrophies: old and new players. *Nature reviews. Molecular cell biology*. 7:762–73.

Deconinck, A.E. 1997. Postsynaptic Abnormalities at the Neuromuscular Junctions of Utrophin-deficient Mice. *The Journal of Cell Biology*. 136:883–894.

Van Deutekom, J.C., M. Bremmer-Bout, A.A. Janson, I.B. Ginjaar, F. Baas, J.T. den Dunnen, and G.J. van Ommen. 2001. Antisense-induced exon skipping restores dystrophin expression in DMD patient derived muscle cells. *Human molecular genetics*. 10:1547–54.

Ervasti, J.M. 2003. Costameres: the Achilles' heel of Herculean muscle. *The Journal of Biological Chemistry*. 278:13591–4.

Ervasti, J.M. 2007. Dystrophin, its interactions with other proteins, and implications for muscular dystrophy. *Biochimica et biophysica acta*. 1772:108–17.

Ervasti, J.M., and K.P. Campbell. 1991. Membrane organization of the dystrophin-glycoprotein complex. *Cell*. 66:1121–31.

Ervasti, J.M., and K.P. Campbell. 1993. A role for the dystrophin-glycoprotein complex as a transmembrane linker between laminin and actin. *The Journal of cell biology*. 122:809–23.

Ervasti, J.M., K. Ohlendieck, S.D. Kahl, M.G. Gaver, and K.P. Campbell. 1990. Deficiency of a glycoprotein component of the dystrophin complex in dystrophic muscle. *Nature*. 345:315–9.

Flanigan, K.M., K. Campbell, L. Viollet, W. Wang, A.M. Gomez, C.M. Walker, and J.R. Mendell. 2013. Anti-dystrophin T cell responses in duchenne muscular dystrophy: prevalence and a glucocorticoid treatment effect. *Human gene therapy*. 24:797–806.

Förstermann, U., E.I. Closs, J.S. Pollock, M. Nakane, P. Schwarz, I. Gath, and H. Kleinert. 1994. Nitric oxide synthase isozymes. Characterization, purification, molecular cloning, and functions. *Hypertension*. 23:1121–31.

Förstermann, U., and H. Kleinert. 1995. Nitric oxide synthase: expression and expressional control of the three isoforms. *Naunyn-Schmiedeberg's archives of pharmacology*. 352:351–64.

Górecki, D.C., A.P. Monaco, J.M.J. Derry, A.P. Walker, E.A. Barnard, and P.J. Barnard. 1992. Expression of four alternative dystrophin transcripts in brain regions regulated by different promoters. *Human Molecular Genetics*. 1:505–510.

Gramolini, a O., C.L. Dennis, J.M. Tinsley, G.S. Robertson, J. Cartaud, K.E. Davies, and B.J. Jasmin. 1997. Local transcriptional control of utrophin

expression at the neuromuscular synapse. *The Journal of Biological Chemistry*. 272:8117–20.

Hammond, J.W., D. Cai, and K.J. Verhey. 2008. Tubulin modifications and their cellular functions. *Current Opinion in Cell Biology*. 20:71–6.

Hardham, A. 1987. Microtubules and the flagellar apparatus in zoospores and cysts of the fungus Phytophthora cinnamomi. *Protoplasma*. 137:109–24.

Henderson, D.M., J.J. Belanto, B. Li, H. Heun-Johnson, and J.M. Ervasti. 2011. Internal deletion compromises the stability of dystrophin. *Human Molecular Genetics*. 20:2955–63.

Henderson, D.M., A. Lee, and J.M. Ervasti. 2010. Disease-causing missense mutations in actin binding domain 1 of dystrophin induce thermodynamic instability and protein aggregation. *Proceedings of the National Academy of Sciences*. 107:9632–7.

Henderson, D.M., A.Y. Lin, D.D. Thomas, and J.M. Ervasti. 2012. The carboxy-terminal third of dystrophin enhances actin binding activity. *Journal of Molecular Biology*. 416:414–24.

Hendricks, A.G., J.E. Lazarus, E. Perlson, M.K. Gardner, D.J. Odde, Y.E. Goldman, and E.L.F. Holzbaur. 2012. Dynein tethers and stabilizes dynamic microtubule plus ends. *Current Biology*. 22:632–7.

Hillier, B.J. 1999. Unexpected Modes of PDZ Domain Scaffolding Revealed by Structure of nNOS-Syntrophin Complex. *Science*. 284:812–815.

Hoffman, E., R.B. Jr, and L. Kunkel. 1987. Dystrophin: the protein product of the Duchenne muscular dystrophy locus. *Cell*. 919–28.

Imai, Y., Y. Matsushima, T. Sugimura, and M. Terada. 1991. A simple and rapid method for generating a deletion by PCR. *Nucleic Acids Research*. 19:2785.

Khairallah, R.J., G. Shi, F. Sbrana, B.L. Prosser, C. Borroto, M.J. Mazaitis, E.P. Hoffman, A. Mahurkar, F. Sachs, Y. Sun, Y.-W. Chen, R. Raiteri, W.J. Lederer, S.G. Dorsey, and C.W. Ward. 2012. Microtubules underlie dysfunction in duchenne muscular dystrophy. *Science Signaling*. 5:ra56.

Kirschner, M., and T. Mitchison. 1986. Beyond self-assembly: from microtubules to morphogenesis. *Cell*. 329–42.

Kleopa, K.A., A. Drousiotou, E. Mavrikiou, A. Ormiston, and T. Kyriakides. 2006. Naturally occurring utrophin correlates with disease severity in Duchenne muscular dystrophy. *Human Molecular Genetics*. 15:1623–8.

Kobayashi, Y.M., E.P. Rader, R.W. Crawford, N.K. Iyengar, D.R. Thedens, J.A. Faulkner, S. V Parikh, R.M. Weiss, J.S. Chamberlain, S.A. Moore, and K.P. Campbell. 2008. Sarcolemma-localized nNOS is required to maintain activity after mild exercise. *Nature*. 456:511–5.

Koenig, M., and L.M. Kunkel. 1990. Detailed analysis of the repeat domain of dystrophin reveals four potential hinge segments that may confer flexibility. *The Journal of Biological Chemistry*. 265:4560–6.

Koenig, M., A. Monaco, and L. Kunkel. 1988. The complete sequence of dystrophin predicts a rod-shaped cytoskeletal protein. *Cell*. 219.

Kramarcy, N.R., A. Vidal, S.C. Froehner, and R. Sealock. 1994. Association of utrophin and multiple dystrophin short forms with the mammalian M(r) 58,000 dystrophin-associated protein (syntrophin). *The Journal of Biological Chemistry*. 269:2870–6.

Lai, Y., G. Thomas, Y. Yue, and H. Yang. 2009. Dystrophins carrying spectrin-like repeats 16 and 17 anchor nNOS to the sarcolemma and enhance exercise performance in a mouse model of muscular. *The Journal of Clinical Investigation*. 119:624–35.

Lai, Y., J. Zhao, Y. Yue, and D. Duan. 2013. α2 and α3 helices of dystrophin R16 and R17 frame a microdomain in the α1 helix of dystrophin R17 for neuronal NOS binding. *Proceedings of the National Academy of Sciences*. 110:525–30.

Lewis, S., I. Ivanov, G. Lee, and N. Cowan. 1989. Organization of microtubules in dendrites and axons is determined by a short hydrophobic zipper in microtubule-associated proteins MAP2 and tau. *Nature*. 342:498–505.

Li, D., A. Bareja, L. Judge, Y. Yue, Y. Lai, R. Fairclough, K.E. Davies, J.S. Chamberlain, and D. Duan. 2010. Sarcolemmal nNOS anchoring reveals a qualitative difference between dystrophin and utrophin. *Journal of Cell Science*. 123:2008–13.

Li, S., E. Kimura, R. Ng, B.M. Fall, L. Meuse, M. Reyes, J.A. Faulkner, and J.S. Chamberlain. 2006. A highly functional mini-dystrophin/GFP fusion gene for cell and gene therapy studies of Duchenne muscular dystrophy. *Human Molecular Genetics*. 15:1610–22.

Lidov, H.G., S. Selig, and L.M. Kunkel. 1995. Dp140: a novel 140 kDa CNS transcript from the dystrophin locus. *Human molecular genetics*. 4:329–35.

Lyons, P.R., and C.R. Slater. 1991. Structure and function of the neuromuscular junction in young adult mdx mice. *Journal of neurocytology*. 20:969–81.

Matsuda, R., A. Nishikawa, and H. Tanaka. 1995. Visualization of dystrophic muscle fibers in mdx mouse by vital staining with Evans blue: evidence of apoptosis in dystrophin-deficient muscle. *Journal of biochemistry*. 118:959–64.

Matsumura, K., J.M. Ervasti, K. Ohlendieck, S. Kahl, and K.P. Campbell. 1992. Association of dystrophin-related protein with dystrophin-associated proteins in mdx mouse muscle. *Nature*. 360:588–91.

Mattei, E., N. Corbi, M.G. Di Certo, G. Strimpakos, C. Severini, A. Onori, A. Desantis, V. Libri, S. Buontempo, A. Floridi, M. Fanciulli, D. Baban, K.E. Davies, and C. Passananti. 2007. Utrophin up-regulation by an artificial transcription factor in transgenic mice. *PloS one*. 2:e774.

Mendell, J.R., K. Campbell, L. Rodino-Klapac, Z. Sahenk, C. Shilling, S. Lewis, D. Bowles, S. Gray, C. Li, G. Galloway, V. Malik, B. Coley, K.R. Clark, J. Li, X. Xiao, J. Samulski, S.W. McPhee, R.J. Samulski, and C.M. Walker. 2010. Dystrophin immunity in Duchenne's muscular dystrophy. *The New England journal of medicine*. 363:1429–37.

Mendell, J.R., C. Shilling, N.D. Leslie, K.M. Flanigan, R. Al-Dahhak, J. Gastier-Foster, K. Kneile, D.M. Dunn, B. Duval, A. Aoyagi, C. Hamil, M. Mahmoud, K. Roush, L. Bird, C. Rankin, H. Lilly, N. Street, R. Chandrasekar, and R.B. Weiss. 2012. Evidence-based path to newborn screening for Duchenne muscular dystrophy. *Annals of Neurology*. 71:304–13.

Menke, A., and H. Jockusch. 1991. Decreased osmotic stability of dystrophin-less muscle cells from the mdx mouse. *Nature*. 349:69–71.

Michel, T., and O. Feron. 1997. Nitric oxide synthases: which, where, how, and why? *The Journal of clinical investigation*. 100:2146–52.

Mirza, A., M. Sagathevan, N. Sahni, L. Choi, and N. Menhart. 2010. A biophysical map of the dystrophin rod. *Biochimica et Biophysica Acta*. 1804:1796–809.

Moens, P., P.H. Baatsen, and G. Maréchal. 1993. Increased susceptibility of EDL muscles from mdx mice to damage induced by contractions with stretch. *Journal of muscle research and cell motility*. 14:446–51.

Mokri, B., and A. Engel. 1998. Duchenne dystrophy: electron microscopic findings pointing to a basic or early abnormality in the plasma membrane of the muscle fiber. *Neurology*. 25:1111.

Niesen, F.H., H. Berglund, and M. Vedadi. 2007. The use of differential scanning fluorimetry to detect ligand interactions that promote protein stability. *Nature Protocols*. 2:2212–21.

Nudel, U., D. Zuk, P. Einat, E. Zeelon, Z. Levy, S. Neuman, and D. Yaffe. 1989. Duchenne muscular dystrophy gene product is not identical in muscle and brain. *Nature*. 337:76–8.

O'Brien, E.T., E.D. Salmon, and H.P. Erickson. 1997. How calcium causes microtubule depolymerization. *Cell Motility and the Cytoskeleton*. 36:125–35.

Ohlendieck, K., and K.P. Campbell. 1991. Dystrophin-associated proteins are greatly reduced in skeletal muscle from mdx mice. *The Journal of cell biology*. 115:1685–94.

Pearce, M., D.J. Blake, J.M. Tinsley, B.C. Byth, L. Campbell, A.P. Monaco, and K.E. Davies. 1993. The utrophin and dystrophin genes share similarities in genomic structure. *Human molecular genetics*. 2:1765–72.

Percival, J.M., P. Gregorevic, G.L. Odom, G.B. Banks, J.S. Chamberlain, and S.C. Froehner. 2007. rAAV6-microdystrophin rescues aberrant Golgi complex organization in mdx skeletal muscles. *Traffic*. 8:1424–39.

Perez, O.D., Y.-T. Chang, G. Rosania, D. Sutherlin, and P.G. Schultz. 2002. Inhibition and reversal of myogenic differentiation by purine-based microtubule assembly inhibitors. *Chemistry & biology*. 9:475–83.

Petrof, B.J., J.B. Shrager, H.H. Stedman, A.M. Kelly, and H.L. Sweeney. 1993. Dystrophin protects the sarcolemma from stresses developed during muscle contraction. *Proceedings of the National Academy of Sciences of the United States of America*. 90:3710–4.

Pillers, D.A., D.E. Bulman, R.G. Weleber, D.A. Sigesmund, M.A. Musarella, B.R. Powell, W.H. Murphey, C. Westall, C. Panton, and L.E. Becker. 1993. Dystrophin expression in the human retina is required for normal function as defined by electroretinography. *Nature genetics*. 4:82–6.

Ponting, C., D. Blake, K. Davies, J. Kendrick-Jones, and S. Winder. 1996. ZZ and TAZ: new putative zinc fingers in dystrophin and other proteins. *Trends in Biological Science*. 21:11–13.

Porter, G.A., G.M. Dmytrenko, J.C. Winkelmann, and R.J. Bloch. 1992. Dystrophin colocalizes with beta-spectrin in distinct subsarcolemmal domains in mammalian skeletal muscle. *The Journal of Cell Biology*. 117:997–1005.

Prins, K.W., J.L. Humston, A. Mehta, V. Tate, E. Ralston, and J.M. Ervasti. 2009. Dystrophin is a microtubule-associated protein. *The Journal of Cell Biology*. 186:363–9.

Prosser, B.L., C.W. Ward, and W.J. Lederer. 2011. X-ROS signaling: rapid mechano-chemo transduction in heart. *Science*. 333:1440–5.

Rall, S., and T. Grimm. 2012. Survival in Duchenne muscular dystrophy. *Acta Myologica*. 117–120.

Ralston, E., Z. Lu, and T. Ploug. 1999. The organization of the Golgi complex and microtubules in skeletal muscle is fiber type-dependent. *The Journal of Neuroscience*. 19:10694–705.

Ralston, E., T. Ploug, J. Kalhovde, and T. Lomo. 2001. Golgi complex, endoplasmic reticulum exit sites, and microtubules in skeletal muscle fibers are organized by patterned activity. *The Journal of Neuroscience*. 21:875–83.

Randazzo, D., E. Giacomello, S. Lorenzini, D. Rossi, E. Pierantozzi, B. Blaauw, C. Reggiani, S. Lange, A.K. Peter, J. Chen, and V. Sorrentino. 2013. Obscurin is required for ankyrinB-dependent dystrophin localization and sarcolemma integrity. *The Journal of Cell Biology*. 200:523–36.

Roberts, R., A. Coffey, M. Bobrow, and D. Bentley. 1993. Exon structure of the human dystrophin gene. *Genomics*. 16:536–8.

Roberts, R.G., R.J. Gardner, and M. Bobrow. 1994. Searching for the 1 in 2,400,000: a review of dystrophin gene point mutations. *Human mutation*. 4:1–11.

Rybakova, I.N., and J.M. Ervasti. 1997. Dystrophin-glycoprotein complex is monomeric and stabilizes actin filaments in vitro through a lateral association. *The Journal of Biological Chemistry*. 272:28771–8.

Rybakova, I.N., J.L. Humston, K.J. Sonnemann, and J.M. Ervasti. 2006. Dystrophin and utrophin bind actin through distinct modes of contact. *The Journal of Biological Chemistry*. 281:9996–10001.

Rybakova, I.N., J.R. Patel, K.E. Davies, P.D. Yurchenco, and J.M. Ervasti. 2002. Utrophin binds laterally along actin filaments and can couple costameric actin

with sarcolemma when overexpressed in dystrophin-deficient muscle. *Molecular Biology of the Cell*. 13:1512–1521.

Saitoh, O., T. Arai, and T. Obinata. 1988. Distribution of microtubules and other cytoskeletal filaments during myotube elongation as revealed by fluorescence microscopy. *Cell and tissue research*. 252:263–73.

Schmidt, H.H., G.D. Gagne, M. Nakane, J.S. Pollock, M.F. Miller, and F. Murad. 1992. Mapping of neural nitric oxide synthase in the rat suggests frequent co-localization with NADPH diaphorase but not with soluble guanylyl cyclase, and novel paraneural functions for nitrinergic signal transduction. *Journal of Histochemistry & Cytochemistry*. 40:1439–1456.

Schoenmakers, T., G. Visser, G. Flik, and A. Theuvenet. 1992. CHELATOR: an improved method for computing metal ion concentrations in physiological solutions. *Biotechniques*. 12:870–9.

Schwarze, S.R., K.A. Hruska, and S.F. Dowdy. 2000. Protein transduction: unrestricted delivery into all cells? *Trends in cell biology*. 10:290–5.

Sonnemann, K.J., H. Heun-Johnson, A.J. Turner, K. a Baltgalvis, D. a Lowe, and J.M. Ervasti. 2009. Functional substitution by TAT-utrophin in dystrophin-deficient mice. *PLoS Medicine*. 6:e1000083.

Suzuki, A., M. Yoshida, and E. Ozawa. 1995. Mammalian alpha 1- and beta 1-syntrophin bind to the alternative splice-prone region of the dystrophin COOH terminus. *The Journal of cell biology*. 128:373–81.

Tinsley, J., N. Deconinck, R. Fisher, D. Kahn, S. Phelps, J.M. Gillis, and K. Davies. 1998. Expression of full-length utrophin prevents muscular dystrophy in mdx mice. *Nature Medicine*. 4:1441–4.

Wade, R., and D. Chrétien. 1993. Cryoelectron microscopy of microtubules. *Journal of Structural Biology*. 110:1–27.

Wang, Z., J.M. Allen, S.R. Riddell, P. Gregorevic, R. Storb, S.J. Tapscott, J.S. Chamberlain, and C.S. Kuhr. 2007. Immunity to adeno-associated virus-mediated gene transfer in a random-bred canine model of Duchenne muscular dystrophy. *Human Gene Therapy*. 18:18–26.

Warner, L.E., C. DelloRusso, R.W. Crawford, I.N. Rybakova, J.R. Patel, J.M. Ervasti, and J.S. Chamberlain. 2002. Expression of Dp260 in muscle tethers the actin cytoskeleton to the dystrophin-glycoprotein complex and partially prevents dystrophy. *Human molecular genetics*. 11:1095–105.

Way, M., B. Pope, R.A. Cross, J. Kendrick-Jones, and A.G. Weeds. 1992. Expression of the N-terminal demonstration domain of dystrophin in E . coli and of binding to F-actin. *FEBS Letters*. 301:243–5.

Weisenberg, R. 1972. Microtubule formation in vitro in solutions containing low calcium concentrations. *Science*. 177:1104–1105.

Winder, S.J., L. Hemmings, S.K. Maciver, S.J. Bolton, J.M. Tinsley, K.E. Davies, D.R. Critchley, and J. Kendrick-Jones. 1995. Utrophin actin binding domain: analysis of actin binding and cellular targeting. *Journal of Cell Science*. 108:63–71.

Worton, R.G., and M.W. Thompson. 1988. Genetics of Duchenne muscular dystrophy. *Annual Review of Genetics*. 22:601–29.

Yin, H., H.M. Moulton, C. Betts, Y. Seow, J. Boutilier, P.L. Iverson, and M.J.A. Wood. 2009. A fusion peptide directs enhanced systemic dystrophin exon skipping and functional restoration in dystrophin-deficient mdx mice. *Human molecular genetics*. 18:4405–14.

Zhang, T., K.J.M. Zaal, J. Sheridan, A. Mehta, G.G. Gundersen, and E. Ralston. 2009. Microtubule plus-end binding protein EB1 is necessary for muscle cell differentiation, elongation and fusion. *Journal of cell science*. 122:1401–9.

Appendix

Generation of a transgenic mouse model expressing a dystrophin lacking microtubule binding activity

Joseph Belanto performed all experiments.

Chapter 3 outlines the delineation of the minimal microtubule binding domain of dystrophin, the data from which we used to generate a transgenic mouse model expressing a dystrophin-utrophin hybrid protein in which the microtubule binding domain of dystrophin was replaced with the homologous region of utrophin (Dys R20-24$_{Utr}$). This hybrid protein retains the nNOS binding domain (Lai et al., 2009) but fails to bind microtubules (Figure 3-5). Dys R20-24$_{Utr}$ was engineered under the control of the human skeletal alpha-actin promoter, restricting expression to skeletal muscles, the same strategy used for generation of the Fiona-*mdx*, the Dys-TG-*mdx*, and the mini-Dys-TG-*mdx* mouse models (Figure A-1). Transgenic founder mice have been produced and bred, the details of which are outlined in Table A-1.

Our current mouse lines express 15% (Ln2), 30% (Ln2^2), and 160% (Ln4) levels of WT dystrophin on the *mdx* mouse background (Figure A-2 and Table A-1). Line Ln2^2 is line Ln2 bred to be homozygous for the transgene. A last transgenic mouse line (Ln3) is still being bred onto the *mdx* background. These mice will be utilized in future experiments to further delineate phenotypes specific to the loss of microtubule organization. Initial characterization of the Ln2^2-*mdx* and Ln4-*mdx* mouse lines is detailed below.

To initially determine that the transgenic dystrophin protein was properly localized within muscle and that it had integrated into the DGC, we performed wheat germ agglutinin (WGA) chromatography to enrich whole muscle lysates for DGC components. WGA is a lectin which binds to N-acetyl-D-glucosamine and sialic acid, both of which are abundant on the surface of α-dystroglycan. We

show that in both Ln2^2-*mdx* and Ln4-*mdx* mice, transgenic dystrophin incorporates into the DGC as evidenced by its presence in the elution fraction of the WGA enrichment (Figure A-3). Additionally, known DGC components such as the dystroglycans and syntrophin are present in the WGA elution fraction.

We next sought to determine whether DGC components showed proper sarcolemmal localization in our transgenic mice. Dystrophin, α-dystroglycan, β-dystroglycan, α-sarcoglycan, γ-sarcoglycan, dystrobrevin, syntrophin, nNOS, and laminin show sarcolemmal localization in WT mice (Figure A-4). Utrophin levels in WT mice are reduced compared to *mdx* mice, which upregulate utrophin in the absence of dystrophin. Utrophin in *mdx* mice shows greater sarcolemmal localization than in any other line. Transgenic line Ln2^2-*mdx* and Ln4-*mdx* show presence of all DGC components at the sarcolemma, with Ln2^2-*mdx* mice showing relatively reduced levels of all components, except utrophin, as compared to WT and Ln4-*mdx* mice. Ln2^2-*mdx* mice show increased levels of utrophin at the sarcolemma as compared to WT but lower than that seen in *mdx* mice, most likely due to the lower dystrophin expression of this line. These data indicate that the low levels of dystrophin present in Ln2^2-*mdx* mice partially restores the DGC, but not to levels present in WT mice whereas Ln4-*mdx* mice show sarcolemmal localization of all DGC components comparable to WT.

Additionally, we analyzed the patterning of the neuromuscular junction in our transgenic mice. Like WT mice, we find that Ln2^2-*mdx* and Ln4-*mdx* mice show the pretzel-like patterning of the neuromuscular junction (Figure A-5). This is in contrast to the grape-like patterning of the *mdx* neuromuscular junction.

These data indicate to us that even relatively low levels of dystrophin present in Ln2^2-*mdx* mice are sufficient to rescue the disorganized neuromuscular junction patterning of the *mdx* mouse.

Lastly, we analyzed the subsarcolemmal microtubule lattice organization in our transgenic mice. As shown in Figure 2-2, the WT subsarcolemmal microtubule lattice adopts a rectilinear lattice organization whereas the *mdx* microtubule lattice lacks such organization (Figure A-6). The microtubule lattice of the Ln2^2-*mdx* mouse appears disorganized while the Ln4-*mdx* mouse appears somewhat intermediate between organized and disorganized. While we have shown that the transgene used to generate our mice lacks any *in vitro* microtubule binding activity (Figure 3-5), this does not preclude the hypothesis that reintroducing the other muscle stabilizing functions of dystrophin allows for partial rescue of microtubule lattice morphology.

Taken together, all current data for our transgenic mice suggest that they are good model for elucidating specific phenotypes of the *mdx* mouse specifically related to lack of WT microtubule lattice organization.

Figures

Figure A-1: Plasmid map of construct used to generate transgenic mice. Constructs used to generate transgenic mice expressing a muscle-specific dystrophin incapable of binding microtubules. Ovals represent spectrin-like repeats, diamonds represent hinge regions. Red and yellow represent portions of dystrophin whereas blue represents portions of utrophin. HSA, human skeletal α-actin promoter; NT, N-terminus; CT, C-terminus; CR, cysteine rich domain.

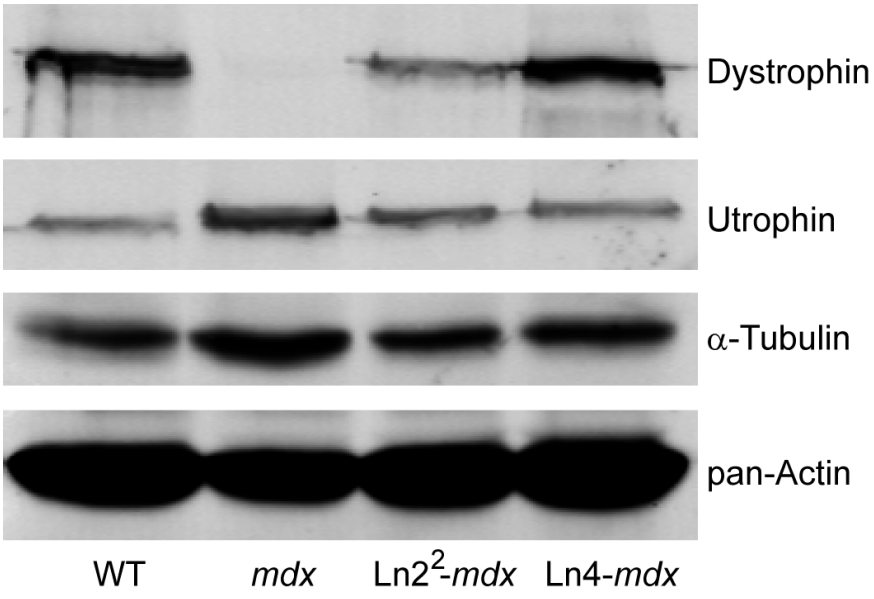

Figure A-2: Western blot of Ln2^2-*mdx* and Ln4-*mdx* transprotein expression. Dystrophin levels in Ln2^2-*mdx* mice is approximately 30% of WT levels whereas dystrophin levels in Ln4-*mdx* mice is approximately 160% of WT levels. Utrophin levels are elevated in *mdx* mice as compared to WT levels, but are reduced in the presence of transgenic dystrophin. Tubulin and actin shown as loading controls.

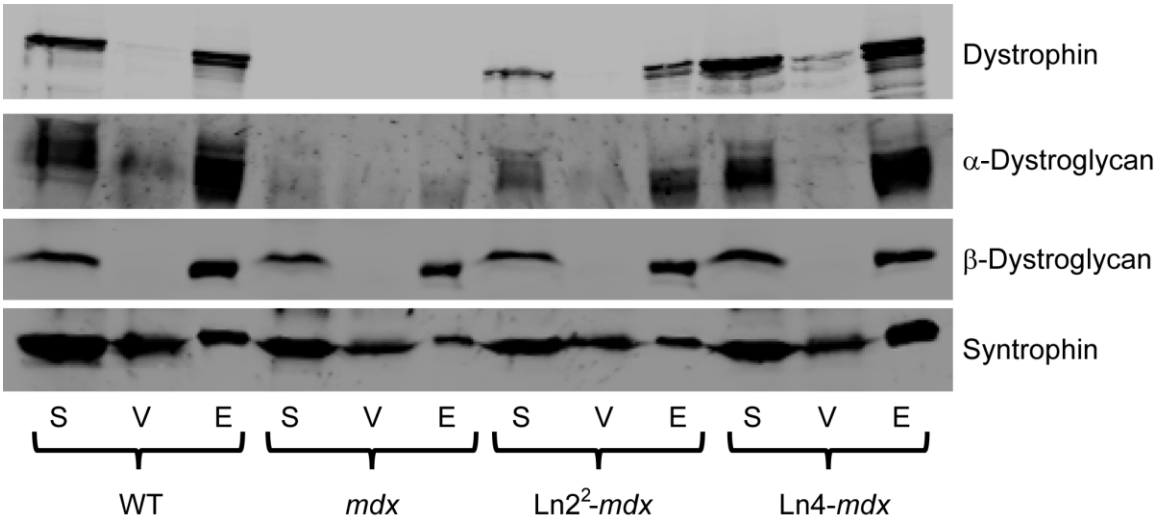

Figure A-3: Wheat germ agglutinin enrichment of DGC components in Ln2^2-*mdx* and Ln4-*mdx* mice. Transgenic dystrophin incorporates into the DGC as evidenced by its presence in the elution fraction of the WGA enrichment. The dystroglycans and syntrophin are also present in the elution fraction, with their relative abundance proportional to the levels of dystrophin present in each mouse line. S, starting lysate; V, void fraction not bound to WGA beads; E, elution fraction from WGA beads.

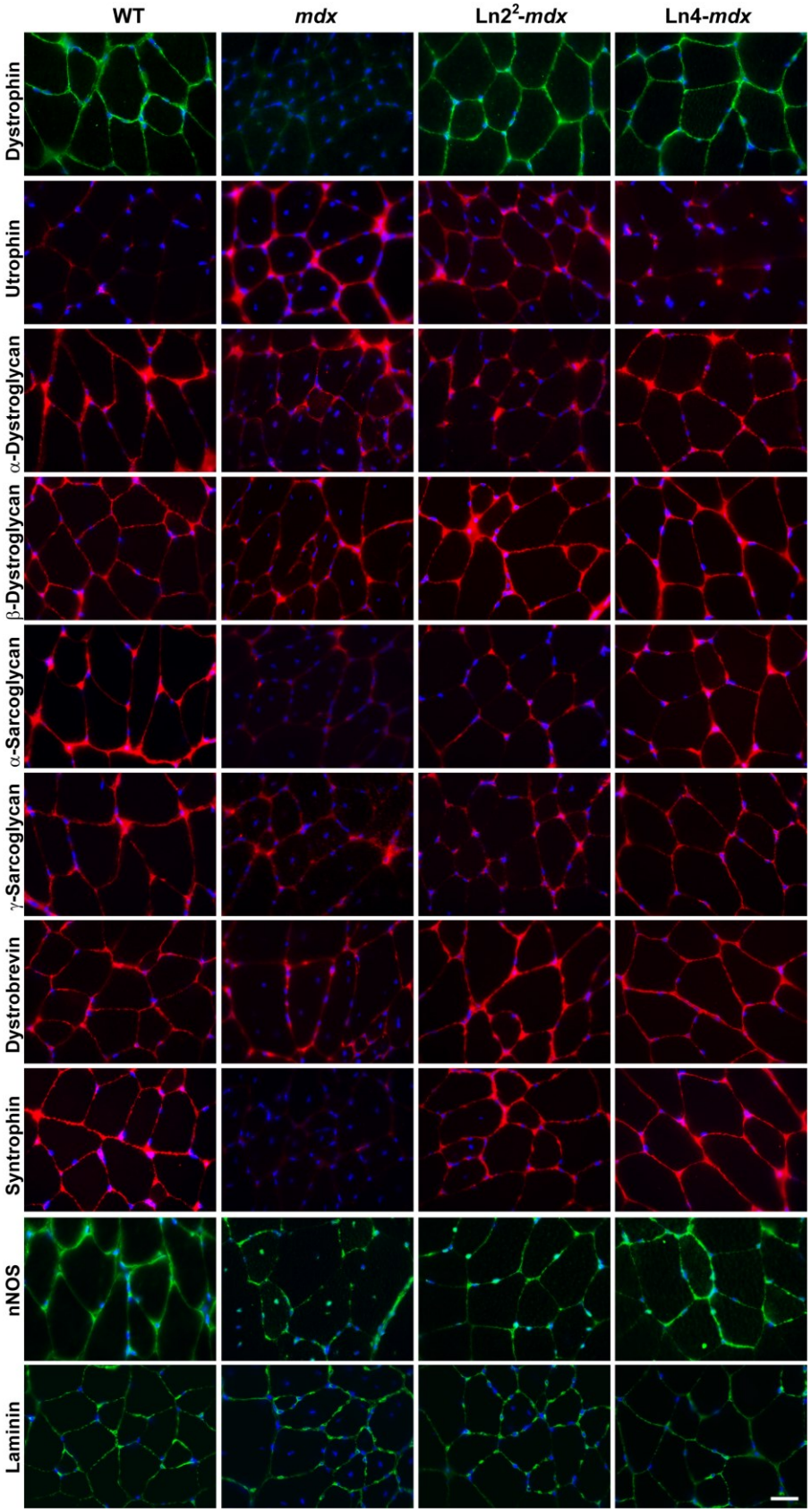
WT
mdx
Ln2²-mdx
Ln4-mdx
Dystrophin
Utrophin
α-Dystroglycan
β-Dystroglycan
α-Sarcoglycan
γ-Sarcoglycan
Dystrobrevin
Syntrophin
nNOS
Laminin

Figure A-4: Immunofluorescence analysis of Ln2^2-mdx and Ln4-mdx mice. Dystrophin, utrophin, α-dystroglycan, β-dystroglycan, α-sarcoglycan, γ-sarcoglycan, dystrobrevin, syntrophin, nNOS, and laminin immunofluorescent localization in WT, *mdx*, Ln2^2-*mdx*, and Ln4-*mdx* mice. Dystrophin is absent in *mdx* mice. Utrophin levels are upregulated in *mdx* mice as compared to other lines. Ln2^2-*mdx* and Ln4-*mdx* mice show presence of all DGC components at the sarcolemma. Bar, 20μm.

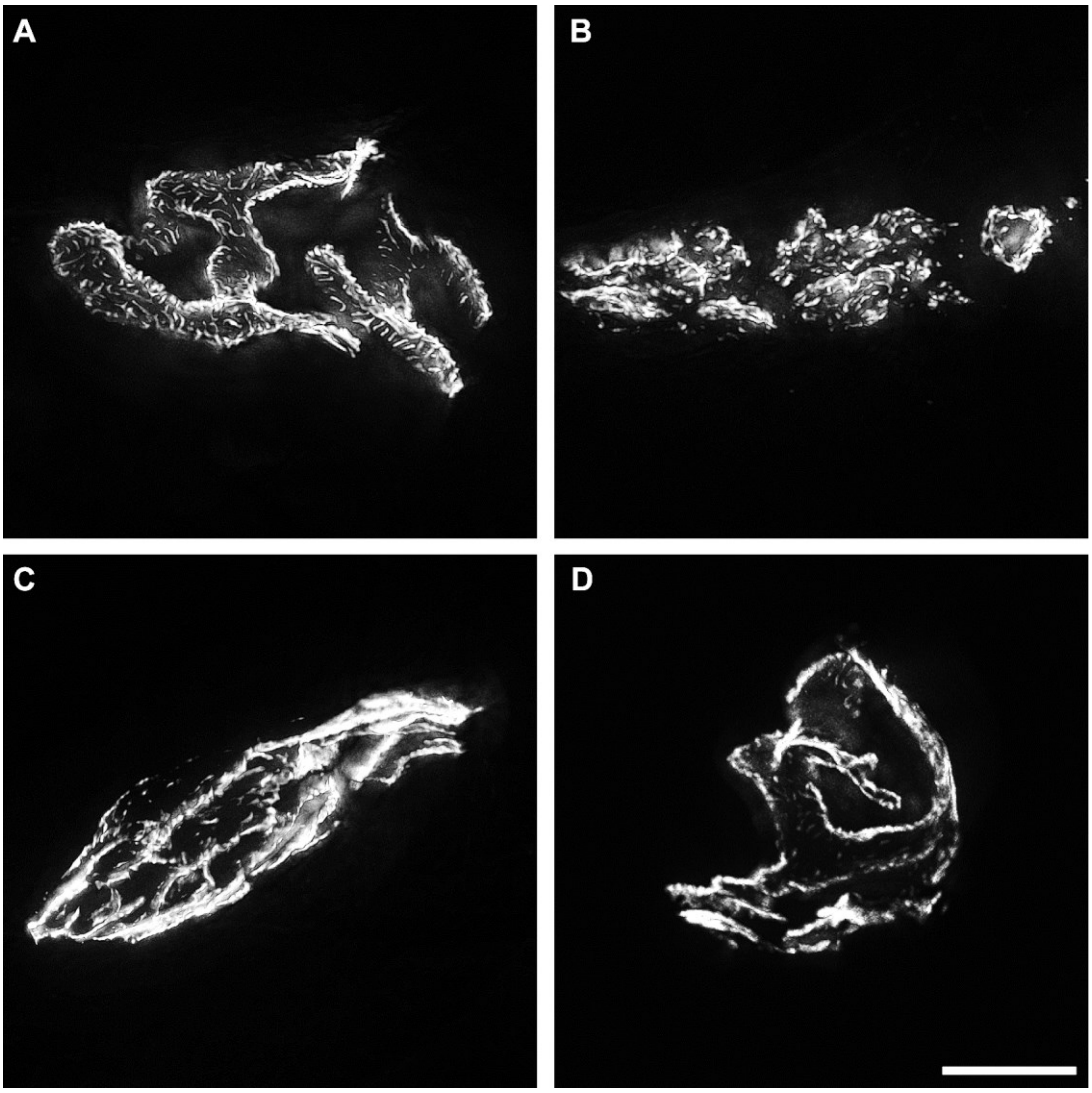

Figure A-5: Neuromuscular junction imaging in Ln2^2-mdx and Ln4-mdx mice. (A) Neuromuscular junction morphology in a WT mouse resembles a pretzel. (B) This morphology is lost in the *mdx* mouse and instead appear as a cluster of grapes. (C) The Ln2^2-*mdx* mouse shows rescued neuromuscular junction morphology. (D) The Ln4-*mdx* mouse shows rescued neuromuscular junction morphology. Bar, 5μm.

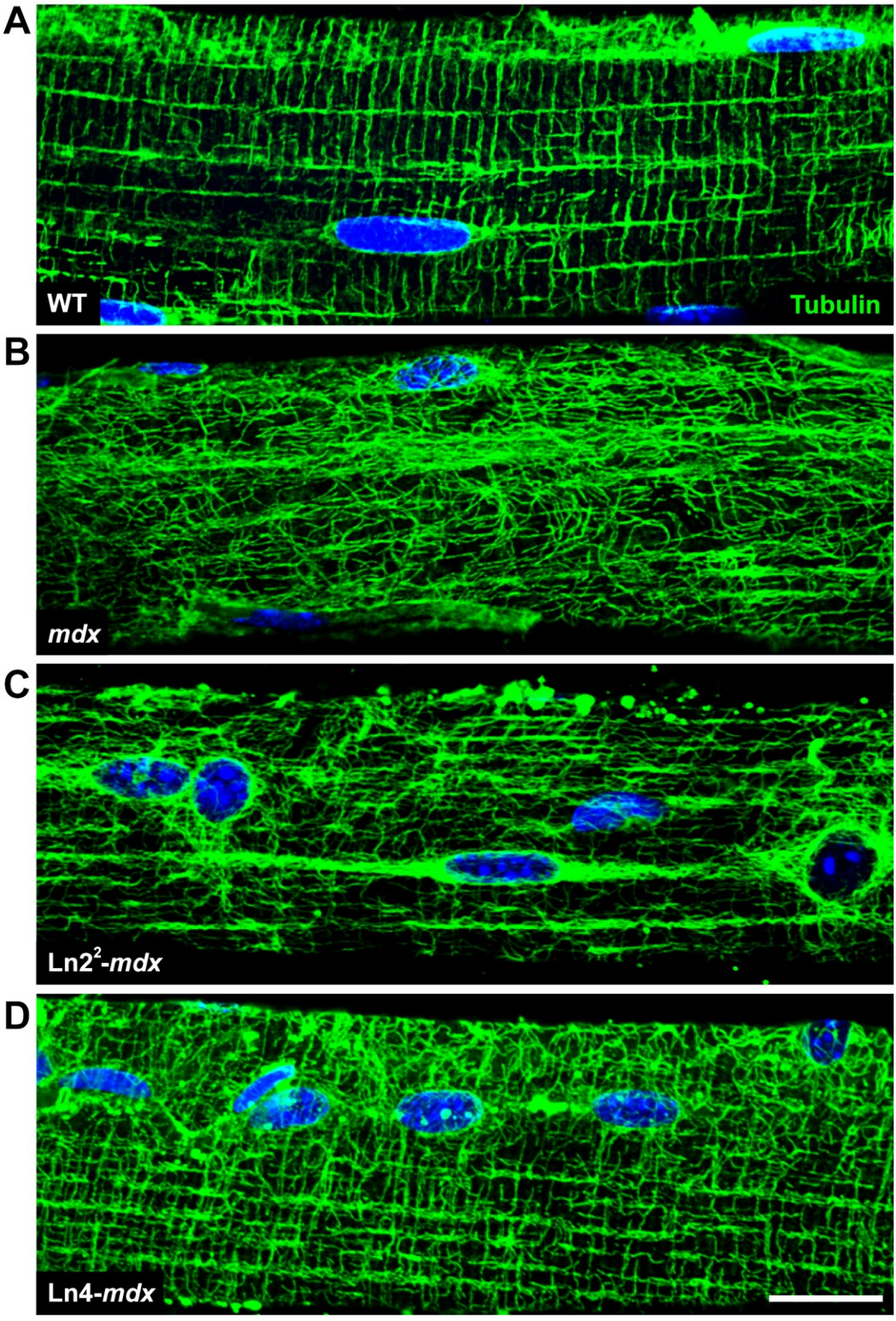
A
WT
Tubulin
B
mdx
C
Ln2²-mdx
D
Ln4-mdx

Figure A-6: Extensor digitorum longus muscle sarcolemmal microtubule imaging in Ln2^{2}-*mdx* and Ln4-*mdx* mice. (A) When dystrophin is present (WT), microtubules are organized into a rectilinear lattice beneath the sarcolemma. Image is identical to Figure 2-2A. (B) In the absence of dystrophin (*mdx*), the microtubule lattice becomes disordered. (C-D) Transgenic expression of dystrophin lacking the microtubule binding domain does not fully rescue the disorganized microtubule lattice. Single extensor digitorum longus muscle fibers were mechanically teased from profusion fixed mice and immunostained for tubulin and counterstained with DAPI to visualize nuclei. Bar, 20μm.

Tables

Mouse ID	Date Of Birth	Sex	Transgene Transmission?	Transprotein Expression?	Mouse Line
1	7/31/2012	F	Yes	Yes	Ln3
4	7/31/2012	M	Yes	No	Ln1
5	7/31/2012	M	Never Bred	-	-
7	7/31/2012	F	Never Bred	-	-
10	7/31/2012	F	Never Bred	-	-
13	7/31/2012	M	Yes	Yes (15% WT)	Ln2
				Yes (30% WT)	$Ln2^2$
16	7/31/2012	F	Yes	Yes (160% WT)	Ln4
21	8/28/2012	F	No	-	-
23	8/28/2012	M	No	-	-
25	8/28/2012	M	Never Bred	-	-

Table A-1: Summary of transgenic Dys R20-24$_{Utr}$ founder mice received, transgene transmission, and transprotein expression. Transgenic line 2 was bred to be homozygous for the transgene ($Ln2^2$) to increase the level of protein expression. Transgenic line 3 has not been bred onto the *mdx* background yet, therefore no protein expression level is listed.